



NTNU – Trondheim
Norwegian University of
Science and Technology

Buckling of cylindrical members with respect to axial loads

Julie Lund

Master of Science in Mechanical Engineering

Submission date: June 2014

Supervisor: Nils Petter Vedvik, IPM

Norwegian University of Science and Technology
Department of Engineering Design and Materials

THE NORWEGIAN UNIVERSITY
OF SCIENCE AND TECHNOLOGY
DEPARTMENT OF ENGINEERING DESIGN
AND MATERIALS

**MASTER THESIS SPRING 2014
FOR
STUD.TECHN. JULIE LUND**

Buckling of cylindrical members with respect to axial loads

Interwell is a Norwegian based oil service company which was founded in 1988 by recognizing the need for an independent supplier with focus on operation and maintenance of down-hole tool such as plugs, packers and straddles with associated running & pulling tools, and niche completion products and services.

In many of Interwell's product lines, cylindrical rods and pipes are being exposed to axial compressive loads in both static and dynamic conditions. Several methods have been developed to determine the allowed buckling loads for various geometries and constraints. Interwell suspects that these calculation methods are more conservative than needed for Interwell's equipment and industry. One of the main goals in any structural design is optimization of the different parameters involved. Interwell would like to perform full scale tests to give answers to how well Interwell's equipment, with given constraints and load conditions, perform when comparing to the established theory. The motivation for this study is to gain knowledge facilitating full utilization of the limited design space available for Down Hole Equipment.

This study aims to verify build in functionalities and constructional integrity of the Setting Chamber Mandrel in the Hydrostatic Setting Unit, as well as give the preliminaries to establish an acceptable method of predicting the buckling load of a structural member due to axial compression. The most severe load is during operation in maximum pressure conditions, when the compression is relaxed by applied axial tension, only to be restored in a very abrupt manner when breaking a weak point in the product to be set. The Setting Chamber Mandrel also has to resist compression caused by increasing well pressure while running in hole.

FE- analyses and tests of the Setting Chamber Mandrel shall be carried out to study buckling characteristics under uniform axial compression from well pressure. To determine the critical quality attributes likely to influence the quality and performance of the Setting Chamber Mandrel five different parameter tests will be performed; length, diameter, surface treatment (hardening), temperature and dynamic effects from tool operation in well pressure. Linear static buckling analysis and non-linear static analysis will be done using the finite element software package ABAQUS 6.13. If inertia effects shows to be important for the understanding of the instability mechanisms, non-linear dynamic analysis will be carried out using the same software package. The gathered data set should result in a recommendation on Safety Factors for calculations and analyses of different types of equipment. Knowledge on how tool components exposed to buckling loads perform would provide; a safety of result in the design process, technical competitive edge, and a reassuring credibility towards customers in need of reliable answers.

Three weeks after start of the thesis work, an A3 sheet illustrating the work is to be handed in. A template for this presentation is available on the IPM's web site under the menu "Masteroppgave" (<http://www.ntnu.no/ipm/masteroppgave>). This sheet should be updated one week before the Master's thesis is submitted.

Performing a risk assessment of the planned work is obligatory. Known main activities must be risk assessed before they start, and the form must be handed in within 3 weeks of receiving the problem text. The form must be signed by your supervisor. All projects are to be assessed, even theoretical and virtual. Risk assessment is a running activity, and must be carried out before starting any activity that might lead to injury to humans or damage to materials/equipment or the external environment. Copies of signed risk assessments should also be included as an appendix of the finished project report.

The thesis should include the signed problem text, and be written as a research report with summary both in English and Norwegian, conclusion, literature references, table of contents, etc. During preparation of the text, the candidate should make efforts to create a well arranged and well written report. To ease the evaluation of the thesis, it is important to cross-reference text, tables and figures. For evaluation of the work a thorough discussion of results is appreciated.

The thesis shall be submitted electronically via DAIM, NTNU's system for Digital Archiving and Submission of Master's thesis.

The contact person at Interwell: Eirik Grande



Torgeir Welo
Head of Division



Nils Petter Vedvik
Professor/Supervisor

Abstract

Managing technology and taking advantage of the opportunities to further development is essential to ensure increased hydrocarbon recovery and barrier security for upstream energy companies. Interwell is a well intervention company operating globally, with main competence in plug and straddle solutions with related setting, pulling and measurement tools. In many of Interwell's product lines, cylindrical members and pipes are being exposed to axial compressive loads in both static and dynamic conditions. The purpose of this study was to increase the knowledge on how to facilitate full utilization of the limited design space available for Down Hole Equipment by minimizing the gap between the numerical and the experimental results and to find global safety factors. This study introduces options to supplement the safe design of axially loaded members, focusing mainly on the Setting Chamber Mandrel, a cylindrical member in the Hydrostatic Setting Unit. The Setting Chamber mandrel has to resist compression caused by increasing well pressure while running in hole. The prominence of the failure mode depends on several factors including member slenderness, section slenderness, strength, influence of connections and restrains, geometric imperfections and residual stresses.

The members in this study have been characterized into three general types depending on their proneness to buckling; short, intermediate and long. The dividing lines between short, intermediate and long members shall not be considered as accurately defined; furthermore the maximum load-carrying capacity of a member in each category is based upon different types of mechanical failure scenarios. The Setting Chamber Mandrel is classified as intermediate and will fail by both yielding and buckling; i.e. inelastic buckling behavior. Failure of intermediate members could be progressive and unpredictable, and it is common practice to use large safety factors when predicting the buckling strength. A safe design approach has been suggested for predicting the critical load and critical stresses of intermediate members by comparing experimental results to existing literature.

The experimental study consists of three experimental tests; TEST 1: length and diameter, TEST 2: temperature and TEST 3: well pressure. The results obtained from the experimental study were compared with NS-EN 1993-1-1:2005, FE-analyses and established linear buckling theory; Euler and J.B. Johnsons equations. Linear elastic eigenvalue buckling analysis and nonlinear static buckling analyses were performed with finite element software package Abaqus 6.12. In order to understand the buckling behavior of the Setting Chamber Mandrel elastic-plastic material properties was added to the nonlinear large deformation buckling analysis. The results from the analyses were used as a pre-study for the experimental testing and for post-buckling analysis to validate the results to establish the reliability and uncertainties of the numerical methods. Results indicate that NS-EN 1993-1-1:2005 and the nonlinear analysis techniques are suitable to accurately predict the critical buckling load of an axially loaded compression member. The results from the nonlinear static large deformation buckling analysis using elastic-plastic material properties show most agreement with the experimental studies.

The partial safety factors in the global safety factor presented in this study are utilized based on anticipated conditions to ensure that build in functionality and constructional integrity of the Setting Chamber Mandrel will not affect the overall integrity of the Hydrostatic Setting Unit. The appropriate global safety factor for intermediate members with similar shape and boundary conditions as the Setting Chamber Mandrel is concluded to be 1.5 when calculating buckling strength with Interwell's safe design procedure. In order to obtain a high degree of confidence in the design of axially loaded compression members it is recommended to follow the complete methodology provided in this study.

Sammendrag (Norwegian)

Interwell er et oljeserviceselskap med kjernekompetanse innen plugger og pakninger som brukes i olje- og gassbrønner for å sikre og/eller forbedre produksjonen. I mange av produktene til Interwell finner man sylindervede deler som blir utsatt for aksiale trykkbelastninger både i statiske og dynamiske lasttilfeller. Formålet med denne oppgaven var å øke kunnskap innen knekkingsteori og dermed oppnå full utnyttelse av tilgjengelig plass ved å lage en sikker designprosess basert på eksperimentelle og teoretiske resultater. I denne oppgaven beskrives derfor muligheter og utfordringer knyttet til redegjørelse av potensialet og til videreutvikling av eksisterende knekkingsteorier. En grundig analyse av de klassiske metodene for å beregne knekktilfeller på deler som Setting Chamber Mandrel (en sylindervedet stang i Hydrostatic Setting Unit) ble gjennomført.

Setting Chamber Mandrel er klassifisert som en mellomslank stang der inndelingen er basert på slankheten til stangen, m.a.o. forholdet mellom stangens tverrsnittsareal og lengde. I motsetning til en del andre sammenbrudd kan knekking skje uten særlig deformasjon i forkant og man får derfor ingen forvarsel før den kritiske grensetilstanden til stangen er nådd. Elastisk eller plastisk ustabilitet som forårsakes av trykkspenninger er avhengig av flere faktorer; slankhet, tverrsnittstyrke, grensebetingelser, avvik fra nominell geometri og residualspenninger fra fabrikasjon. For mellomslanke stenger kan man få en ustabilitet med plastisk deformasjon, dvs. plastisk knekking.

Denne oppgaven tar i bruk tilgjengelig litteratur, numeriske analyser, standarder og tester for å oppnå nødvendig forståelse av knekkingsteori for trykkstenger som utsettes for aksiale krefter. Det eksperimentelle studiet består av tre tester; TEST 1: lengde og diameter, TEST 2: temperatur, TEST 3: brønntrykk. De oppnådde resultatene fra testene er blitt sammenlignet med nåværende standard NS-EN 1993-1-1:2005, FE-analyser og lineær knekkings teori; Euler og J.B. Johnsons ligninger. Lineær-elastisk knekkingsanalyse og ikke-lineær knekkingsanalyse ble utført med elementprogrammet Abaqus 6.12. I den lineær-elastiske knekkingsanalysen ble aktuelle knekkformer med tilhørende egenverdi funnet. Kapasitetsberegningene som fulgte i de ikke-lineære analysene benyttet knekkformene fra lineær-elastisk analyse som formfeil. Beregningene av lastvirke og deformasjoner sammen med sammenligningen mellom de ulike modellene la grunnlag for etablering av pålitelighet og usikkerhet i de numeriske metodene. Resultatene fra studiet viser at NS-EN 1993-1-1:2005 og de ikke-lineære metodene er egnet ved bruk av beregning av knekklast og spenninger på en stang utsatt for aksiale krefter. I dette studiet viste det seg at ved å innføre elastisk-plastisk materialegenskaper til modellen fikk man en knekkingsrespons som er sammenlignbar med testene.

Den viktigste barrieren mot progressivt sammenbrudd av Setting Chamber Mandrel er kvalitet i designprosessen og klare retningslinjer ved bruk av partisalfaktorer sammen med NS-EN 1993-1-1:2005. Oppgaven introduserer et beregningsgrunnlag ved dimensjonering av lastbærende integritet med partisalfaktorer i kombinasjon med flere analytiske fremgangsmåter.

Preface

This study is the final work after a 5-year Master programme in Mechanical Engineering at the Department of Engineering Design and Material, Norwegian University of Science and Technology, NTNU, Spring 2013. The assignment was provided by Eirik Grande at Interwell. This study has been written to provide a safe design approach for axially loaded compression members with similar shape and boundary conditions as the Setting Chamber Mandrel.

Although great care has been taken to ensure the accuracy of the material presented in this study, responsibility for its use for any purpose rests with the user.

A handwritten signature in black ink, reading "Julie Lund". The signature is written in a cursive style with a large initial 'J' and 'L'. Below the signature is a solid horizontal line.

Julie Lund

June 10, 2014

NTNU, Trondheim

Table of Contents

1	INTRODUCTION	1
1.1	BACKGROUND AND MOTIVATION	1
1.2	SCOPE.....	3
1.2.2	<i>Structure of Thesis.....</i>	4
1.2.3	<i>Limitations.....</i>	5
2	PRELIMINARIES.....	7
2.1	HYDROSTATIC SETTING UNIT	7
2.1.1	<i>Setting Chamber Mandrel</i>	8
2.2	BUCKLING ANALYSIS	8
2.2.1	<i>Linear Elastic Eigenvalue Buckling Analysis</i>	9
2.2.2	<i>NS-EN 1993-1-1:2005</i>	11
2.2.3	<i>Nonlinear Static Buckling Analysis.....</i>	15
2.2.4	<i>Riks analysis.....</i>	15
2.2.5	<i>Dynamic Buckling Analysis</i>	16
2.3	INTERMEDIATE MEMBERS.....	16
3	PROOF OF CONCEPT	19
3.1	TEST SETUP	19
3.1.1	<i>Strain Gauges</i>	20
3.2	TEST PARTS	21
3.2.1	<i>Uniaxial Tensile Testing of 34CrNiMo6 steel.....</i>	23
3.3	EVALUATION.....	27
4	ANALYSIS.....	29
4.1	EULER AND J.B JOHNSON BUCKLING	29
4.1.1	<i>NS-EN 1993-1-1:2005</i>	30
4.2	FE-ANALYSIS.....	32
4.2.1	<i>Model Calibration</i>	32
4.2.2	<i>Linear Elastic Eigenvalue Buckling Analysis</i>	36
4.2.3	<i>Nonlinear Static Analysis.....</i>	38
5	EXPERIMENTAL STUDIES.....	51
5.1	BUCKLING WITH HYDRAULIC PRESS	52
5.1.1	<i>Preparation of test pieces.....</i>	52
5.1.2	<i>Instrumentation</i>	52
5.1.3	<i>Test Setup and Procedure.....</i>	54
5.1.4	<i>TEST 1: Length and Diameter.....</i>	56

5.1.5	TEST 2: Temperature.....	66
5.2	BUCKLING IN TEST CASING	70
5.2.1	TEST 3: Well Pressure.....	70
6	DISCUSSION.....	77
6.1.1	Safety Factor	85
7	CONCLUSION	91
	REFERENCES	93
	ACKNOWLEDGEMENT	94
	APPENDIX.....	97
	LIST OF APPENDIX.....	97
	APPENDIX A: MATERIAL CERTIFICATE FOR 34CRNIMO6.....	98
	APPENDIX B: DERIVATION OF EULER AND J.B. JOHNSONS EQUATION.....	100
	EULERS EQUATION FOR LONG COLUMNS.....	100
	J.B. JOHNSONS EQUATION FOR INTERMEDIATE MEMBERS	101
	APPENDIX C: BUCKLING CALCULATIONS ACCORDING TO NS-EN 1993-1-1:2005	103
	APPENDIX D: RESULTS FROM NONLINEAR RIKS ANALYSIS	106
	APPENDIX E: M-BOND ADHESIVES MANUAL.....	109
	APPENDIX F: DATA SHEET TC8.212.R4.....	113
	APPENDIX G: INTERWELL SAFE DESIGN PROCEDURE.....	115
	APPENDIX H: UNIAXIAL TENSILE TEST	118
	APPENDIX I: RISK ASSESSMENT	122

List of Tables

TABLE 2.1: MATERIAL SPECIFICATIONS FOR 34CrNiMo6 STEEL.....	8
TABLE 2.2: SELECTION OF FLEXURAL BUCKLING CURVE FOR A CROSS-SECTION [5].....	12
TABLE 3.1: MATERIAL SPECIFICATION FOR TEST SPECIMEN IN PROOF OF CONCEPT ANALYSIS.	19
TABLE 3.2: OVERVIEW OVER THE TEST SPECIMENS. THE CURVE SHOWS THE REDUCTION FACTOR χ VS THE NON-DIMENSIONAL SLENDERNESS λ	21
TABLE 3.3: DESIGN OF THE UNIAXIAL TENSILE TEST SPECIMENS OF 34CrNiMo6 STEEL FROM EN ISO 6892-1.....	23
TABLE 3.4: INFORMATION ABOUT UNIAXIAL TENSILE TESTING.....	24
TABLE 3.5: TEST RESULTS FROM UNIAXIAL TENSILE TESTING.	25
TABLE 3.6: COMPARISON BETWEEN THE MEAN UNIAXIAL TENSILE TEST RESULTS AND THE MECHANICAL PROPERTIES FROM THE MATERIAL CERTIFICATES (APPENDIX A).....	25
TABLE 3.7: DIFFERENT TESTS AND TEST PARTS FOR BUCKLING ANALYSIS OF SETTING CHAMBER MANDREL.....	28
TABLE 4.1: RESULTS FROM EULER AND J.B. JOHNSONS EQUATIONS.	29
TABLE 4.2: RESULTS FROM BUCKLING CALCULATION WITH NS-EN 1993-1-1:2005.	31
TABLE 4.3: MATERIAL SPECIFICATION FOR 34CrNiMo6 STEEL.	33
TABLE 4.4: MESH CONVERGENCE FOR REFERENCE TEST PART TP-000274-OD15.....	35
TABLE 4.5: RESULTS FROM LINEAR ELASTIC EIGENVALUE BUCKLING ANALYSIS.....	37
TABLE 4.6: RESULTS FROM NONLINEAR STATIC LARGE DEFORMATION BUCKLING ANALYSIS.	40
TABLE 4.7: PLASTIC STRAIN VALUES IN THE NONLINEAR ABAQUS ANALYSIS.....	44
TABLE 4.8: RESULTS FROM NONLINEAR STATIC LARGE DEFORMATION BUCKLING ANALYSIS WITH ELASTIC-PLASTIC MATERIAL.....	44
TABLE 4.9: RESULTS FROM THE NONLINEAR STATIC RIKS ANALYSIS.....	49
TABLE 5.1: RESULTS FROM TEST1: LENGTH AND DIAMETER.....	58
TABLE 5.2: RESULTS FROM TEST 2: TEMPERATURE TESTS COMPARED WITH TP-000274-4-OD15.....	68
TABLE 5.3: RESULTS FROM TEST 3: WELL PRESSURE.....	73
TABLE 6.1: OVERVIEW OVER THE FINAL RESULTS FROM EXPERIMENT, NS-EN 1993-1-1:2005 AND FE-ANALYSES.	79
TABLE 6.2: EULER AND J.B JOHNSONS FAILURE STRESS COMPARED WITH EXPERIMENTAL RESULTS FROM HP.....	84
TABLE 6.3: INTERWELL SAFE DESIGN PROCEDURE VS NS-EN 1993-1-1:2005 GRAPH.	87
TABLE 6.4: PARTIAL SAFETY FACTORS OBTAINED FROM EXPERIMENTAL STUDIES AND STANDARDS.....	87
TABLE 6.5: VALIDATION OF GLOBAL SAFETY FACTOR.....	88
TABLE 6.6: ALLOWED BUCKLING LOAD.....	88
TABLE 6.7: CORRELATION FACTOR FOR A LINEAR ELASTIC EIGENVALUE BUCKLING ANALYSIS.	88
TABLE 6.8: CORRELATION FACTOR FOR A NONLINEAR STATIC LARGE DEFORMATION BUCKLING ANALYSIS.	89
TABLE 6.9: CORRELATION FACTOR FOR A NONLINEAR RIKS BUCKLING ANALYSIS.	89
TABLE 6.10: CORRELATION FACTOR FOR A NONLINEAR STATIC LARGE DEFORMATION BUCKLING ANALYSIS-EP.....	90

List of Figures

FIGURE 2.1: 2.70" HSU 10" STROKE	7
FIGURE 2.2: SETTING CHAMBER MANDREL IN 2.70" HSU 10" STROKE (A) SHAPE OF SETTING CHAMBER MANDREL (B) QUARTER CUT VIEW	8
FIGURE 2.3: EULER CURVE	10
FIGURE 2.4: BUCKLING CURVES FOR NON-DIMENSIONAL SLENDERNESS [5].	12
FIGURE 2.5: LOAD CASE (A) INITIALLY STRAIGHT COLUMN WITH EULER LOAD; (B) MEMBERS WITH INITIAL CURVATURE AND DEFLECTION; (C) COLUMN CROSS-SECTION	14
FIGURE 2.6: BUCKLING CURVE C OBTAINED FROM LITERATURE STUDY IMPLEMENTED IN MICROSOFT EXCEL 2010.....	15
FIGURE 2.7: AVERAGE COMPRESSIVE CRITICAL BUCKLING STRESS VERSUS THE SLENDERNESS RATIO FOR 34CrNiMo6 STEEL	17
FIGURE 3.1: FINAL TEST SET UP WITH STRAIN GAUGE POSITIONS	20
FIGURE 3.2: TEST PARTS FROM SPECIALIZATION PROJECT WITH OLD DIMENSIONS.	22
FIGURE 3.3: REFERENCE TEST PART TP-000274-OD15.....	22
FIGURE 3.4: MACHINED TEST PIECED OF ROUND CROSS-SECTIONS (A) BEFORE TESTING; (B) AFTER TESTING.....	24
FIGURE 3.5: STRESS-STRAIN CURVE FOR (A) HT: 170807; (B) HT: 168232	26
FIGURE 3.6: STRESS-STRAIN CURVES (A) COMPARISON BETWEEN HT: 170807 AND HT: 168232; (B) TYPICAL STRESS-STRAIN BEHAVIOR OF 34CrNiMo6.....	26
FIGURE 3.7: TT4: (A) IN HYDRAULIC PRESS; (B) COMPARISON BETWEEN BEFORE AND AFTER UNIAXIAL TENSILE TEST FOR TT4, SEE APPENDIX H.....	26
FIGURE 3.8: RESULTS FROM THE CONCEPT ANALYSIS; STRAIN-TIME VS FORCE-TIME.	28
FIGURE 4.1: THE REDUCTION FACTOR X VS THE NON-DIMENSIONAL SLENDERNESS λ FOR NS-EN 1993-1-1:2005 CURVE C POLYNOMIAL AND THE CURVE C OBTAINED FROM DATA.	31
FIGURE 4.2: BASE SKETCHES (IN THIS FIGURE: TP-000274-OD15) (A) CROSS-SECTION AREA; (B) EFFECTIVE LENGTH.....	33
FIGURE 4.3: REVOLVED AND PARTITIONED PARTS (IN THIS FIGURE: TP-000274-OD15) (A) VERTICAL CUTTING PLANE; (B) HORIZONTAL CUTTING PLANE; (C) PARTITIONED FACE OF CROSS-SECTION; (D) PARTITIONED FACE OF OUTER CELL.....	33
FIGURE 4.4: TP-000274-OD15 (A) BOUNDARY CONDITIONS AND LOAD APPLIED TO THE MODEL; (B) ABAQUS MODEL	34
FIGURE 4.5: TP-000274-OD15 (A) CROSS-SECTION AREA; (B) FRONT-ISO VIEW; (C) C3D8R ELEMENT; (D) FULLY MESHED PART	35
FIGURE 4.6: BASE STATE AND BUCKLING MODES FOR TP-000274-OD15 (A) BASE STATE; (B) MODE 1 WITH EIGENVALUE OF 633.1 MPA, (C) MODE 3 WITH AN EIGENVALUE OF 1282.2 MPA.	38
FIGURE 4.7: STRESSES FROM NONLINEAR STATIC LARGE DEFORMATION BUCKLING ANALYSIS (A) TP-000274-OD12; (B) TP-000272; (C) TP-000274-OD15; (D) TP-000274-OD15-L350; (E) TP-000274-OD18; (F) TP-000273-OD12; (G) TP-000274 ..	43
FIGURE 4.8: TP-000274-OD15: STRESSES FROM APPLIED LOAD WITH ELASTIC-PLASTIC MATERIAL PROPERTIES.....	45
FIGURE 4.9: LOAD-DISPLACEMENT CURVES FOR NONLINEAR ELASTIC AND NONLINEAR ELASTIC-PLASTIC MATERIAL FOR TP-000274-OD15.	45
FIGURE 4.10: LOAD-DISPLACEMENT CURVES FOR NONLINEAR ELASTIC AND NONLINEAR ELASTIC-PLASTIC MATERIAL FOR (A) TP-000274-OD12; (B) TP-000272; (C) TP-000274-OD15-L350; (D) TP-000274-OD18; (E) TP-000273-OD12; (F) TP-000274 ..	46
FIGURE 4.11: DIFFERENT PLASTICITY PROPERTIES FOR TP-000274-OD15.	47
FIGURE 4.12: LPF-ARC LENGTH CURVES FOR TP-000274-OD15.....	48

FIGURE 4.13: FORCE-DISPLACEMENT CURVES COMPARING THE NONLINEAR STATIC RIKS BUCKLING ANALYSIS RESULTS FOR ALL THE MODELS.	49
FIGURE 4.14: TP-000274-OD15: STRESSES FROM APPLIED LOAD.	50
FIGURE 5.1: SURFACE PREPARATION OF STRAIN GAUGE (A) TEST SPECIMEN IN ALUMINUM CLAMPS; (B) CLEANED SURFACE.	52
FIGURE 5.2: NI CIRCUIT BOARD (A) NI 9237 WITH DSUB PIN ASSIGNMENTS; (B) QUARTER-BRIDGE CIRCUIT DIAGRAM; (C) THE CIRCUIT ON THE NI CIRCUIT BOARD; (D) NI 9923 37-PIN DSUB TO SCREW-TERMINAL CONNECTOR BLOCK CONNECTED TO STRAIN GAUGES (GREY CABLES) AND LOADCELL (COLORED CABLES)	53
FIGURE 5.3: TEST-SETUP IN INTERWELL'S PREMISES.	55
FIGURE 5.4: BTE CONNECTED TO THE LOAD CELL.....	55
FIGURE 5.5: INFLUENCE OF GEOMETRIC ATTRIBUTES; DIAMETER AND EFFECTIVE LENGTH: (A) FORCE-DIAMETER CURVE FOR L_e OF 344 MM (B) FORCE-EFFECTIVE LENGTH CURVE FOR OD12 AND OD20.	57
FIGURE 5.6: PICTURES FROM BUCKLING IN HP (A) TP-000272; (B) TP-000274-OD15.	59
FIGURE 5.7: RESULTS FROM TEST 1: LENGTH AND DIAMETER	59
FIGURE 5.8: RESULTS FROM TEST 1 WITH 5% ERROR BARS.	60
FIGURE 5.9: FORCE-TIME CURVES FOR TP-000274-OD15.....	60
FIGURE 5.10: STRESS-STRAIN CURVES FOR TP-000274-OD15.....	61
FIGURE 5.11. STRAIN-TIME CURVES VS FORCE-TIME CURVE FOR TP-000274-OD15	61
FIGURE 5.12: FORCE-TIME CURVES: (A) TP-000274-OD12; (C) TP-000272; (E) TP-000274-OD15-L350; (G) TP-000274-OD18; (I) TP-000273-OD12; (K) TP-000274. FORCE-DISPLACEMENT CURVES: (B) TP-000274-OD12; (D) TP-000272; (F) TP-000274-OD15-L350; (H) TP-000274-OD18; (J) TP-000273-OD12; (L) TP-000274.	63
FIGURE 5.13: THE BUCKLING SHAPES FOR THE TEST PARTS OF DIFFERENT GEOMETRY WITH THE INFLUENCE OF AN AXIAL LOAD (A) TP-000274-OD12; (B) TP-000272; (C) TP-000274-OD15; (D) TP-000274-OD15-L350; (E) TP-000274-OD18; (F) TP-000273-OD12; (G) TP-000274.	65
FIGURE 5.14: TEMPERATURE CALIBRATION: TIME-TEMPERATURE CURVES FOR T1 AND T2 SENSOR.	66
FIGURE 5.15: TEST SETUP FOR TEMPERATURE TESTS IN INTERWELL'S PREMISES.	67
FIGURE 5.16: TEST RESULTS FROM TEST 2 (A) TP-000274-OD15-T200 AFTER BUCKLING; (B) TP-000274-OD15-T150 TO THE LEFT AND TP-000274-OD15-T200 TO THE RIGHT	68
FIGURE 5.17: FORCE-TIME CURVES FOR TP-000274-OD15-T150, TP-000274-OD15-T200 AND TP-000274-4-OD15.....	69
FIGURE 5.18: FORCE-DISPLACEMENT CURVES FOR TP-000274-OD15-T150, TP-000274-OD15-T200 AND TP-000274-4-OD15	69
FIGURE 5.19: STRAIN-TIME CURVES FOR TP-000274-OD15-T150 AND TP-000274-OD15-T200.....	70
FIGURE 5.20: ASSEMBLY OF BUCKLING TEST EQUIPMENT FOR HSU	71
FIGURE 5.21: SHEAR SCREW WITH A REDUCER FITTING CONNECTED TO THE SEALING CAP	72
FIGURE 5.22: TEST SETUP FROM INTERWELL'S WORKSHOP (A) TEST PART IN 2.70"HSU; (B) 2.70" HSU TO THE LEFT AND TEST CASING TO THE RIGHT.....	72
FIGURE 5.23: PRESSURE-TIME CURVES FOR THE DIFFERENT TESTS IN THE 2.70" HSU	74
FIGURE 5.24: PRESSURE-TIME CURVES FOR THE STATIC COMPRESSION TEST IN 2.70" HSU.	74
FIGURE 5.25: BEFORE AND AFTER CRITICAL LOAD FOR BUCKLING TEST IN TEST CASING (A) TP-000274-OD15-T1; (B) TP-000274-OD15-T5; (C) TP-000274-OD15-T6	75
FIGURE 5.26: RESULTS AFTER STATIC COMPRESSION TEST IN HSU (A) TP-000274-OD15-T9; (B) TP-000274-OD15-T8 COMPARED WITH TP-000274-10-OD15.....	76
FIGURE 6.1: COMPARISON BETWEEN THE DIFFERENT CRITICAL FORCES OBTAINED VS THE SLENDERNESS RATIO FOR EACH TEST PART.....	79

FIGURE 6.2: PERCENTAGE DIFFERENCE BETWEEN THE EXPERIMENTS AND THE THEORETICAL ANALYSES.	80
FIGURE 6.3: BUCKLED TEST PARTS SORTED BY SLENDERNESS-RATIO FROM LEFT; LOWEST TO HIGHEST.	80
FIGURE 6.4: FORCE-DISPLACEMENT CURVES FOR THE DIFFERENT RESULTS OBTAINED FROM EXPERIMENTAL STUDY IN HP AND ABAQUS 6.12 TP-000274-OD15 FOR TP-000274-OD15.	81
FIGURE 6.5: FORCE-DISPLACEMENT CURVES FOR THE DIFFERENT RESULTS OBTAINED FROM EXPERIMENTAL STUDY IN HP AND ABAQUS 6.12 TP-000274-OD15 FOR (A) TP-000274-OD12; (B) TP-000272; (C) TP-000274-OD15-L350; (D) 000274-OD18; (E) TP-000273-OD12; (F) TP-000274.....	82
FIGURE 6.6: COMPARISON BETWEEN THE DIFFERENT TESTS; TEST 1= LENGTH AND DIAMETER, TEST 2 = TEMPERATURE, TEST 3 = WELL PRESSURE, FOR TP-000274-OD15.....	83
FIGURE 6.7: J.B. JOHNSON-EULER CURVE WITH THE EXPERIMENTAL AND ABAQUS ANALYSES RESULTS.....	84
FIGURE 6.8: J.B. JOHNSON-EULER CURVE WITH THE EXPERIMENTAL AND THE ANALYSIS RESULTS WITH TEST PARTS REPRESENTING THE SCATTER IN THE RESULTS.	85
FIGURE H.0.1: BEFORE AND AFTER UNIAXIAL TENSILE TEST (A) TT1; (B) TT2; (C) TT3; (D) TT4; (E) TT5; (F) TT6; (G) TT7	121

List of Abbreviations

BTE	Buckling Test Equipment
BTEHP	Buckling Test Equipment for Hydraulic Press
BTETC	Buckling Test Equipment for Test Casing
CAD	Computer Aided Design
CPU	Central Processing Unit
EP	Elastic-plastic
FE	Finite Element
FEA	finite element analysis
HP	Hydraulic Press
HSU	Hydrostatic Setting Unit
HT	Heat
LPF	Load Proportionality Factor
NI	National Instrument
NTNU	Norwegian University of Science and Technology
OD	Outer Diameter
UTS	Ultimate Tensile Strength
PEEQ	Equivalent Plastic Strain
QPQ	Quench Polish Quench

List of Nomenclatures

A	Cross-section area
A_0	Original cross-section area of the parallel length
A_f	Final cross-section area
A_s	area of shear screw
d_0	Initial diameter
E	Modulus of elasticity
E_T	Tangent modulus of elasticity
i	Radii of gyration
I_{\min}	smallest moment of inertia
K	strength constant
K^{MN}	tangent stiffness matrix
K_{Δ}^{MN}	geometric stiffness matrix
K_0^{MN}	material stiffness matrix
L_0	original gauge length
L_c	parallel length
L_e	Effective Length
L_f	final length
L_k	Buckling length
$\ln(\sigma_{\text{true}})$	logarithmic plastic strain
L_t	
n	strain-hardening coefficient
P	Axial compression load
P_0	dead load
P_{cr}	Critical buckling load
$P_{cr,25^\circ\text{C}}$	critical buckling load for 25°C
$P_{cr,T}$	critical buckling load for temperature tests
P_{ref}	load magnitude
R	transition radius
R_0	initial resistance
U_{\max}	Maximum displacement
v_i^M	Buckling mode shapes
v_m	nontrivial displacement solutions
z_0	eccentricity and amplitude of initial curve
γ_g	partial safety factor for Geometric
γ_{ls}	partial safety factor for Load and support
γ_{ms}	partial safety factor for Material strength
γ_p	partial safety factor for Well Pressure
γ_t	partial safety factor for Temperature
δ	deflection

δ_0	initial deflection
ΔA	change in cross-section area
ΔL	change in length
ϵ_{nom}	nominal stress
ϵ_{true}	true stress
η	imperfection parameter
λ	Slenderness ratio
$\bar{\lambda}$	reference slenderness
λ_i	Eigenvalues
λ_p	Minimum slenderness ratio
$\sigma_{0.2\%}$	Yield 0.2%
σ_{cr}	critical stress
σ_{max}	maximum stress
σ_r	residual stress
σ_{TS}	ultimate tensile stress
σ_y	yield stress
φ	capacity reduction factor
ϕ_D	diameter of shear screw
χ	reduction factor

CHAPTER 1

1 Introduction

1.1 Background and Motivation

Interwell is a Norwegian based oil service company which was founded in 1988 by recognizing the need for an independent supplier with focus on operation and maintenance of down-hole tool such as plugs, packers and straddles with associated running & pulling tools, and niche completion products and services. In many of Interwell's product lines, cylindrical rods and pipes are being exposed to axial compressive loads in both static and dynamic conditions. Several methods have been developed to determine the allowed buckling load for various geometries and constraints. Interwell suspects that these calculation methods are more conservative than needed for Interwell's equipment and industry. One of the main goals in any structural design is optimization of the different parameters involved. The Setting Chamber Mandrel is an essential part in the Hydrostatic Setting Unit (HSU), a setting device used for installation of Downhole Tools. The effect of geometric quantities and material properties of the Setting Chamber Mandrel can be determined using parametric studies. The Setting Chamber Mandrel has to resist compression caused by increasing well pressure while running in hole. The most severe load for the Setting Chamber Mandrel is during operation in maximum pressure conditions. In this situation the compression of the Setting Chamber mandrel is relaxed by applied axial tension, only to be restored in a very abrupt manner when breaking a weak point in the product to be set.

There are two primary categories leading to failure of a mechanical component; material failure and structural instability, which is often called buckling. The prominence of these failure modes depends on several factors including member slenderness, section slenderness, strength, influence of connections and restrains, as well as level of material and geometric imperfections and residual stresses. Due to the geometry of the Setting Chamber Mandrel and the design criteria of minimizing the compression margin, buckling is one of the most critical failure criteria. Safety issues coupled with the difficulty to predict buckling behavior makes it important to calculate the critical buckling load accurately. Buckling is defined as instability of equilibrium in members due to compressive action on the structural member or element involved. Instability is a state in which small perturbations can result in change in deformation mode or displacement value, causing the system to not return to its original equilibrium state. The term small is a relative term that indicates that the behavior remains in the immediate vicinity of the equilibrium state. In practice, buckling is characterized by a sudden failure of a structural member subjected to high compressive stress, where the actual compressive stress at the point of failure is less than the ultimate

compressive stresses that the material is capable of withstanding. There is a critical value of the load at which the current equilibrium state suddenly changes from stable to unstable and small perturbations result in large responses and sudden catastrophic damage to the material.

Buckling may be classified into two categories depending on material behavior [1]: (1) elastic buckling and (2) inelastic buckling. The members in this study have been characterized into three general types depending on their proneness to buckling; short, intermediate and long. Structural optimization is an important part of system optimization and is based on the assumption that certain parameters affecting the overall system are given (i.e. nonstructural weight, size and shape, performance ect.). Design of Down Hole Equipment is often based on strength and stiffness considerations. In this context strength is defined to be the ability to resist stress in the form of applied pressure, while stiffness is the resistance to deformation (i.e., the structure is sufficiently stiff not to deform beyond permissible limits). Nevertheless, a structure may become unstable before the maximum strength and stiffness criteria. The dividing lines between short, intermediate and long members are not accurately defined, but it is useful to make these distinctions because the maximum load-carrying capacity of a member in each category is based upon different mechanical failure scenarios. There is need for a simplified but reliable analysis method that can readily be used for quick and safe estimates of strength of specific Down Hole Equipment. This study defines critical stress and critical load and differentiates between short, intermediate and long members.

Strength analysis is often conducted using finite element (FE) analysis. In order to understand the buckling behavior of the Setting Chamber Mandrel, linear elastic eigenvalue buckling analysis and nonlinear static buckling analysis in Abaqus 6.12 were performed, as well as compression tests on test specimens with different geometric quantities. FE analysis of ultimate strength tends to be complex. The obtained results are compared with established theory [2]. Different values of geometric imperfections of the Setting Chamber Mandrel as well as different constraint conditions are investigated. The boundary conditions determine the mode of bending and the distance between inflection points on the deflected Setting Chamber Mandrel. This study will look at the different geometric parameters involved, the effect of the end condition of the Setting Chamber Mandrel, as well as the material properties on the compressive behavior and buckling. The design parameters and buckling modes will show different levels of imperfections related to empirical design factors for buckling loads establishing lower bounds to test data. This study aims to verify build in functionalities and constructional integrity of the Setting Chamber Mandrel, as well as give the preliminaries to establish an acceptable method of predicting the buckling load of a structural member due to axial compression.

1.2 Scope

This study includes all work necessary to provide a global safety factor and correlation factors for calculations and analyses of different types of Down Hole Equipment with similar geometrical shape and boundary conditions as the Setting Chamber Mandrel. Interwell is currently using NS 3472:2001 to calculate buckling of cylindrical parts [3]. NS 3472:2001 was replaced with NS-EN 1993-1-1:2005 in 2010. NS-EN 1993-1-1:2005 calibrates elastic critical buckling analysis and nonlinear analysis to experimental data to established practice as found in full-scale experiments. This study includes evaluation of existing literature and describes all required subsequent steps of the research, such as: research on the development of the different buckling theories, choice of appropriate methods and techniques to test the theoretical model and discussion of the contribution of the research to the current literature. This study analyze all available alternatives and recommend a design process to supplement the safe design of axially loaded members i.e. identifying critical parameters likely to influence the quality and performance of the Setting Chamber Mandrel.

General layout and instrumentation for the test-setup and references to existing facilities is described for the three different experimental studies; TEST 1: length and diameter, TEST 2: temperature and TEST 3: well pressure. FE – analyses and experimental studies of the simplified model of Setting Chamber Mandrel have been carried out to study buckling characteristics under uniform axial compression from well pressure. This study aims to verify build in functionalities and constructional integrity of the Setting Chamber Mandrel in the Hydrostatic Setting Unit, as well as give the preliminaries to establish an acceptable method of predicting the critical load of a structural member due to axial compression. Knowledge on how tool components exposed to buckling loads perform would provide; a safety of result in the design process, technical competitive edge, and a reassuring credibility towards customers in need of reliable answers.

Below follows a short overview of the programs used in this study:

- Microsoft Word 2010
- Microsoft Excel 2010
- Mathcad 15
- Solid Edge
- Abaqus 6.12
- LabVIEW SignalExpress
- catmanAP v3.4.2

1.2.2 Structure of Thesis

Chapter 1: Introduction	The introduction presents the general outline of this study.
Chapter 2: Preliminaries	This chapter will briefly outline some background information of the Hydrostatic Setting Unit and buckling analysis. The theoretical analyses discussed in this chapter are NS-EN 1993-1-1:2005, linear elastic eigenvalue buckling analysis and nonlinear static buckling analysis. The intermediate member chapter discusses some commonly used inelastic buckling theories that fill the gap between short and long members.
Chapter 3: Proof of concept	In order to demonstrate a full functionality and provide early feedback on the integrity and completeness of the test setup from the Specialization Project a validation and stability study on the test concept in NTNU premises was performed.
Chapter 4: Analysis	This study divides members into short, intermediate and long length, where Johnson's equation is valid for intermediate members and Euler's equation is valid for long members. Results from Euler and Johnson's equation are presented in this chapter as well as the Abaqus analyses. Four kinds of buckling analysis were conducted in Abaqus; a linear elastic eigenvalue buckling analysis, a nonlinear static large deformation buckling analysis (one with elastic material properties, and one with plasticity properties added to the material) and a nonlinear Riks buckling analysis.
Chapter 5: Experimental Studies	The object of the experimental studies was to study the real behavior of the test parts under axial compression load and make sure that the design of the Setting Chamber Mandrel will withstand the expected loading in well. The experimental studies are divided into three different test-setups; TEST1 = length and diameter, TEST2 = temperature and TEST 3 = well pressure
Chapter 6: Discussion	This chapter discusses buckling in the context of axially compressed members and identifies the parameters governing the buckling behavior comparing the analyses and experimental studies. Four kinds of buckling analysis were done in Abaqus; a linear elastic eigenvalue buckling analysis, a nonlinear static large deformation buckling analysis (one with elastic material properties, and one with

plasticity properties added to the material) and a nonlinear Riks buckling analysis. Results from Euler and J.B. Johnsons equations have also been compared with the experimental results in this chapter.

Chapter 7: Conclusion

This chapter presents the conclusion of this study by summarizing the results and discussion.

1.2.3 Limitations

The theory covered in this study has involved certain simplifying assumptions. The linear analysis contains the following key assumptions; linear elastic material behavior, small deflection theory (small deflections prior to buckling) and that the reference equilibrium position is the initial geometry of the model. Therefore, linear analysis does not account for geometric imperfections and permanent deformation and true material behavior is not represented. The models in Abaqus are limited to very simple, small geometric shapes because of the need for a high-density mesh at the cross-section. However, the analysis techniques outlined in this study can be used for any intermediate member that cannot fully rely on the assumptions and boundary conditions in Eulers linear buckling theory.

Due to the scope of this thesis only a limited number of cases have been investigated and the number of tests on each test part has been specified to two or three tests. Interwell's workshop is not a lab facility, and imperfections such as radial play between the parts in the hydraulic press and inaccurate calibration of instrumentation is expected to influence the results. Information about the test parts have been obtained from the machine drawings made in the Specialization Project. Compared to the anticipated geometric dimensions from the Specialization Project some of the test parts have new dimensions. Because of the new dimensions the tests are limited to TEST 1: length and dimension, TEST 2: temperature and TEST 3: well pressure. The parameter test with surface treatment hardening was therefore not conducted. Design considerations for altering of excising facilities are not included in this study.



CHAPTER 2

2 Preliminaries

This section will briefly outline some background information of the Hydrostatic Setting Unit and buckling analysis.

2.1 Hydrostatic Setting Unit

The Hydrostatic Setting Unit (HSU) is a setting device used for the installation of Downhole Tools such as Bridge Plugs, High Expansion Gauge Hangers, and Straddles. The hydrostatic pressure of the well fluid can be converted and utilized to supply the force necessary to perform the setting operations. The HSU has a Trigger Mechanism that prevents well fluid and pressure from entering the tool until being activated by an Electronics Cartridge. Once activated, an electric motor serves as an actuator for the Trigger Mechanism that in turn retracts a barrier valve pin allowing well fluid (pressure) to access the tool. The HSU converts the hydrostatic pressure into an axial force.

The different HSUs will operate in temperatures ranging from 0°C to 200°C and pressures up to 20,000 psi. The selected tool for this study, the 2.70" HSU 10" Stroke is rated for pressure up to 10,000 psi and 200°C. The maximum setting force depends on both size and in-situ well pressure. The allowed utilized setting force is limited to maximum of 37,000 lbf due to a designed 45,000 lbf weak point in the tool's lower connection [4].



Figure 2.1: 2.70" HSU 10" Stroke

2.1.1 Setting Chamber Mandrel

The Setting Chamber Mandrel is a component in the HSU, designed to apply tension to the setting kit and to resist the compression caused by well pressure, see Figure 2.2. The effective length of the Setting Chamber Mandrel is equal to the distance between the points where buckling induced moment is equal to zero. The notations for the cylindrical coordinate system is (ρ, ϕ, z) , which in this study represents the Cartesian (x, y, z) coordinates respectively. The upper end of the Setting Chamber Mandrel connected to the Hydraulic Housing is held from translating in the axial (z) direction and from rotating in the radial (x) and circumferential (y) directions. The opposite end connected to the Sealing Cap is held from rotating in the radial (x) and circumferential (y) directions. Materials with optimized properties for certain applications are more and more demanded in the industry. The minimum yield criterion is specified from the material certificate to 900 MPa, see Appendix A.

Table 2.1: Material specifications for 34CrNiMo6 steel.

Young's modulus, E [MPa]	Yield Stress, σ_{cr} [MPa]	Poisson's ratio, ν	Thermal Conductivity
2.05	900	0.290	0.016

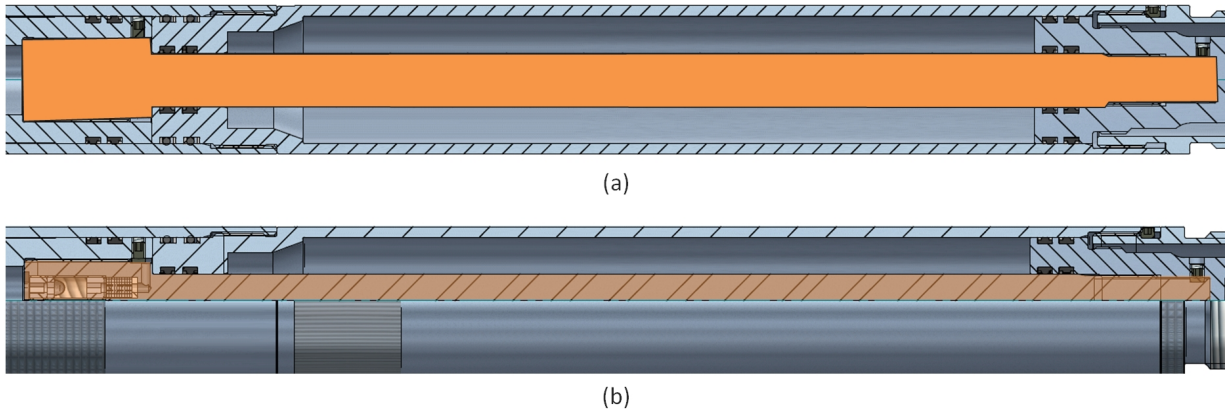


Figure 2.2: Setting Chamber Mandrel in 2.70" HSU 10" Stroke (a) shape of Setting Chamber Mandrel (b) quarter cut view

2.2 Buckling Analysis

In all analyses a specific definition of failure should be formulated. In this case the failure definition needs to correspond with the functional requirements of the Setting Chamber Mandrel. The term buckling and collapse are often used interchangeably in the literature. Buckling is defined as instability of equilibrium in members due to compressive action on the structural member or element involved, while collapse is a general failure of the entire cross-section by flattening due to external pressure. The distinction between types of members is not well defined, but a generally accepted classification of a member is short, intermediate or long. This classification depends not only on the effective length of the member, but also on its cross-section and material properties; this property is often called slenderness ratio. Slenderness

ratio, λ , is quantitatively expressed as the effective length of the member divided by its radius of gyration, i , and is used to determine elastic or inelastic mode of buckling failure.

$$\lambda = \frac{L_k}{\sqrt{I_{min}/A}} = \frac{L_k}{i} \quad (1)$$

The theoretical equations discussed in this study will hopefully give reasonable values for critical loads and critical stresses causing buckling. Buckling is a complicated phenomenon, and the buckling in any individual member may be influenced by imperfections such as; variations in straightness, misalignment in loading, unknown residual stresses and defects in the material. Traditionally, the ultimate strength of offshore structures and products are analyzed by linear methods to determine the resistances of cross-sections and internal distribution of forces and moments. The results are then checked according to design resistances found in design codes.

Interwell is currently using NS 3472:2001 to calculate buckling of cylindrical parts [3]. This method is calibrating elastic critical buckling analysis and nonlinear analysis to experimental data to established practice as found in full-scale experience. NS 3472:2001 has so far been a satisfactory method, but Interwell suspects that this method is more conservative than needed for Interwell's equipment and industry. In order to correctly decide the capacity of the Setting Chamber Mandrel residual stresses and imperfections have to be included, which cannot be done analytically. For this study, the theoretical analysis will consist of linear eigenvalue analysis with NS-EN 1993-1-1:2005: Design of steel structures [5], Euler and J.B. Johnsons equations, as well as FE-analyses; linear elastic eigenvalue buckling analysis and nonlinear static buckling analysis. Linear elastic eigenvalue buckling analysis and nonlinear static buckling analysis will be performed using Abaqus 6.12, a general-purpose finite element program with linear static, dynamic and nonlinear analysis capabilities. Unless otherwise is stated the preceding discussions of elastic and inelastic buckling are based upon idealized members.

2.2.1 Linear Elastic Eigenvalue Buckling Analysis

The elastic buckling strength of a structural member has been studied extensively in the past [1] - [3], [10] - [12] and the load at which linear eigenvalue buckling occurs is important because it provides the basis for commonly used buckling equations used in designed codes. Linear eigenvalue buckling is the most elementary form of buckling, and its study is an essential step towards understanding the buckling behavior of more complex structures; structures combining initial imperfection, residual stresses and inelastic behavior.

The behavior of an ideal column is represented by Eulers curve, which is shown in Figure 2.3 for 34CrNiMo6. The critical stress developed in a long member depends inversely on the square of the slenderness ratio and can at buckling be expressed as:

$$\sigma_{cr} = \frac{P_{cr}}{A} = \frac{\pi^2 E (Ar^2)}{AL^2} = \frac{\pi^2 E}{(L_k/r)^2} \quad (2)$$

The buckling load predicted by linear elastic buckling equation without imperfections was published by Euler [2] in 1744, and applies to a simply supported member of constant cross-section and a length L . The Euler equation for critical load (equation (3)) is for elastic buckling and is only valid when the material everywhere in the cross-section is in the elastic region, i.e. the axial compressive critical stress remains below the proportional limit. The proportional limit of a material is defined as the highest unit stress for which the strain is proportional to the stress. Furthermore, the elastic limit of a material is the highest unit stress to which the material may be imposed to before onset of permanent deformation. If the material goes inelastic the Euler equation becomes useless and the slope of the stress-strain curve for the material is less than the modulus of elasticity; hence the critical load of inelastic buckling will always be less than the load obtained from Eulers equation. The equation can also be used when the member is not simply supported, the only change being the addition of a suitably altered value of the buckling length L_k , whose value depends on the effective length and boundary conditions of the member. It is clear that the buckling load in Eulers equation is dependent only on the geometry (cross-section and length) and the stiffness represented by the modulus of elasticity, and not by the strength of material.

$$P_{cr} = \frac{\pi^2 EI}{L_k^2} \quad (3)$$

The minimum slenderness ratio, λ_p , ensuring that Euler's equation is valid is found by substituting the proportional limit for the critical stress.

$$\lambda_p = \pi \sqrt{\frac{E}{\sigma_y}} \quad (4)$$

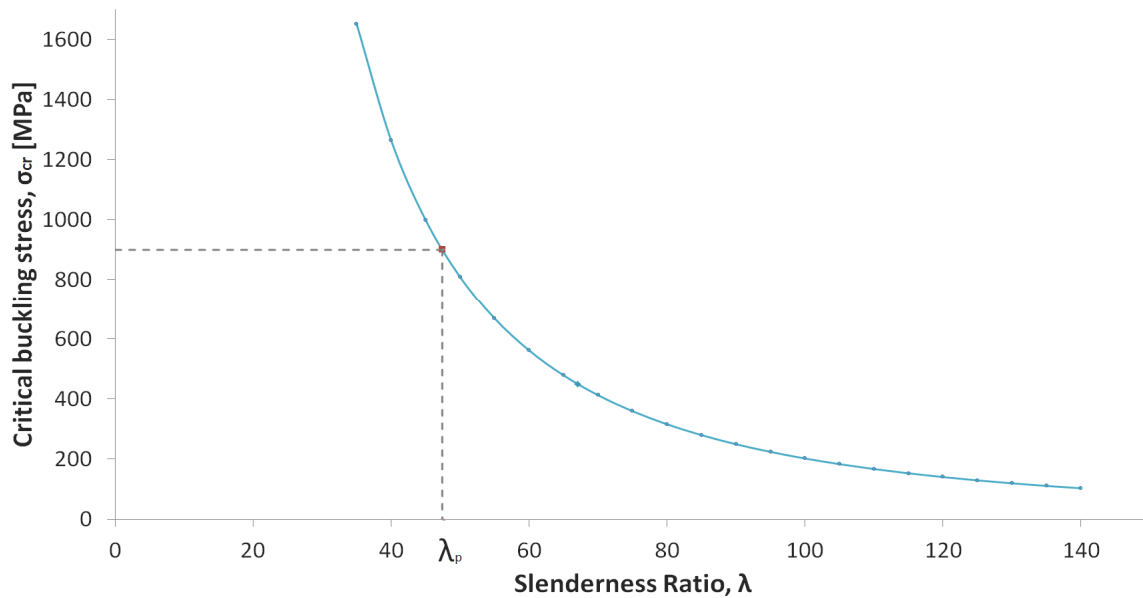


Figure 2.3: Euler curve

2.2.1.1 Linear Elastic Eigenvalue Buckling Analysis in ABAQUS

Linear eigenvalue buckling analysis in Abaqus is based on linear perturbation, and predicts the buckling strength (the bifurcation point) of an ideal linear elastic member. In a linear elastic eigenvalue buckling analysis we search for the loads for which the model stiffness matrix becomes singular, so that the equation;

$$\mathbf{K}^{MN}\mathbf{v}^M = \mathbf{0} \quad (5)$$

has nontrivial solutions. \mathbf{K}^{MN} is the tangent stiffness matrix when the loads are applied, while \mathbf{v}^M are nontrivial displacement solutions. M and N in equation (5) refer to the degrees of freedom [6]. The eigenvalue problem yields the first load level where a system becomes unstable and is derived by splitting the tangent stiffness matrix to find a solution to equation (5). The tangent stiffness matrix consists of two parts, the material stiffness matrix, \mathbf{K}_0^{NM} , which is related to the deformational stiffness of the components, and the geometric stiffness matrix, \mathbf{K}_Δ^{NM} , which is related to the component forces. In equation (6) λ_i are the eigenvalue and v_i^M are the buckling mode shapes.


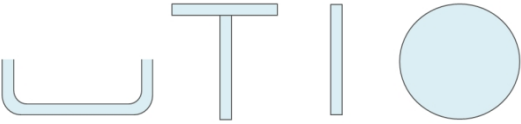
$$(\mathbf{K}_0^{NM} + \lambda_i\mathbf{K}_\Delta^{NM})v_i^M = 0 \quad (6)$$

However, nonlinearities and imperfections tend to prevent most members from achieving their theoretical elastic buckling strength. Thus, linear elastic eigenvalue analysis often yields excessive results and eigenvalue buckling load factors are therefore somewhat overestimated. A nonlinear static analysis including imperfections and elastic-plastic material properties can be done to get a more accurate result.

2.2.2 NS-EN 1993-1-1:2005

All engineering methods need to be calibrated against an empirical basis in the form of full scale tests or laboratory experiments. NS-EN 1993-1-1:2005 is grouping the different profiles based on cross-sectional area, validity, residual stresses and flange thickness [5]. The buckling resistance of a member is determined by applying a reduction factor χ to the yield strength. The reduction factor χ is a function of the non-dimensional slenderness and depending on the buckling mode. The five buckling curves presented in Figure 2.4 were found using experimental and simulated data, including cross-section area, geometric imperfections and residual stresses due to rolling or welding. In this case, the cross-section is solid and buckling can take place about any axis, which implies that the choice of curve for this problem should be c [7].

Table 2.2: Selection of flexural buckling curve for a cross-section [5].

Cross-section	Validity	Buckling about axis	Reduction curve	
			S 235 S 275 S 355 S 420	S 460
Hollow sections 	Hot finished	any	a	a ₀
	Cold formed		c	c
U-, T- and solid sections 			c	c

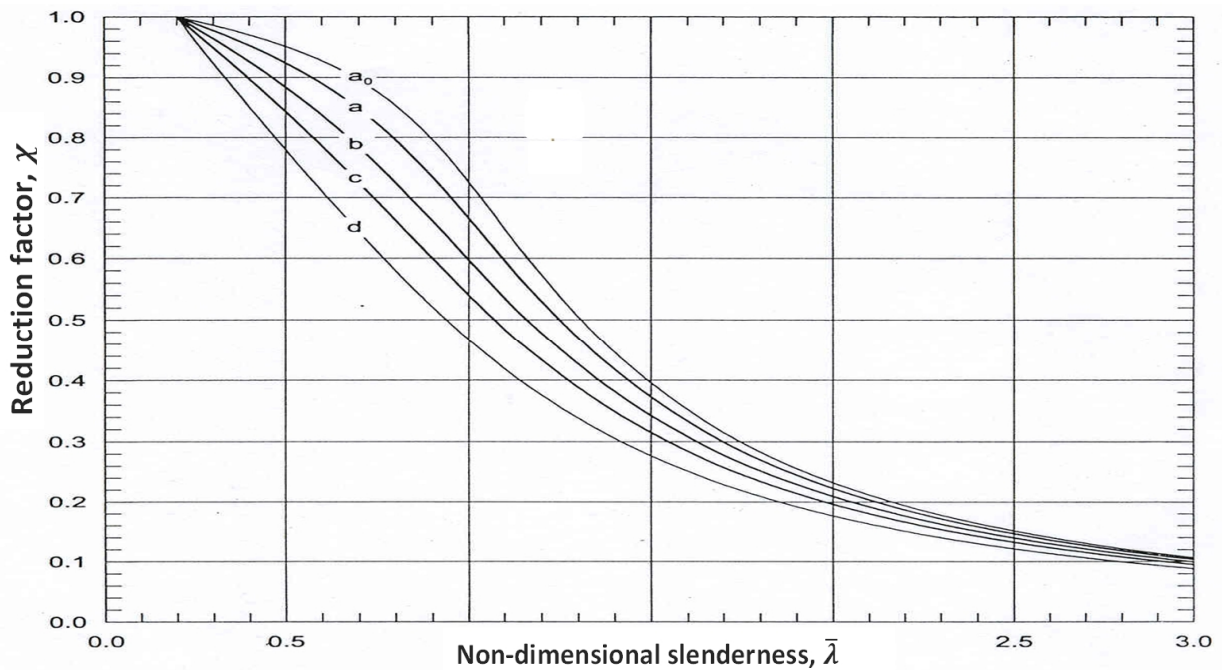


Figure 2.4: Buckling curves for non-dimensional slenderness [5].

2.2.2.1 Imperfection: Initial curvature

In reality, columns are generally not perfectly straight, and the effect of out of straightness on column strength is studied in this section. This section will hopefully help determine the value of applied axial load, which causes the largest stress in the member to reach the yield stress, σ_y . The axially compressive load gives the highest stress location on the inside of the member where the deflection is greatest. This is the point where yield first will be reached as the load is increased. Assuming a pin-ended column with initial curvature bent in a half sine wave, as shown in Figure 2.5, the initial deflection at x from A is z_0 and the struts deflects $z = \sin(\pi x/L)$ further under the axial compression load P . The equilibrium equation for this situation is given by:

$$EI_z \frac{d^2 z}{dx^2} + P(z + z_0) = 0 \quad (7)$$

Combining the above differential equation with $z = \sin(\pi x/L)$, and considering the boundary conditions, it can be shown that the initial deflection δ_0 at the center of the member and the deflection δ caused by the compression load can be written as follows:

$$\delta = \delta_0 \left[\frac{(P/P_{cr})}{1 - (P/P_{cr})} \right] \quad (8)$$

For which the earlier elastic analysis is valid, the maximum stresses at the center of the member is given by:

$$\sigma_{max} = \frac{P}{A} + \frac{P(\delta_0 - \delta) \times (L_e/2)}{I} \quad (9)$$

Recalling the maximum deflection from the above equation (8) and solving for the value for which the mean axial stress causes yield stress (at the maximum deflection point) gives the Perry Robertson Equation [8];

$$\sigma = \frac{\sigma_y + (1 + \eta)\sigma_{cr}}{2} - \sqrt{\left(\frac{\sigma_y + (1 + \eta)\sigma_{cr}}{2}\right)^2 - \sigma_y \sigma_{cr}} \quad (10)$$

where η is the imperfection parameter given by $\eta = [\delta_0(L_e/2)]/r^2$. The Euler buckling curves in NS-EN 1993-1-1:2005 uses the Perry Robertson equation (10) for the mean axial stress to cause failure with different values of imperfection factors. The dimensionless reduction factor can be written as;

$$\chi = \frac{1}{\phi + \sqrt{\phi^2 - \bar{\lambda}^2}} \quad (11)$$

in which the capacity reduction factor, ϕ , is a knockdown factor for nominal strength of compression members, and $\bar{\lambda}$ is the reference slenderness given in equation (12). For curve c in NS EN-1993-1-1:2005 $\eta = \alpha(\bar{\lambda} - 0.2)$, where α is an imperfection factor with a value of 0.49, and the constant 0.2 is a Robertson value depending on the cross-section of the member.

$$\phi = \frac{1 + \eta + \bar{\lambda}^2}{2}, \quad \bar{\lambda} = \sqrt{\sigma_y / \sigma_{cr}} \quad (12)$$

From these equations the data to obtain curve c from NS-EN 1993-1-1:2005 were implemented in Microsoft Excel 2010, see Figure 2.6.

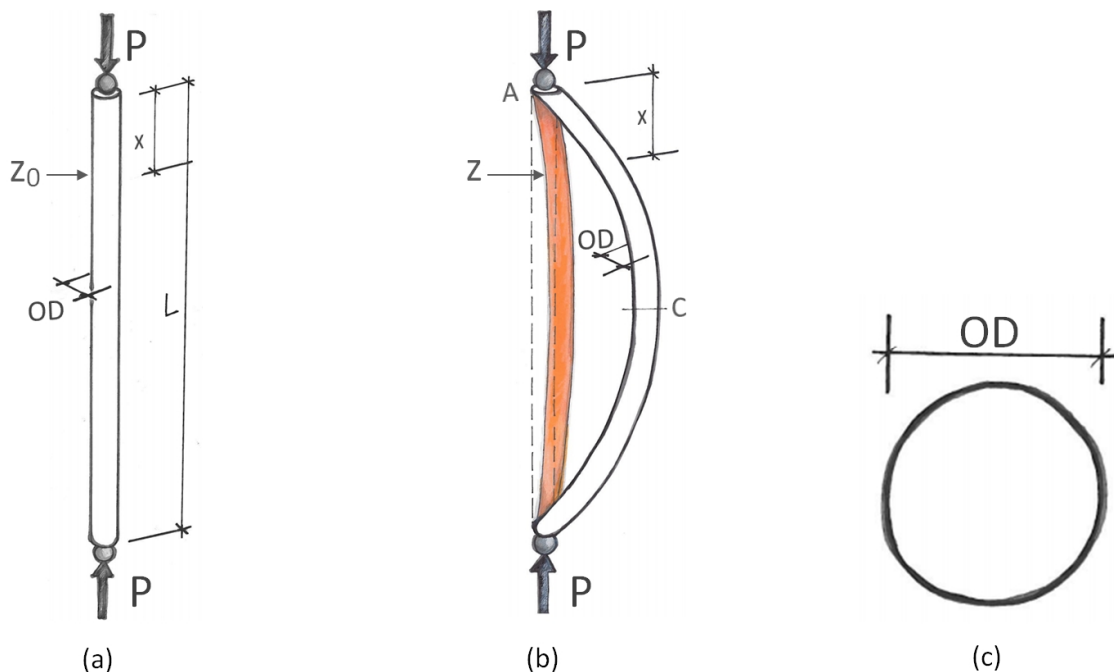


Figure 2.5: Load case (a) initially straight column with Euler load; (b) members with initial curvature and deflection; (c) column cross-section

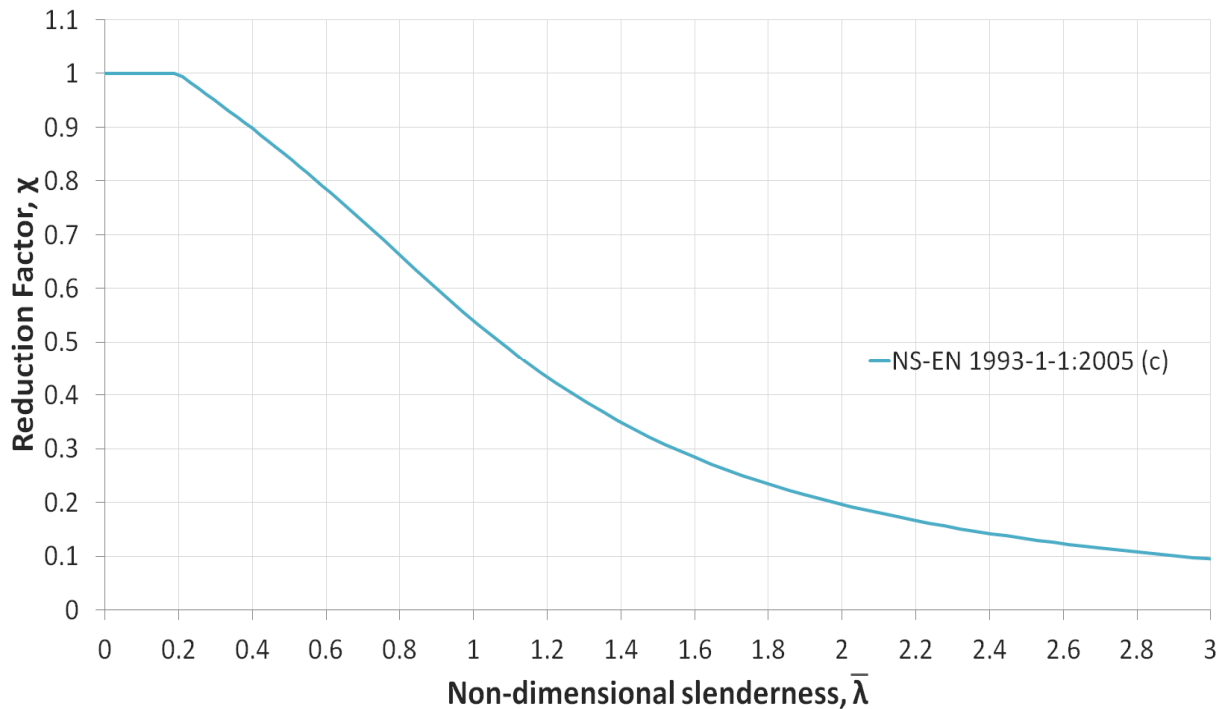


Figure 2.6: Buckling curve c obtained from literature study implemented in Microsoft Excel 2010.

2.2.3 Nonlinear Static Buckling Analysis

The design resistance formulas from design codes often require deformations well into the inelastic range before collecting code-defined resistances. In case of variable loading or cyclic loading additional checks of accumulated plastic deformations and repeated yielding will be needed. Steel members loaded to their limit behave more or less nonlinear. Nonlinear effects that may be included in the analyses are geometrical and material nonlinearity. Nonlinear static buckling analysis is usually more accurate than eigenvalue buckling analysis and is therefore recommended for design and evaluation of members.

The nonlinear large displacement method increases the load in steps, solving for displacement. The stiffness matrix in the nonlinear static analysis is updated periodically based on the current deformed shape of the member. The increment size is established based on the nonlinear analysis technique used. The load is increased until instability occurs and the stiffness of the member approaches zero. A nonlinear static analysis has the ability to estimate the response of the member at a specific load level and detect at what load the instability occurs.

2.2.4 Riks analysis

For imperfection-sensitive members it would probably be more realistic to perform a Riks analysis in Abaqus. The Riks method is typically used to predict geometrically unstable nonlinear buckling of a member by using the load magnitude as an additional unknown. This method takes the modified Newton method and requires it to converge along an arc so that it follows the post-buckling nonlinear load-

displacement curve. The arc length is a measure of deformation in Abaqus used to evaluate the progress of the solution and to give an estimate of how much the total deformation have varied throughout the analysis. The size of the fixed increments is limited by moving a given distance along an arc to the current solution point before searching for equilibrium in the orthogonal plane that passes through the point. The minimum and maximum arc length increments can be used to control the automatic incrementation in the analysis. The load magnitudes are governed by a single scalar parameter. Constantly incrementing the applied loads prevents unrealistic divergence in the analyses. The only requirement for the basic Riks algorithm is that the system must be continuous or reasonably smooth. The actual load in the Riks analysis is given by;

$$P = P_0 + \lambda(P_{ref} - P_0) \quad (13)$$

where P_0 is the “dead load” at the end of the previous step, λ is the load proportionality factor, and P_{ref} is the load magnitude prescribed in the current step [9]. The value of the applied load is irrelevant in this analysis because the load will be increased until collapse occurs, even if the load exceeds the applied load. The key output from this analysis, which is always given as standard, is the load proportionality factor and displacements. The actual values of load magnitudes are computed as the load proportionality factor, LPF. The load proportionality factor is printed out by Abaqus/Standard at each increment.

2.2.5 Dynamic Buckling Analysis

Several approaches are possible for modeling nonlinear static problems of members that involve collapse or buckling behavior. One analysis method is to treat the buckling response dynamically, thus modeling the response with inertia effects included as the structure snaps. Such an analysis is essential for performing proper evaluation of post-buckling behavior of compression members. Utilizing the dynamic buckling analysis is an efficient way to find the ultimate strength in the final stage of deformed members, as well as evaluating the effect due to initial imperfections. However, for this challenge there are no requirements to clarify the post-buckling behavior, i.e. the behavior of the member exhibited after passing through the critical load, and dynamic buckling analysis will therefore not be conducted in this study.

2.3 Intermediate members

This section discusses some commonly used inelastic buckling theories that fill the gap between short and long members. Consequently, the mathematics of intermediate members is based on empirical tests of actual members, as well as interpolation between expressions relating to short and long members. There are a number of empirical design equations for buckling in the intermediate length range, all of which embody the slenderness ratio. This section will focus on three of the most common theory that describes the intermediate member response; Engesser’s tangent modulus approach, J.B. Johnson equation and Shanley’s theory.

Engesser's tangent modulus approach replaces the elastic modulus of elasticity with the tangent modulus of elasticity, $E_T = d\sigma/d\epsilon$. The tangent modulus is the tangent line of the stress-strain curve at a particular value of strain once the stress on the concave side of the axially loaded compression member exceeds the proportional limit. As a result, the tangent modulus theory tends to underestimate the strength of the member, since the convex side of the member is still below the elastic limit of the material. In reality, the tangent modulus depends on stress, which is defined as a function of bending moment that varies with the displacement of the member, δ [10].

$$P_{cr,T} = \frac{\pi^2 E_T I}{L_k^2}, \text{ or } \sigma_{cr} = \frac{\pi^2 E_T}{(L_k/r)^2} \quad (14)$$

For members with intermediate length account must be taken of possible interaction between yielding and buckling. The critical load in J.B. Johnson equation (15) is affected by the strength of the material in addition to its stiffness, E , and geometry. The J.B. Johnson equation is the equation of a parabola that has its vertex at the value of the yield stress on the y-axis and tangent the Euler curve at half the yield stress [11]. For this particular case, the tangent point between the Euler curve and the J.B. Johnson's parabola, λ_0 value is 67.1, and the minimum slenderness ratio is 47.5. In Figure 2.7 below, we have a 34CrNiMo6 steel member with a yield stress of 900 MPa.

$$P_{cr} = \sigma_y A \left[1 - \left(\frac{\sigma_y}{4\pi^2 E} \right) \cdot \left(\frac{L_k}{r} \right)^2 \right] \quad (15)$$

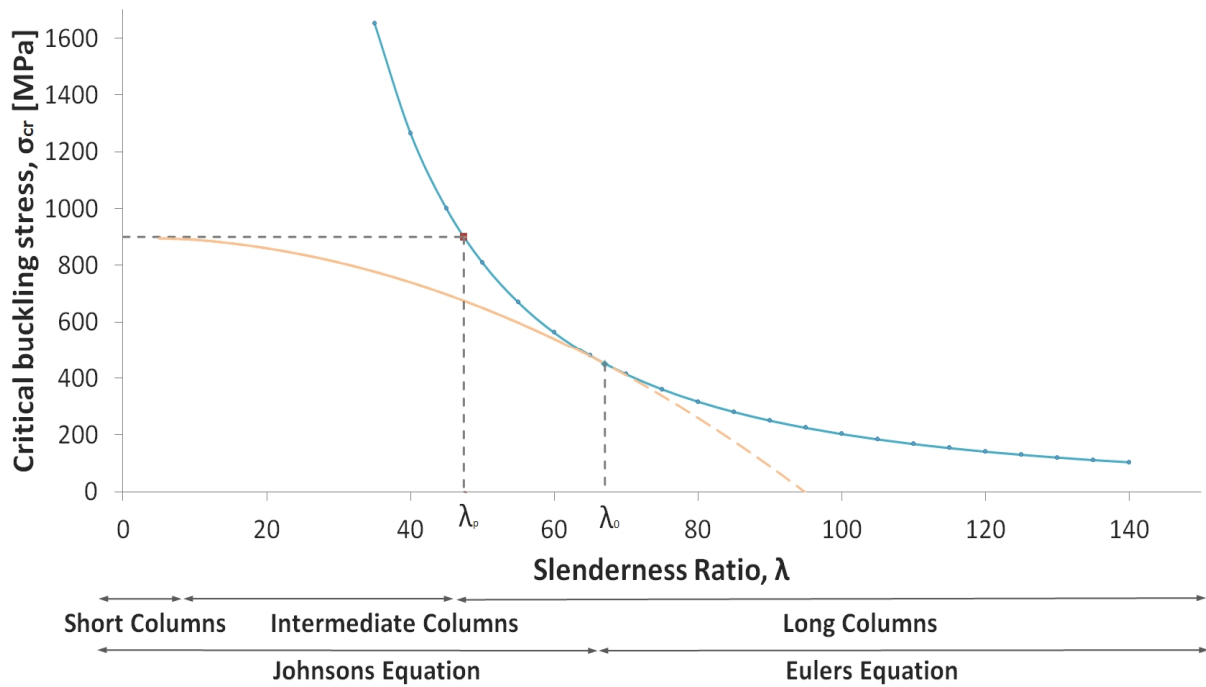


Figure 2.7: Average compressive critical buckling stress versus the slenderness ratio for 34CrNiMo6 steel.

Shanleys theory replaces the tangent modulus with a reduced modulus and assumes that the true deformation mechanism of a compression member will be between two extreme conditions corresponding to the tangent modulus theory and the upper-bound reduced modulus theory. The critical load of inelastic buckling is then a function of the transverse deflection, δ . [12] However, when imperfections such as manufacturing defects and geometric inaccuracies are taken into account, the difference between Shanleys theory and Engessers theory is not significant enough to justify a much more complicated equation in practical applications.

CHAPTER 3

3 Proof of Concept

In order to demonstrate full functionality of the test setup a validation and stability study on the test concept in NTNU premises with an INSTRON (model 1342) universal testing machine was performed. The Hydraulic Press consists of a basic frame, guide columns and a load cross bar. The height of the load cross bar can be adjusted along the guide columns and allows specimens with different buckling lengths to be examined. The Hydraulic Press used is a high rigidity machine that uses a hydraulic cylinder to generate a compressive force up to 100 kN. The purpose of this study was to establish, based on the information on the HSU a scenario where buckling of the Setting Chamber Mandrel models could be tested. This analysis includes the software model and the physical environmental aspects of the system. Analysis results from this study have provided early feedback on the integrity and completeness of the system and can be used to define expected behavior of the specimens for further design refinement.

3.1 Test Setup

The test specimen was loaded with a rate of 1 mm/min. The specimen was mounted by parallel jaw faces, and the strain gauges were connected to the National Instrument sensor measurement system. NI offers modules to use interchangeably in NI CompactDAQ for measurements including strain and voltage modules. Furthermore NI CompactDAQ chassis is shipped with NI LabVIEW SignalExpress LE software. NI LabVIEW data-logging software is a highly productive graphical platform for problem solving that combines easy-to-use graphical development with the flexibility of a powerful programming language. This system design software is providing an ideal measurement and control system for this type of study and will also be used in the experimental study. The final test setup is shown in Figure 3.1.

Table 3.1: Material specification for test specimen in proof of concept analysis.

Material	L_e [mm]	OD [mm]	λ	Young's modulus, E [MPa]	Poisson's ratio, ν
Stainless steel	590.0	15.0	78.67	2.10	0.3

3.1.1 Strain Gauges

Strain can be defined as the measurement of deformation in a material produced by stress. The increase in the original length of the specimen at any moment during test is defined as the percentage elongation. Stress is measured as a force applied over a given cross-sectional area of an element and has the same units as pressure; N/mm^2 . Strain gauges will measure the deformation in units of distance deformed by unit of distance placed under strain. The total displacement of the specimen can be determined by knowing the length of the specimen placed under strain. The length of the wire in the strain gauges and the electrical resistance increases when the specimen is exposed to axial compression. As electrical current flows through the coil of a conductor, the electrical resistance and can be readily measured. The change in resistance is given by [13]:

$$\Delta R \cong 2R_0 \frac{\Delta L}{L_0} \quad (16)$$

This concept analysis will measure applied force and strain from three strain gauges. The strain gauges are attached to the specimen and spaced at 120 degrees to represent the x-, y- and z-plane with CN adhesive cyanoacrylate. Location of the strain gauges on the surface of the test part is shown in Figure 3.1. The orange color applied on the test specimen in this figure represents the effective buckling length, and the maximum deflection is expected to be at the mid-point of the specimen. When the specimen is deflected the upper half and the lower half should be reasonably identical and symmetric about the mid-point. The strain gauges used in this study is FLA-5-11-1L from Tokyo Sokki Kenkyujo Co [14].

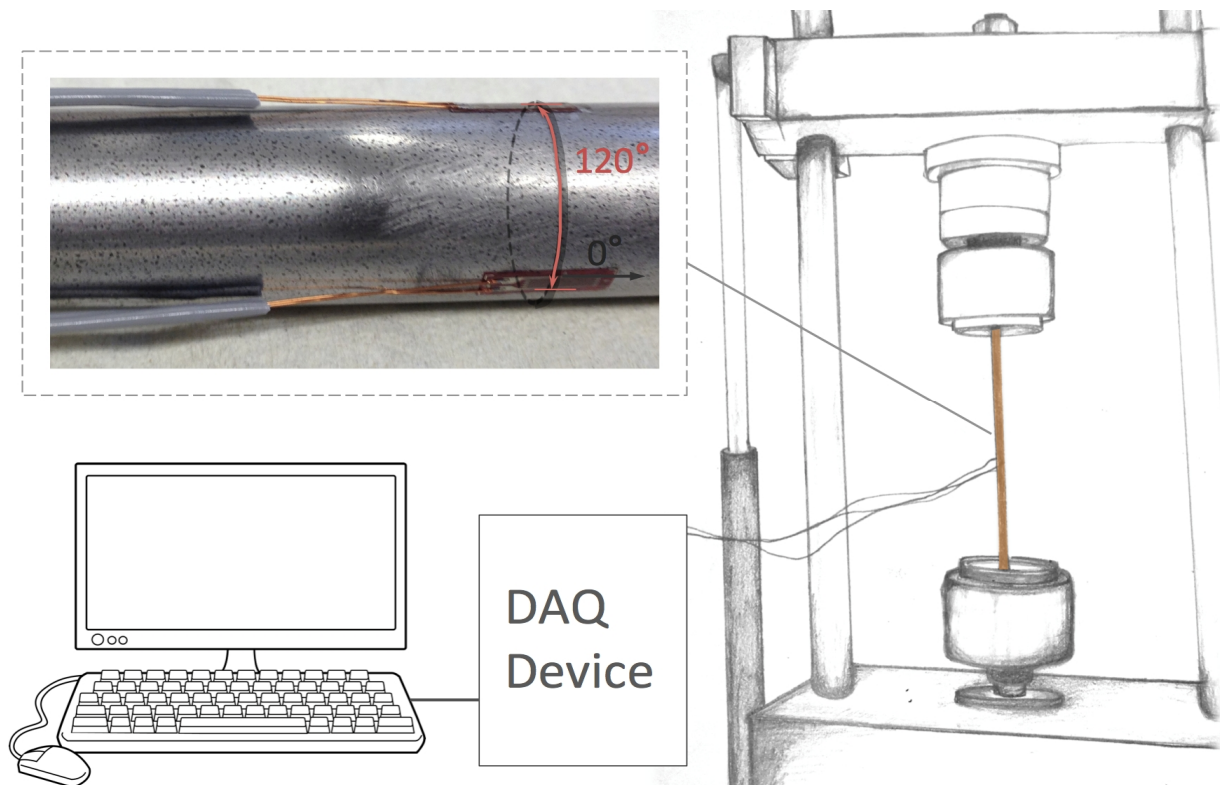


Figure 3.1: Final test set up with strain gauge positions

3.2 Test Parts

The slenderness of the Setting Chamber Mandrel is estimated to be about 27. From calculations done in the Specialization Project [15] the reference test part should be in 34CrNiMo6 steel, and have an effective length of 344 mm and an OD of 20 mm. Consequently it has been difficult to say that there is an exact theory of inelastic buckling, and in order to get the test specimens closer to the minimum slenderness ratio of 47.5 some of them have new dimensions compared to the anticipated geometric dimensions from the Specialization Project, as seen in Figure 3.2. The specimens were designed by conventional criteria with regard to the production method of the specimens and the equipment designed for using them in experimental studies, Buckling Test Equipment (BTE). The new reference test part has the same effective length of 344 mm, but a new OD of 15 mm, see Figure 3.3. An overview over the different test specimen for FE-analyses and experimental testing is to be found in Table 3.2. All test parts with the same diameter should be from the same material batch.

The naming of the members is of the form TP-000274-0-ODX, where TP stands for Test Part and 000274 is the parent member identification number for Interwell. The number 0 stands for the test numbering, and the last suffix ODX or LX is added on the specimens with new dimensions. Hence all members with the same heat number were cut from the same steel rod. The material certificate is to be found in Appendix A.

Table 3.2: Overview over the test specimens. The curve shows the reduction factor χ vs the non-dimensional slenderness λ .

Part Number	L_e [mm]	OD [mm]	λ	The reduction factor χ vs the non-dimensional slenderness λ w/the test specimens
TP-000274-OD12	344	12	57.3	
TP-000272	476	20	47.6	
Minimum slenderness ratio, $\lambda_p = 47.5$				
TP-000274-OD15	344	15	45.8	
TP-000274-OD15-L350	296	15	39.5	
TP-000274-OD18	344	18	38.2	
TP-000273-OD12	216	12	36.0	
TP-000274	344	20	34.4	



Figure 3.2: Test parts from Specialization Project with old dimensions.

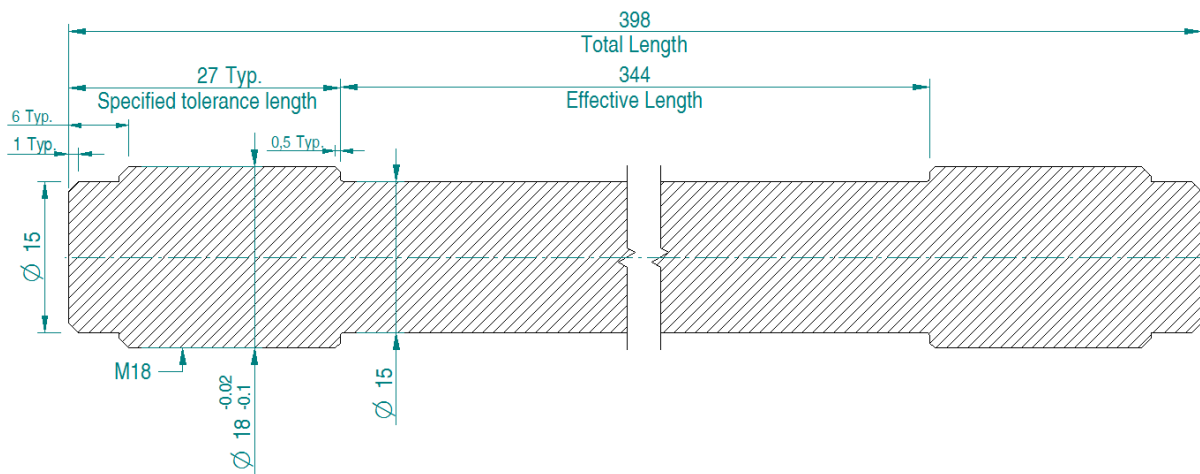


Figure 3.3: Reference test part TP-000274-OD15.

3.2.1 Uniaxial Tensile Testing of 34CrNiMo6 steel

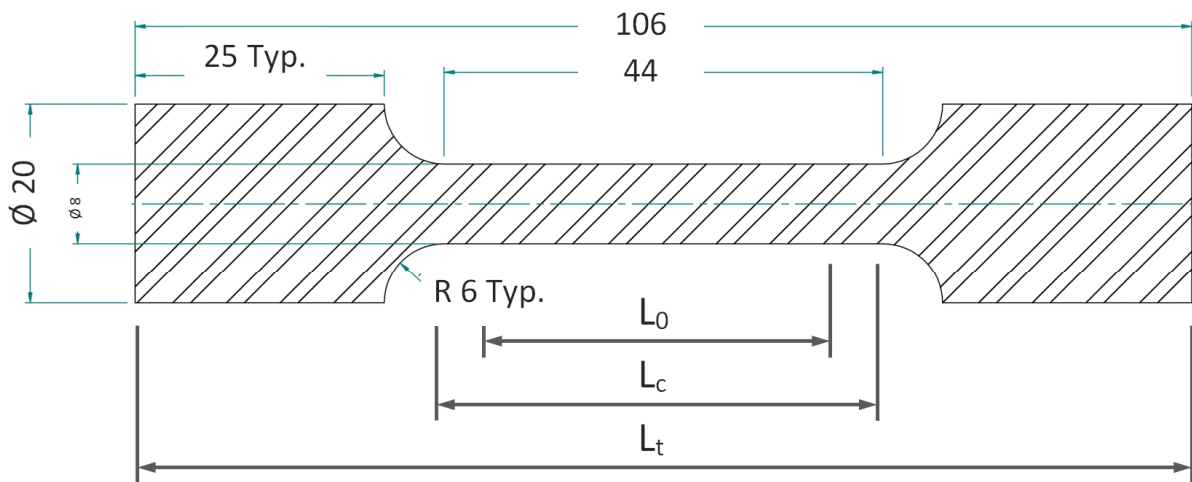
Uniaxial tensile test is a basic and universal engineering test to achieve material parameters such as ultimate strength, yield strength, elongation and percentage area of reduction. The behavior of members in compression and tension depends on the material properties, and this test will establish the behavior and compare it with the manufactures specifications. This test was performed to evaluate and compare existing material data from the Setting Chamber Mandrel with the material data obtained from this test. The tensile testing is carried out by applying axial load at a specific extension rate of 0.66 mm/min to a standard tensile specimen designed from NS-EN ISO 6892-1 until failure occurs. NS-EN ISO 6892-1 specifies the method for tensile testing of metallic materials and defines the mechanical properties, which can be determined at room temperature [16]. The strain rate is calculated with a range 2 and a relative tolerance of $\pm 20\%$. The specimens have a direct relationship between the original gauge length, L_0 , and the original cross-sectional area of the parallel length, A_0 , expressed by the relation;

$$L_0 = k\sqrt{A_0} \quad (17)$$

where k is the coefficient of proportionality with a value of 5.65. In Table 3.3 the parallel length L_c is given by $L_c = L_0 + (d_0/2)$ and the transition radius R is equal to; $R = 0.75d_0$. The relevant dimensions of the specimens have been measured at sufficient cross-sections perpendicular to the longitudinal axis in the central region of the parallel length of the tensile test specimen; see Table 3.3 and Figure 3.4. The specimens have been prepared in accordance to ISO 377.

Table 3.3: Design of the uniaxial tensile test specimens of 34CrNiMo6 steel from EN ISO 6892-1.

σ [MPa]	d_0 [mm]	A_0 [mm ²]	P [kN]	k	L_0 [mm]	L_c [mm]	R [mm]
1300	8.0	50.3	65.3	5.65	40.0	44.0	6.0



(a)

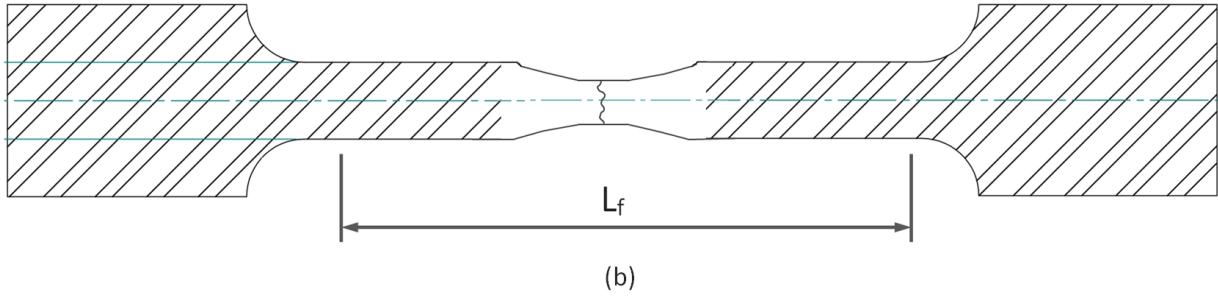


Figure 3.4: Machined test piece of round cross-sections (a) before testing; (b) after testing.

In order to minimize bending of the specimen the axis was coincided with the axis of application of the force. The force-measurement system was not changed after the force zero point was set to ensure alignment of the specimen and the grip arrangement. The specimen was gripped by parallel jaw faces. For data acquisition and visualization of the tensile tests software catmanAP v3.4.2 was used and connected to the hydraulic press and loadcell. The applied tensile load and extensions are recorded during the test for the calculation of the materials tensile strength, yield strength, elongation and area of reduction.

Table 3.4: Information about uniaxial tensile testing

Specimen	Material	Sample rate	Testing Rate
TT	34CrNiMo6 steel	100 Hz	0.66mm/min

3.2.1.1 Results

34CrNiMo6 steel does not show a definite yield point, but a smooth engineering stress-strain curve as shown in Figure 3.5. The yield strength at 0.2 % offset is determined by finding the intersection of the stress-strain curve with a line parallel to the elastic initial slope of the curve which intercepts the stress-strain curve at 0.2 %, see Figure 3.6b. The ultimate tensile strength is the maximum point (UTS, σ_{TS}) of the stress-strain curve. The maximum load is the highest force that the test piece withstands during test after the beginning of workhardening. The results from uniaxial tensile testing are presented in Table 3.5 and Figure 3.5 - Figure 3.7. The material certificate shows about 20 % lower results for $\sigma_{0.2\%}$ and UTS than the results obtained from the uniaxial tensile tests, see Table 3.6.

$$\sigma_{0.2\%y} = \frac{P_{0.2\%}}{A_0} \quad (18)$$

$$\% \varepsilon = \frac{L_f - L_o}{L_o} \times 100 = \frac{\Delta L}{L_o} \times 100 \quad (19)$$

$$\% RA = \frac{A_f - A_o}{A_o} \times 100 = \frac{\Delta A}{A_o} \times 100 \quad (20)$$

Table 3.5: Test results from uniaxial tensile testing.

Details	TT1	TT2	TT3	TT4	TT5	TT6	TT7
Heat	HT:170807	HT:170807	HT:170807	HT:170807	HT:168232	HT:168232	HT:168232
Maximum Load	53.2 kN	53.4 kN	53.4 kN	53.2 kN	60.8 kN	62.2 kN	61.9 kN
Elongation	7.92 mm	7.99 mm	7.29 mm	7.678 mm	7.47 mm	7.40 mm	7.24 mm
Final length, L_f	51.94 mm	51.99 mm	51.29 mm	51.68 mm	51.47 mm	51.40 mm	51.24 mm
Yield 0.2%	1273 MPa	1271 MPa	1269 MPa	1272 MPa	1405 MPa	1480 MPa	1484 MPa
UTS	1381.8 MPa	1388.7 MPa	1387.5 MPa	1381.6 MPa	1581.6 MPa	1616.2 MPa	1609 MPa
Fracture strain	915 MPa	878 MPa	915 MPa	895 MPa	915 MPa	1009 MPa	1006 MPa
% Elongation	18.1 %	18.2 %	16.6 %	17.5 %	16.9%	16.8%	16.5%
% Reduction of area	36.3 %	37.5 %	35.0 %	36.3 %	33.8 %	36.3 %	33.8 %

Table 3.6: Comparison between the mean uniaxial tensile test results and the mechanical properties from the material certificates (Appendix A).

Heat	Yield 0.2 % [MPa]	UTS [MPa]	% Elongation	% Reduction of area
MS: HT: 170807	1004	1107	15.0 %	56.5 %
HT: 170807	1271	1385	17.6 %	36.3 %
MS: HT: 168232	1093	1182	14.9 %	60.4 %
HT: 168232	1456	1602	16.9 %	33.8 %

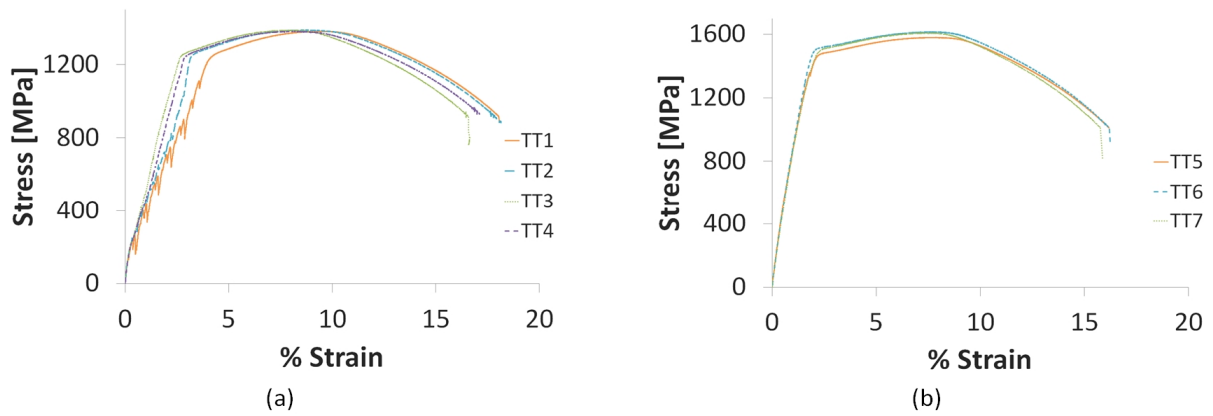


Figure 3.5: Stress-strain curve for (a) HT: 170807; (b) HT: 168232

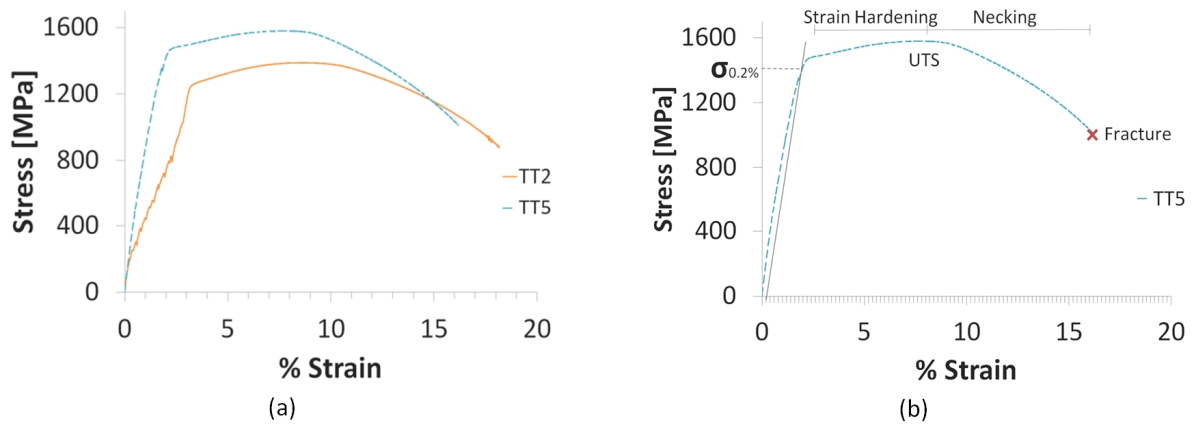


Figure 3.6: Stress-strain curves (a) comparison between HT: 170807 and HT: 168232; (b) typical stress-strain behavior of 34CrNiMo6.

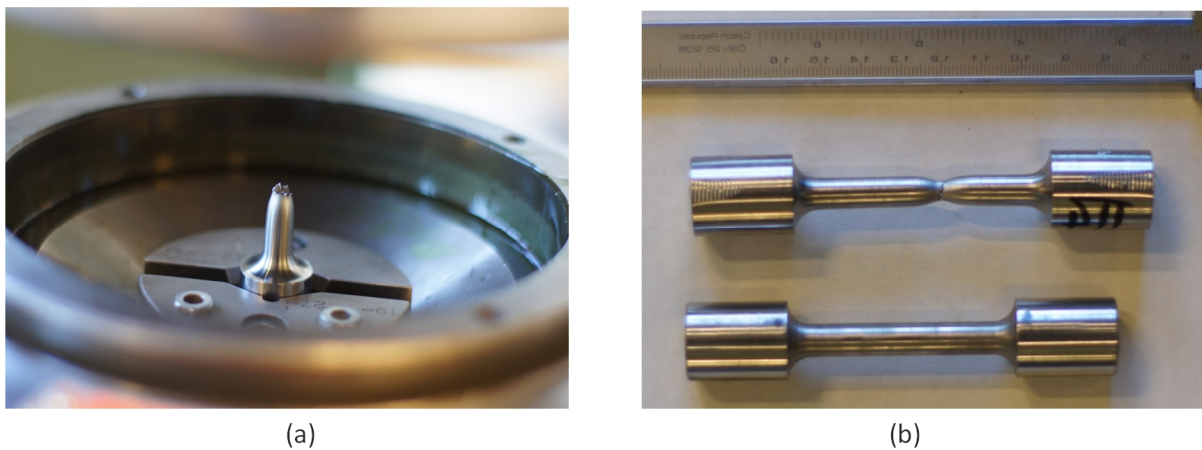


Figure 3.7: TT4: (a) in hydraulic press; (b) comparison between before and after uniaxial tensile test for TT4, see Appendix H.

3.3 Evaluation

A local optimal solution that satisfy the various constraints on the structural behavior is obtained, which include the geometric tolerances and surface quality, as well as the mechanical properties. The correct connections are utilized based on the anticipated condition to ensure that coupling integrity will not affect the overall integrity. The results from the buckling test will aid Interwell to utilize the limited design space available for Down Hole Equipment and also reduce the risk of buckling. The test-setup design is also taking into account the presence of imperfections and their effect on stability. In this case it is useful to distinguish two types of imperfections; one associated with the computational model and the other with the physical structure. The configuration of a mechanical system is the geometric description of the current position of all the particles, or material points, that constitute the system. If there is a change in the configuration this constitutes a displacement. Due to the specimen's dimensions, its axial displacement is going to be very small compared to its lateral deflection. The tendency of the axial compressive force is to increase the lateral displacement.

For this test, the strain gauge signals can be analyzed to determine the quantitative measure that would signal if buckling occurred or not. The initiation of buckling is evident in Figure 3.8, and the results from this concept analysis clearly show the time of lateral deflection. The blue lines in this figure represent the strain gauges, while the load is applied is the orange line. The graph shows noise after 70 second, but this does not affect the overall examination of the result and it is evident from the graph and data sets that buckling occurs after 78 seconds. Results from this analysis show that there is a correlation between the slope and the strain drop-off in the signals at the time of buckling in the specimen. The design and execution of formal stability studies concludes that the BTE can be used for this study. The resulting study of the strain signals can be used to predict time of buckling of the Setting Chamber Mandrel so proper injury predicting criteria and safety factors can be determined and used to improve Interwell's Down Hole Equipment.

On the basis of the Specialization Project, NS-EN 1993-1-1:2005 and this concept analysis three different parameter tests will be performed in Interwell's premises. The attributes likely to influence the quality and performance of the Setting Chamber Mandrel are; length, diameter, material properties, temperature and effects from tool operation in well pressure. The tests that will be conducted in the experimental study, as well as the geometric attributes are to be found in Table 3.7.

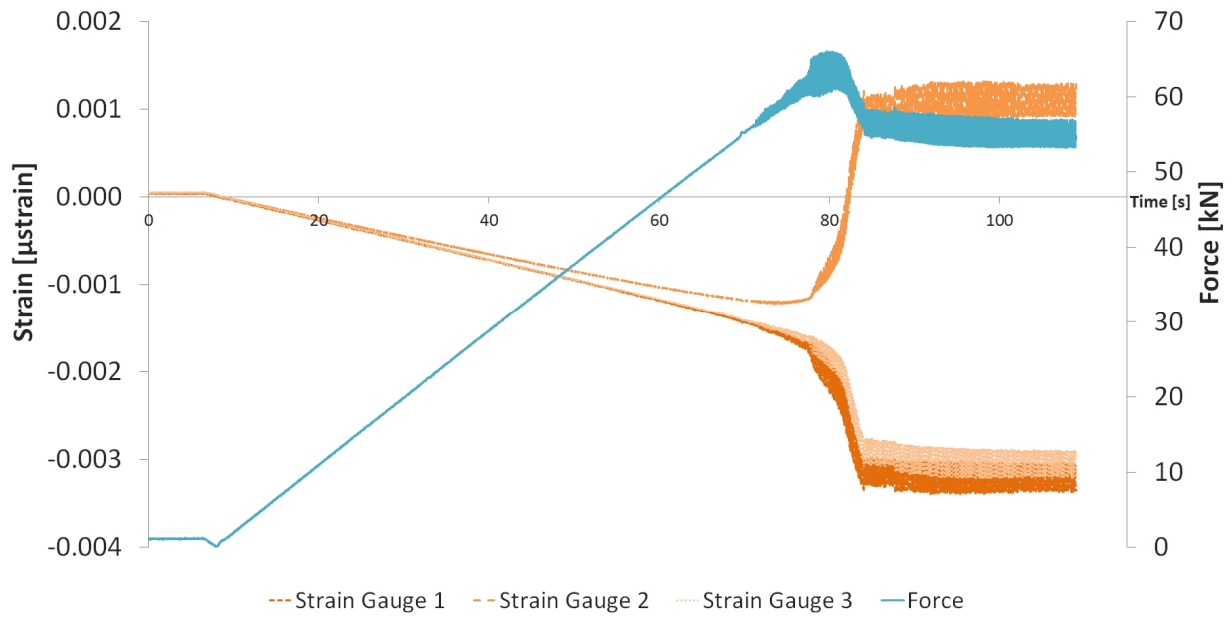


Figure 3.8: Results from the concept analysis; strain-time vs force-time.

Table 3.7: Different tests and test parts for buckling analysis of Setting Chamber Mandrel

Part Number	L_e [mm]	OD [mm]	P_{cr} [kN]	Temperature [°C]
TEST 1: Length and Diameter				
TP-000274-OD12	344	12	34CrNiMo6	25°C
TP-000272	476	20	34CrNiMo6	25°C
TP-000274-OD15	344	15	34CrNiMo6	25°C
TP-000274-OD15-L350	296	15	34CrNiMo6	25°C
TP-000274-OD18	344	18	34CrNiMo6	25°C
TP-000273-OD12	216	12	34CrNiMo6	25°C
TP-000274	344	20	34CrNiMo6	25°C
TEST 2: Temperature				
TP-000274-OD15-T	344	15	34CrNiMo6	150°C
TP-000274-OD15-T	344	15	34CrNiMo6	200°C
TEST 3: Well pressure				
TP-000274-OD15	344	15	34CrNiMo6	25°C

CHAPTER 4

4 Analysis

4.1 Euler and J.B Johnson Buckling

Euler and J.B. Johnson's theory can be used to estimate critical stress with a design factor of 2 or more, and can be useful in the early phases of the design process. This study divides members into short, intermediate and long length, where Johnson's equation (15) is valid for members with intermediate length and Euler's equation (3) is valid for long members. The tangent point between the Euler curve and J.B Johnson curve for 34CrNiMo6 steel member with a yield stress of 900 MPa is $\lambda_0 = 67.1$. Intermediate columns are defined by the minimum slenderness ratio, and for 34CrNiMo6 the value is equal to $\lambda_p = 47.5$. In the section between slenderness ratio 47.4 and 67.1 two of the test parts can be found, both defined as long members, i.e. Euler equation can be used but it should be noted that they are also within J.B. Johnson validations area. J.B. Johnson's equation estimates the critical buckling stress for the test parts to be lower than the critical buckling stress estimated with Eulers equation, see Table 4.1. Derivation of Euler and J.B. Johnsons equation is to be found in Appendix B.

Table 4.1: Results from Euler and J.B. Johnsons equations.

Part Number	L_e [mm]	L_k [mm]	OD [mm]	λ	Euler		Johnson σ_{cr} [MPa]
					P_{cr} [kN]	σ_{cr} [MPa]	
TP-000274-OD12	344	172	12	57.3	67.9	600.3	571.4
TP-000272	476	238	20	47.6	273.7	871.1	673.3
TP-000274-OD15	344	172	15	45.8	165.8	938.2	690.0
TP-000274-OD15-L350	296	148	15	39.4	223.9	1267.0	744.6
TP-000274-OD18	344	172	18	38.2	343.8	1351.0	753.9
TP-000273-OD12	216	108	12	36	172.3	1523.5	770.3
TP-000274	344	172	20	34.4	524.0	1667.9	781.6

4.1.1 NS-EN 1993-1-1:2005

This section will outline the procedure for obtaining a polynomial that describes the test data obtained from section 6.3 Intermediate members. The calculations should reflect the real buckling behavior of a member as close as possible; otherwise the sense of simulating the scenario fades away. Identifying critical parameters for later production is important. The following relation can describe the critical load of a member with imperfections

$$P_{CR} = f(\sigma_y, \sigma_r, z_0, A, E, \lambda) \quad (21)$$

where σ_y = yield stress

σ_r = residual stress

z_0 = eccentricity and amplitude of initial curvature

A = cross-section area

E = Young's modulus

λ = slenderness ratio

It should be emphasized that the variables in the function above are random variables, and that proof of influence of each variable will be obtained from correlation analysis of FE-analyses and experimental results. A good agreement is found between the NS-EN 1993-1-1:2005 for curve c and the polynomial for NS-EN 1993-1-1:2005 using the Microsoft Excel 2010 Trendline option, see Figure 4.1. The computational advantage of this approach depends on the characteristics of the specific problem. To reach an efficient simulation process applicable for a wide range of axial compressive members it is essential to apply a stable solution method for intermediate members that yield reliable results. In Figure 4.1 the non-dimensional slenderness ratio is a primary indicator of the mode of failure one might expect for a compression member. The dotted lines in Figure 4.1 correspond to a buckling curve fitted to the simulated buckling stresses from NS-results and literature study. The polynomial has to variables, where the non-dimensional slenderness can be calculated from geometrical attributes. When calculating buckling with NS-EN 1993-1-1:2005 the buckling stress tends to increase with increasing slenderness ratio, see Table 4.2. The buckling calculations according to NS-EN 1993-1-1:2005 for the reference test part TP-000274-OD15 is to be found in Appendix C.

$$\chi = \begin{cases} 1, & \bar{\lambda} < 0.2 \\ -0.0017\bar{\lambda}^6 + 0.0306\bar{\lambda}^5 - 0.2153\bar{\lambda}^4 + 0.7066\bar{\lambda}^3 - 0.908\bar{\lambda}^2 - 0.0196\bar{\lambda} + 1.0172, & \bar{\lambda} \geq 0.2 \end{cases} \quad (22)$$

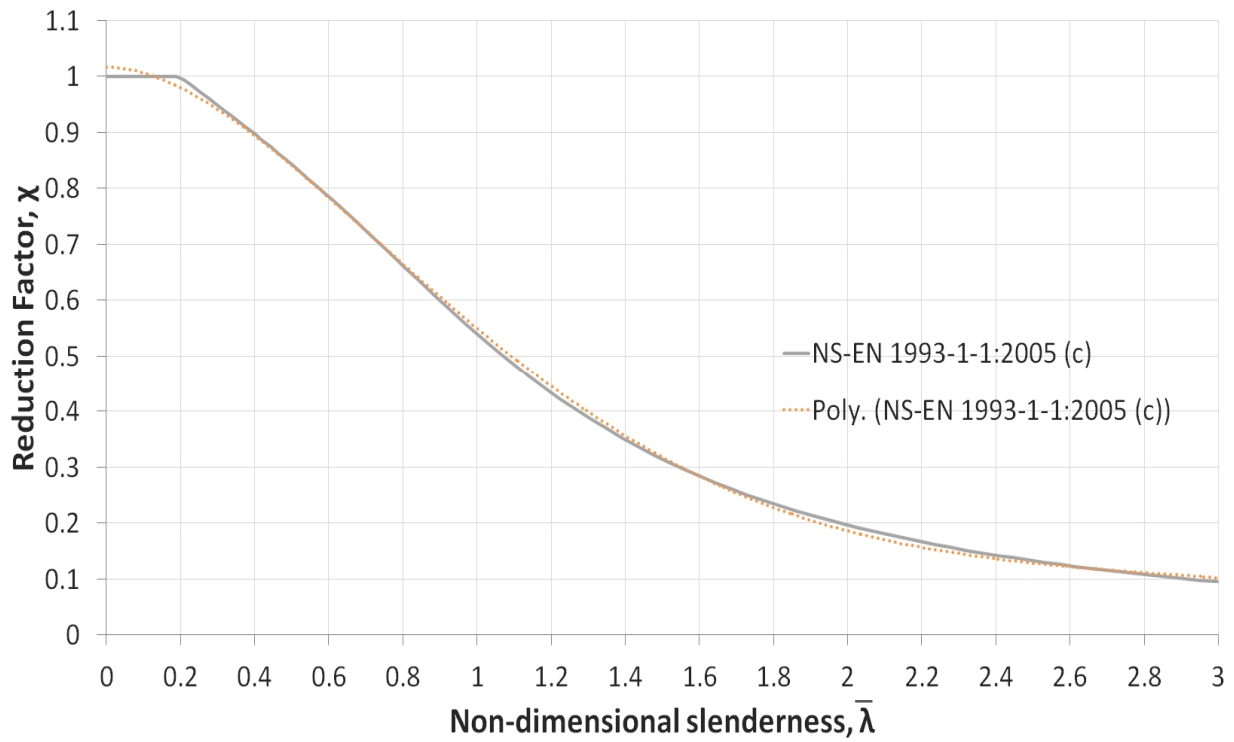


Figure 4.1: The reduction factor χ vs the non-dimensional slenderness λ for NS-EN 1993-1-1:2005 curve c polynomial and the curve c obtained from data.

Table 4.2: Results from buckling calculation with NS-EN 1993-1-1:2005.

Part Number	L_e [mm]	OD [mm]	λ	$\bar{\lambda}$	P_{cr} [kN]	σ_{cr} [MPa]
TP-000274-OD12	344	12	57.3	1.209	47	415.6
TP-000272	476	20	47.6	1.004	147	467.9
TP-000274-OD15	344	15	45.8	0.967	91	514.9
TP-000274-OD15-L350	296	15	39.4	0.832	102	577.2
TP-000274-OD18	344	18	38.2	0.806	174	683.7
TP-000273-OD12	216	12	36	0.759	69	610.1
TP-000274	344	20	34.4	0.726	199	633.4

4.2 FE-analysis

FE-modeling was done in the finite element software package Abaqus 6.12, a product of Dassault Systems. Abaqus is an industry leader in the field of finite element analysis. The development of the finite element method of the test parts illustrates not only the capability of Abaqus 6.12 to represent the behavior, but also the specific capability of the model to predict stresses, strains, and deflections while minimizing not-essential features. This study presents a linear elastic eigenvalue buckling analysis, a nonlinear static large deformation buckling analysis with elastic and elastic-plastic material properties, and a nonlinear Riks buckling analysis. Nonlinear static large deformation buckling analysis with elastic-plastic material properties yielded adequate results and dynamic analysis was therefore not conducted in this study. The analyses were performed in Abaqus 6.12 to see if the results would give better agreement than the results from NS-EN 1993-1-1:2005, increasing the knowledge on how to facilitate full utilization of the limited design space available for Down Hole Equipment. The results from these analyses will be used as a pre-study for the experimental testing and for post-buckling analysis to validate the results to ensure the reliability of the numerical methods.

4.2.1 Model Calibration

4.2.1.1 Geometry

The geometry of the models used in this analysis is based on the design of Setting Chamber Mandrel, see Figure 4.2. The reference test part model comprised a perfectly round cylinder with a uniform cross-section OD of 15 mm. On each side of the model there is a specified tolerance length with 18 mm in OD and 27 mm in length. The total length of the model is 398 mm, and the effective length is 344 mm. The other test parts are partitioned and meshed the same way as the reference test part. To facilitate a more economical and accurate solution, the parts are partitioned into smaller cells before meshed with symmetry. The results of the partitioning operations are shown in Figure 4.3. The load distribution on threads depends on a number of parameters; the pitch, number of engaged threads, form of threads, boundary conditions and the thickness of the wall supporting the threads at the threaded section. It should be noted that the models are simplified by modeling the lower and upper connections without threads, and that neither load distribution between the threads or the stress concentration at the root of the threads are accurately represented in the models.

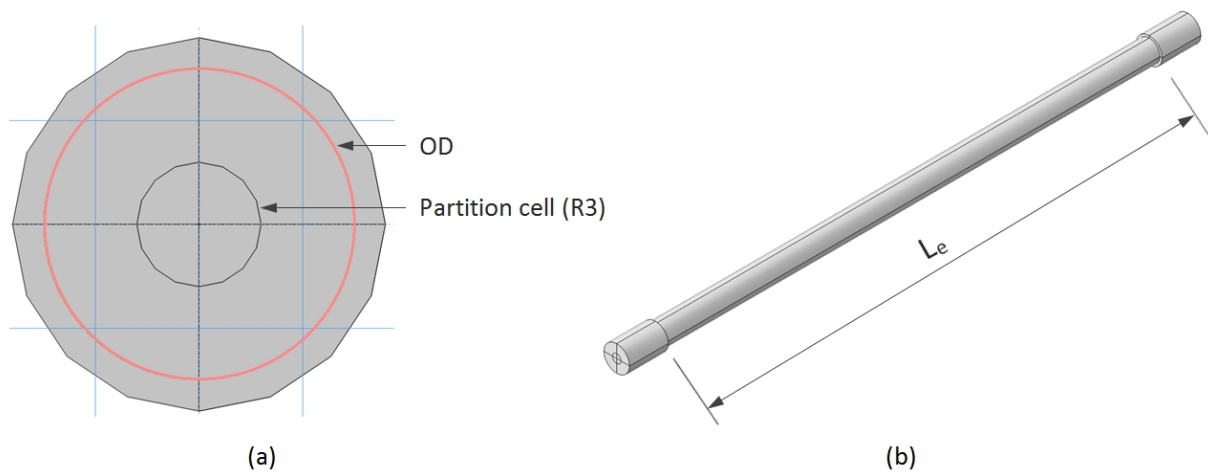


Figure 4.2: Base sketches (in this figure: TP-000274-OD15) (a) cross-section area; (b) effective length

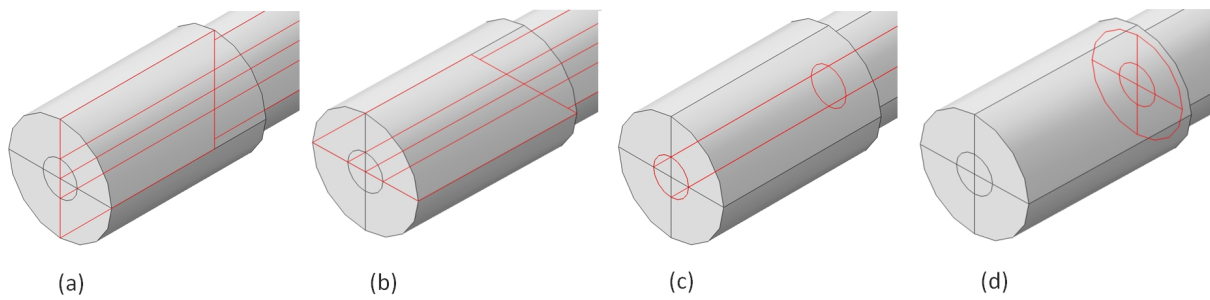


Figure 4.3: Revolved and partitioned parts (in this figure: TP-000274-OD15) (a) vertical cutting plane; (b) horizontal cutting plane; (c) partitioned face of cross-section; (d) partitioned face of outer cell

4.2.1.2 Material Specification

The Setting Chamber Mandrel and the test parts are made from 34CrNiMo6 steel. The material properties for 34CrNiMo6 can be found in Table 4.3 and was assigned to the models by creating a solid, homogenous section. The minimum yield criterion is specified to 900 MPa to make sure that results are on the safe side so that the lowest critical buckling load will be obtained. The models are run at room temperature.

Table 4.3: Material specification for 34CrNiMo6 steel.

Young's modulus, E [MPa]	Yield Stress, σ_{cr} [MPa]	Poisson's ratio, ν
2.05	900	0.29

4.2.1.3 Boundary Conditions and Load

The nodes at the upper end of the Setting Chamber Mandrel are considered fully fixed against translation and rotation. In the model all the six degrees of freedom, three rotations and three translations, have been fixed at current position, though it should be noted that solid bodies (e.g. C3D8R) do not have any rotational degrees of freedom. The lower end of the Setting Chamber Mandrel is also considered fixed, and all the degrees of freedom in the model except the axial deformation have been fixed at current position. The boundary conditions can be seen in Figure 4.4 (note that the inner colored blue line in this figure is representing the transition from the lower and upper test part and is also considered fixed). The selected boundary conditions in the models will represent the real condition so that the results will be as accurate as possible. The axial unit load is applied as pressure to the lower end of the model in the positive z-direction.

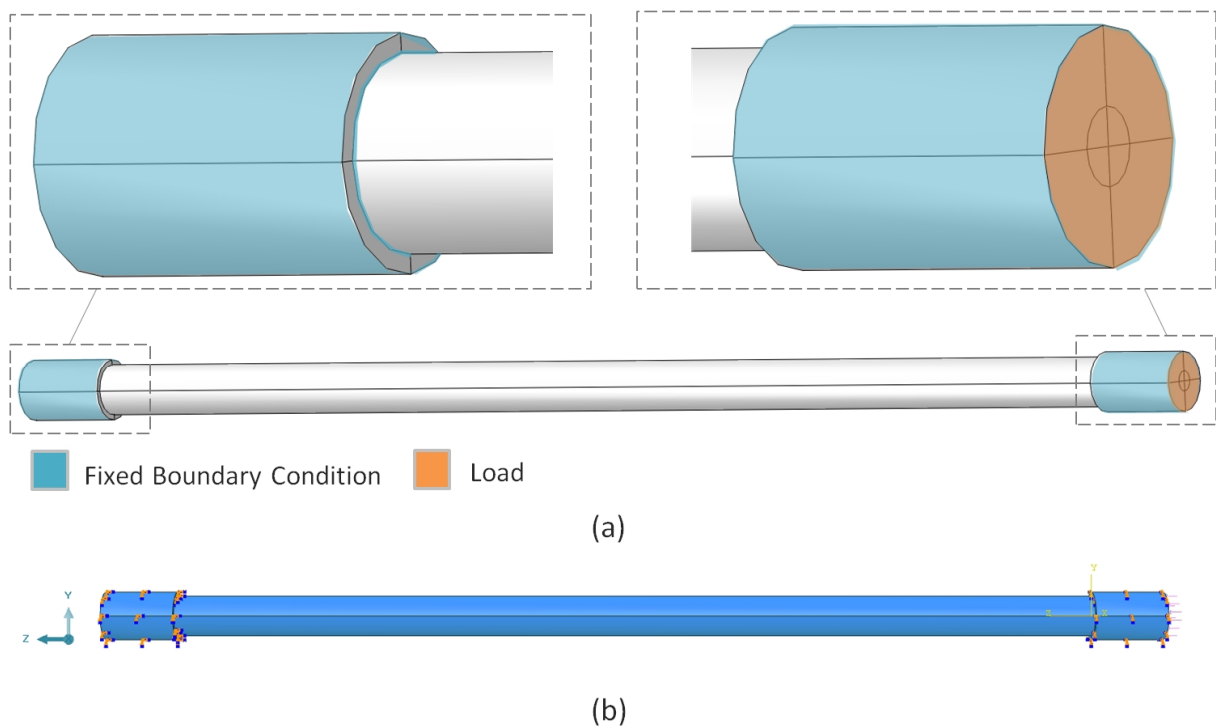


Figure 4.4: TP-000274-OD15 (a) Boundary conditions and load applied to the model; (b) Abaqus model

4.2.1.4 FE-mesh details

FE-mesh was built up on existing CAD geometry. For these analyses, linear hexahedral elements of type C3D8R were used. C3D8R is a general purpose linear 8-node brick element with reduced integration (one integration point) and hourglass control. This element tends to be not stiff enough in bending, and the stresses and strains are most accurate in the integration point. The reference test part is modeled with 62808 linear hexahedral elements of type C3D8R, 100 elements along the model's effective length and 20 elements along the circumference. The total number of nodes is 67655. From mesh convergence study it is

confirmed that the final results from the stress analysis is not affected by changing the size of its mesh. The mesh chosen for the test parts was a good compromise between accuracy and CPU time. These elements were utilized for this study and the results obtained yielded reliable and accurate results by iterating on element size, or mesh density. A finite element mesh sensitivity study was also conducted on each method on the reference test part to verify agreement of the FEA-method and its relationship with the model.

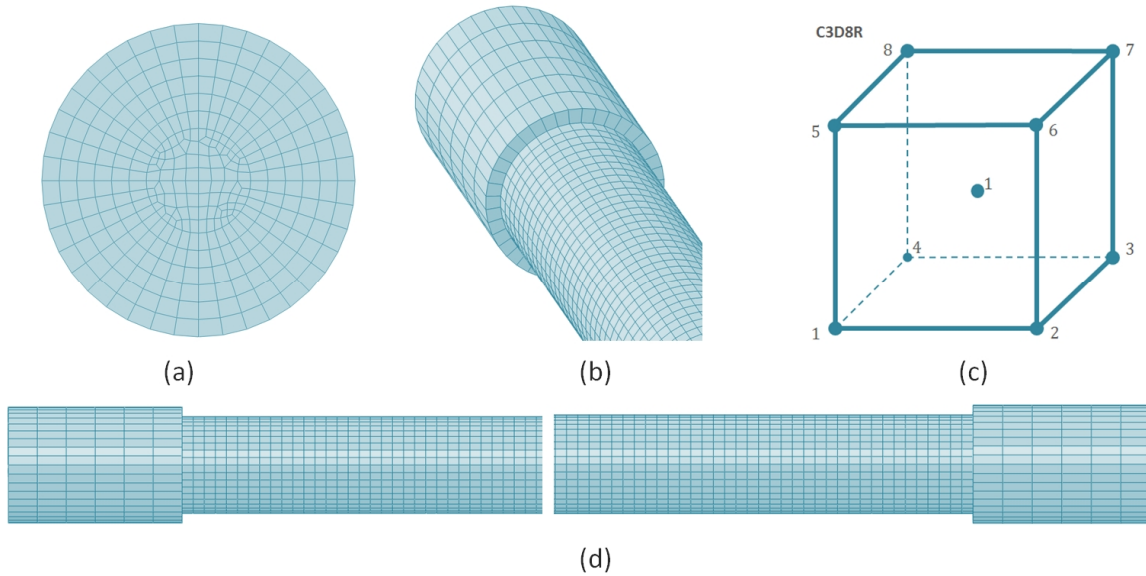
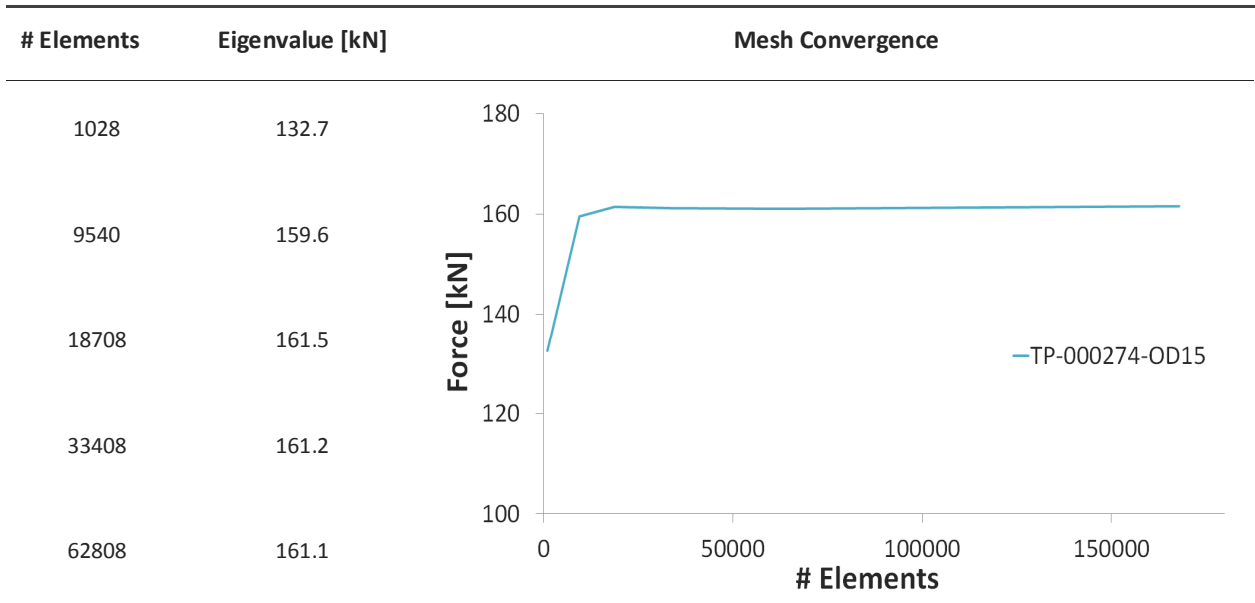


Figure 4.5: TP-000274-OD15 (a) cross-section area; (b) front-iso view; (c) C3D8R element; (d) fully meshed part

Table 4.4: Mesh convergence for reference test part TP-000274-OD15



4.2.1.5 Imperfections

Different imperfections that should be evaluated during a stability analysis are; physical, geometric, load, support and artificial imperfections. The physical imperfections represent deviations of the actual physics from the model used in FE-analysis. Geometric imperfections represent deviations from idealized shape from mechanical drawing to manufacturing processes. Load imperfections are those affecting eccentricities of the axially applied load. Furthermore, load imperfections may include unmodeled effects such as small lateral loads, non-conservativities and fluctuations. Support imperfections represent deviations from idealized boundary conditions i.e. moving foundations and connection eccentricities. Artificial imperfections are not necessarily linked to actual ones and may be added to the FE-model to simulate actual physical imperfections or to trigger the occurrence of certain types of response. Imperfections must be accounted for appropriately in the partial safety factors against instability. One key difficulty with these adjustments to the partial safety factor is the fact that imperfections are probabilistic in nature and statistical methods will be necessary for their correct treatment. Imperfections will be implemented in the nonlinear static analyses. The nonlinear static buckling analyses will study imperfection sensitivity by perturbing the perfect geometry from the linear elastic eigenvalue buckling analysis with different magnitudes of imperfection in the most important buckling mode, and then investigate the effect on the response.

4.2.2 Linear Elastic Eigenvalue Buckling Analysis

Linear elastic eigenvalue buckling analysis is generally used to estimate the critical load and buckling mode shapes of ideal structures by searching for the loads for which the tangent stiffness matrix becomes singular. This type of analysis predicts the theoretical buckling strength of an elastic structure, where the buckling loads are calculated relative to the base of the member. Typically, the material stiffness is positive-definite, whereas the geometric stiffness can admit negative values for certain modes, depending on the applied loading. The effect of a negative geometric stiffness can lead to a singular overall tangent matrix for the member, and hence buckling. This eigenvalue analysis is performed using the *BUCKLE procedure with the live load applied within the step and the eigensolver Subspace [6]. The axially compressive load is applied as a unity value and the resulted eigenvalue will therefore have the same value as the critical load.

The element size used in the analysis is determined by conducting a mesh density study, iterating on element size until the solution converges. The solutions are linear, hence the stiffness matrix is not updated during the solution and the results predict a load carrying capability greater than the member could actually sustain.

4.2.2.1 Results

The response of the test parts is nonlinear before buckling, so the linear buckling analysis is not strictly applicable although it provides a sufficiently good approximation and useful estimates of the different mode shapes. The modes shapes are often the most useful outcome in linear eigenvalue analysis, since

they predict the likely failure mode of the test parts. It is important to note that the buckling mode shapes are normalized vectors and do not represent actual magnitudes of deformation at critical load; i.e. the maximum displacement component is normalized to 1.0. The 1st and 2nd mode of buckling corresponds to a member that snaps into a sinusoidal shape. The 3rd mode of buckling corresponds to a member that snaps into a helical shape. The displacement contours for the base state, mode 1 and mode 3 are illustrated in Figure 4.6, and are the same for all the test parts. In order to see the buckling modes more clearly, a deformation scale factor of 30 was added to the figures. For practical purpose, the minimum critical load corresponding to the first and the second buckling mode is the most important result because the buckling modes are reported in the ascending order according to their numerical value. It is important to note that the geometric stiffness matrix is based only on the component forces, hence the effect of any prebuckling rotations due to moments are ignored in this analysis.

The eigenvalue analysis provides the factor by which the load must be multiplied to reach the buckling load. According to the linear eigenvalue analysis, buckling for TP-000274-OD15 takes place at a critical load of 161.1 kN. The applied load step is set to 1 MPa and the eigenvalue of mode 1 of TP-000274-OD15 is 663.1 MPa, which correspond to a mode 1 buckling load of 161.1 kN. The magnitude of the pressure applied is not important, since it will be scaled by the eigenvalues. The estimated maximum load, for each of the test parts, which can be supported prior to structural instability according to the linear eigenvalue analysis, is to be found in Table 4.5.

Table 4.5: Results from linear elastic eigenvalue buckling analysis

Part Number	L_e [mm]	OD [mm]	# Elements	P_{cr} [kN]	U_{max} [mm]
TP-000274-OD12	344	12	29888	66.7	1.0
TP-000272	476	20	79216	259.9	1.3
TP-000274-OD15	344	15	62808	161.1	1.0
TP-000274-OD15-L350	296	15	63656	215	1.0
TP-000274-OD18	344	18	125772	329.2	1.4
TP-000273-OD12	216	12	84272	165.9	1.3
TP-000274	344	20	80432	482.3	1.0

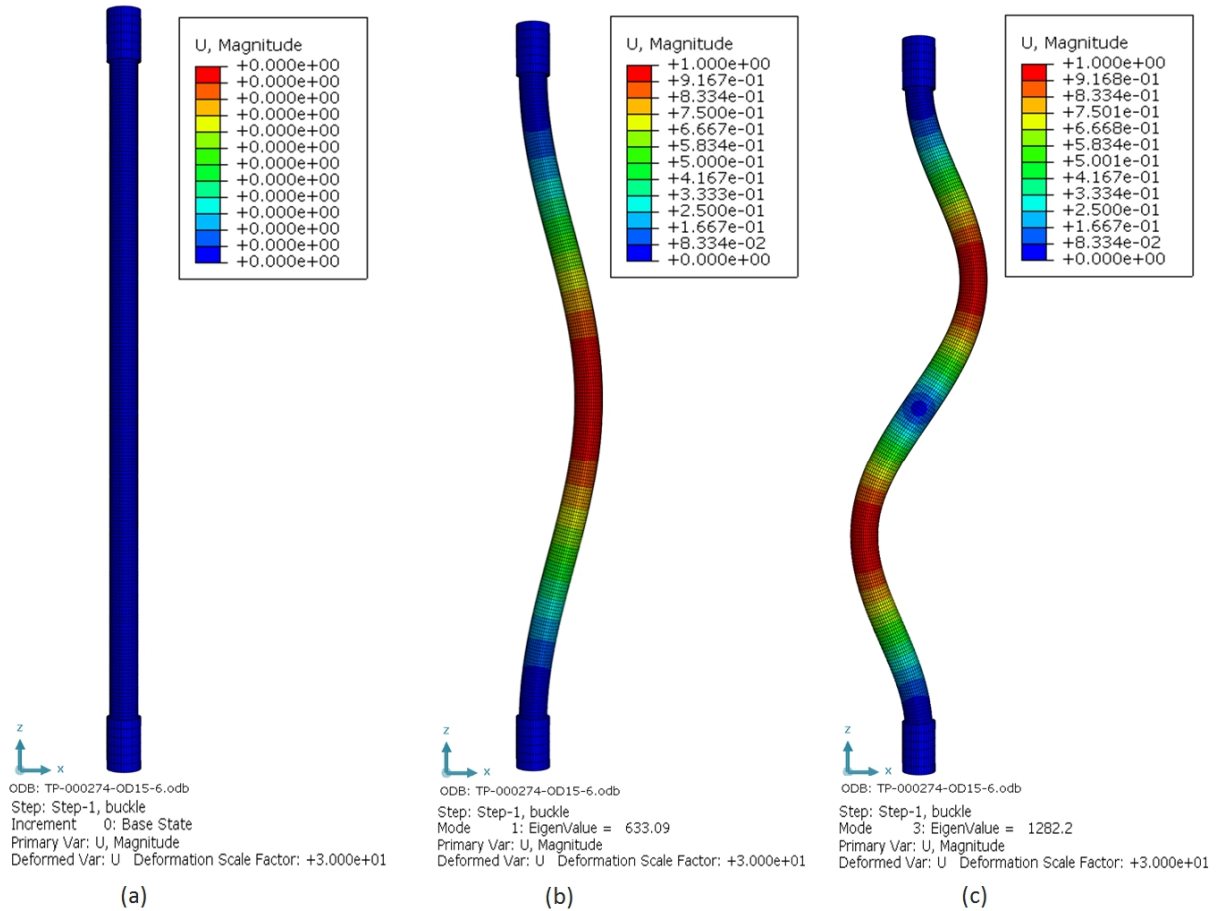


Figure 4.6: Base state and buckling modes for TP-000274-OD15 (a) base state; (b) mode 1 with eigenvalue of 633.1 MPa, (c) mode 3 with an eigenvalue of 1282.2 MPa.

4.2.3 Nonlinear Static Analysis

Linear eigenvalue analysis could be sufficient for a design validation, but since there is concern about material nonlinearity and geometric nonlinearity, load-deflection analysis will be used to investigate the model further. The buckling load predicted by the linear eigenvalue analysis yields to high values for the critical load, since plastic deformation or material failure take place before this point. The buckling loads were calculated relative to the base state of the model. Two nonlinear static analyses were conducted in this study; nonlinear static large deformation buckling analysis and nonlinear static Riks buckling analysis.

Linear eigenvalue buckling analysis provides guidance in mesh design for the nonlinear static analysis because mesh convergence studies are required to ensure that the eigenvalue estimates of the buckling load has converged. The mesh should be adequate to model the buckling modes, which are generally more complex than the prebuckling deformation mode obtained from the linear eigenvalue analysis. The nonlinear static analyses are using mesh and imperfections suggested by the linear eigenvalue analysis.

These analyses are studying imperfection sensitivity by perturbing the perfect geometry of the model with different magnitude of imperfection in the most important buckling mode, as well as the effect of on the response. The stresses in the model will be examined to explain the buckling under axial compressive loading.

4.2.3.1 Nonlinear Static Large Deformation Buckling Analysis

In the previous chapter the buckling loads were determined by using linear material (i.e. strain-displacement) relations. The assumption of linear elastic behavior is only valid if the buckling stress falls below the proportionality limit, and this is generally accurate for slender members. The nonlinear static large deformation buckling analysis is more time consuming and computationally expensive than the linear eigenvalue buckling analysis. However, nonlinear static large deformation buckling analysis yields more accurate results for determining buckling capability of a member. Unlike the linear eigenvalue analysis, the nonlinear analysis is iterative and the load is steadily increased until the solution starts to diverge.

The model consists of an initial eigenvalue analysis with a geometric imperfection imported into a nonlinear static, general step. In this study the geometric imperfection was introduced to the model with the Abaqus command *IMPERFECTION. This command specifies a scaling factor that will be applied to each mode. Different imperfections were added to the models until buckling occurred, starting with small imperfections (0.001) before larger ones were added. Imperfect systems are derived as perturbations of the ideal system and are seldom known precisely, which makes them random quantities that can be rigorously treated by stochastic techniques. A static, general step load was estimated based on the theoretical solution and the eigenvalue results. In order to get Abaqus to account for geometric nonlinearity in the calculations the *nlgeom* setting was turned on. The nonlinear static large deformation buckling analysis estimates the maximum load that can be applied to a geometrically nonlinear member before instability happens. In this analysis an increment of the force is added to the previous value and solved for simultaneously with deformation for the next equilibrium state along a path using Newtons method; therefore, at any time there will be a finite radius of convergence. The onset of buckling is generally indicated by failure to converge for a particular load step and the load increment that failed to converge will correspond to complete collapse of the model. An adequate maximum number of increments were used in this load step for the analysis to complete within reasonable CPU time. The analyses without a maximum number of increments self-aborted at an early stage because the load increased to infinity without any instability occurring to the decreasing structural stiffness.

4.2.3.1.1 Results

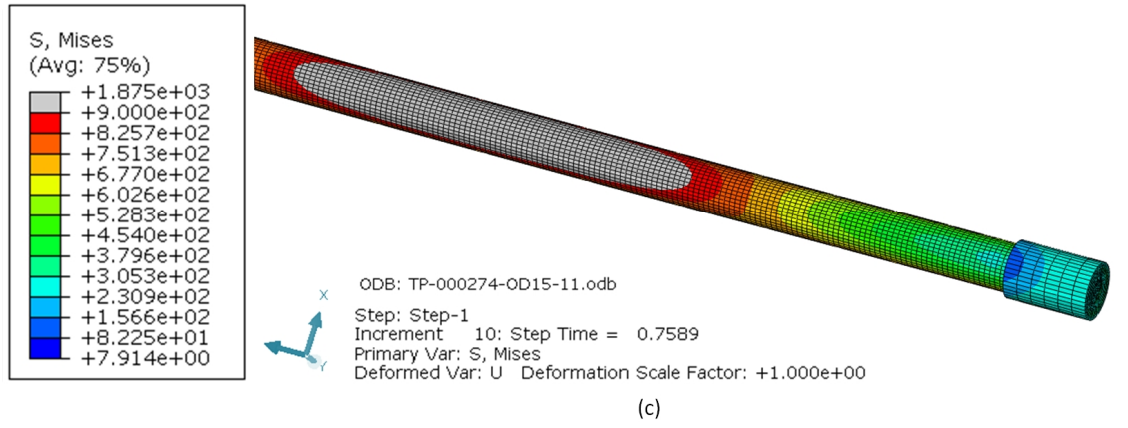
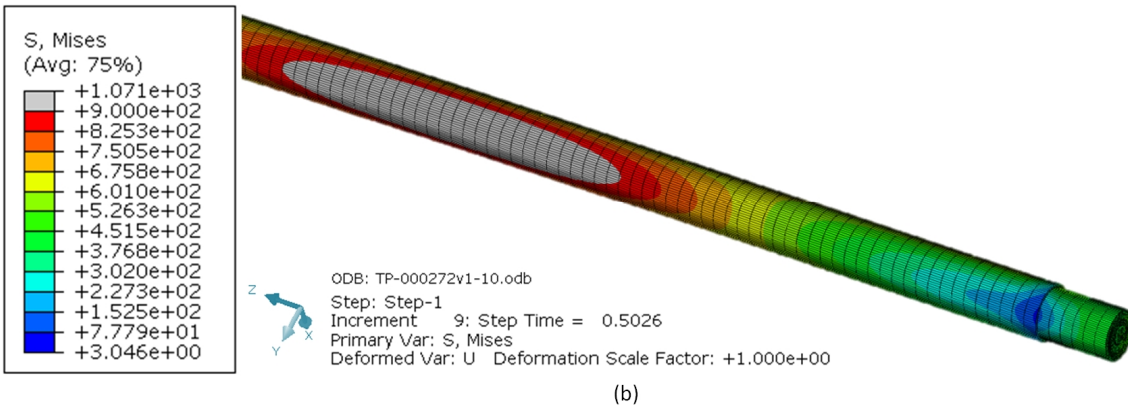
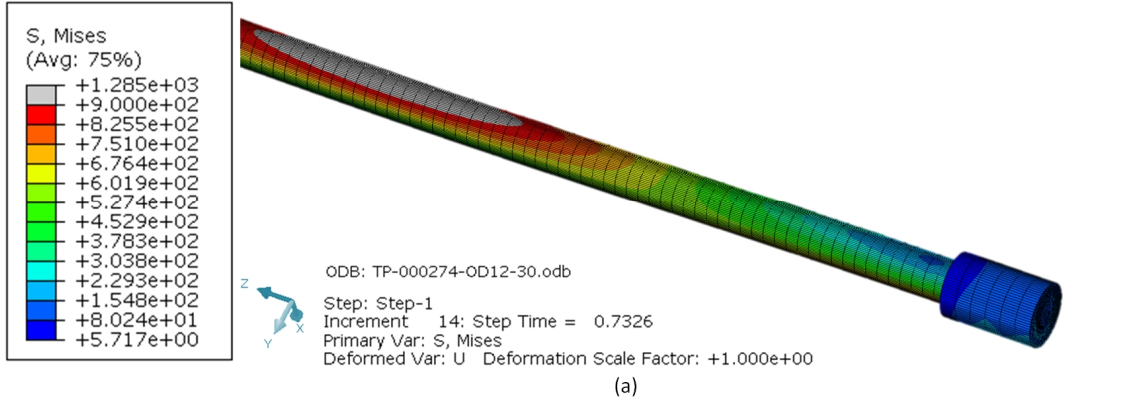
In contrast to the eigenvalue buckling analysis, nonlinear static analysis calculates displacements and stresses. When buckling occurs, the model undergoes a momentary loss of stiffness and the critical load results show numerical instabilities. The bending deformation introduces additional stresses to the model, which becomes larger when the load gets close to the critical load. The bending and membrane stresses in the model reflect the current deformed geometry. By comparing the results of the von Mises stresses from

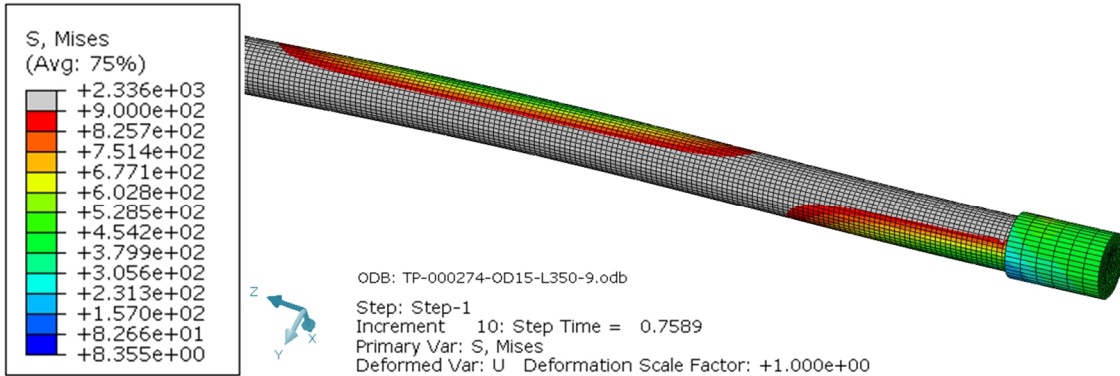
the simulations with lower slenderness ratio with the reference test part's yield strength obtained from the uniaxial tensile test, it is evident that the stresses are too high for the stated displacement, due to the linear-elastic definition of the material. The models with low slenderness tends to start failing by crushing at very high stress levels, well beyond the elastic range of the material. High slenderness ratio corresponds to a lower critical stress that will cause buckling, and conversely, lower slenderness ratio results in higher critical stresses. As the effective length of the model increases with the slenderness, the buckling stress decrease for the same model. The fixed boundary condition could be an excessive constraint. Excessive constraints tend to add stiffness to the model, so that the FE-model is stiffer than the real system.

From the figures it is obvious that as the slenderness decreases, the model undergoes more and more gradual plastification represented with grey areas. The models with lowest slenderness ratio bends without any increase in load, i.e. small deflection theory, and the effect of strain hardening gets more predominant as the value of slenderness decreases. The nonlinear static buckling analysis shows that including only one kind of nonlinearity does not give a realistic situation for the test parts with lower slenderness ratio, see Figure 4.7. Consequently, the models with slenderness ratio lower than 40 gives almost full plastification of cross-section area before buckling, as a result from crushing in the z-direction before buckling. Intermediate columns involve buckling problems with material nonlinearity of plasticity. For the analysis with to small imperfections Abaqus was unable to reach a convergent solution in the initial step of the analysis. After conventional efforts, i.e. refining the mesh, reducing the initial step size, introducing end eccentricity, plastic material specification was considered as the best improvement to the model and was therefore added to the material description.

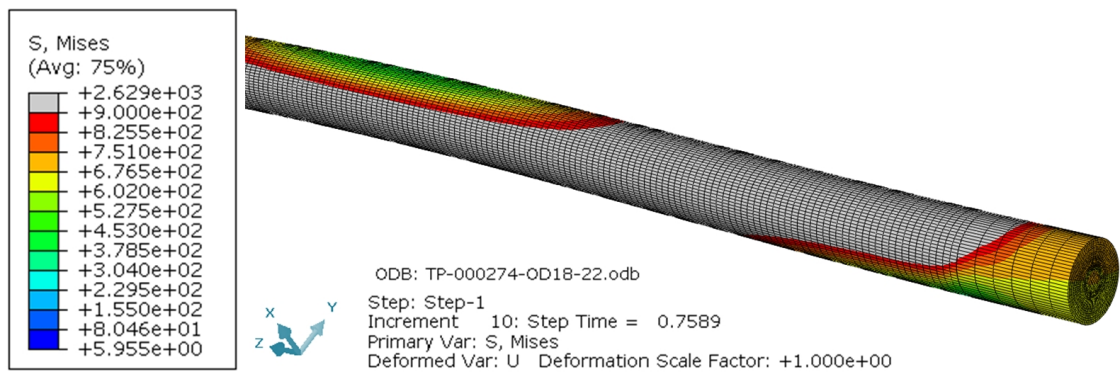
Table 4.6: Results from nonlinear static large deformation buckling analysis.

Part Number	L_e [mm]	OD [mm]	# Elements	P_{cr} [kN]	U_{max} [mm]	S, Mises [MPa]	Imperfection Applied
TP-000274-OD12	344	12	83712	55.9	2.4	1010	0.08
TP-000272	476	20	79216	216.3	1.9	1050	0.5
TP-000274-OD15	344	15	62808	129.4	2.0	1170	0.5
TP-000274-OD15-L350	296	15	63656	173.8	2.2	1620	0.5
TP-000274-OD18	344	18	125772	298.6	2.8	1842	0.3
TP-000273-OD12	216	12	84272	135.2	1.7	1932	0.3
TP-000274	344	20	80432	439.7	2.9	2175	0.3

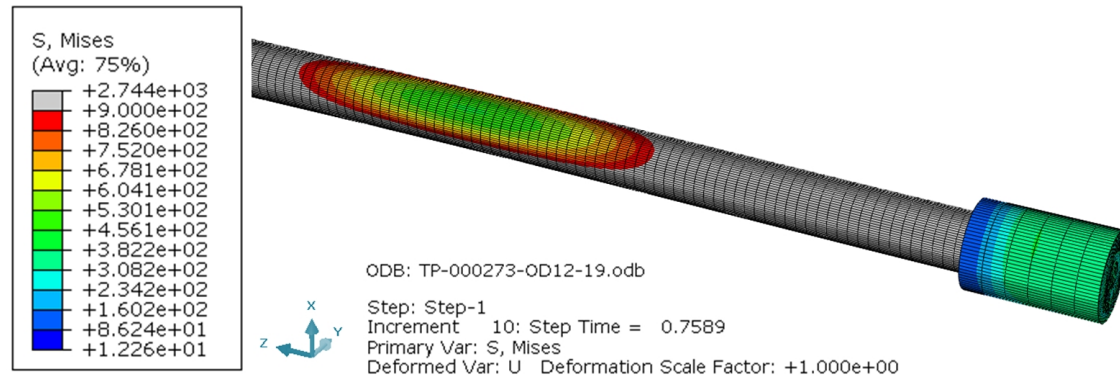




(d)



(e)



(f)

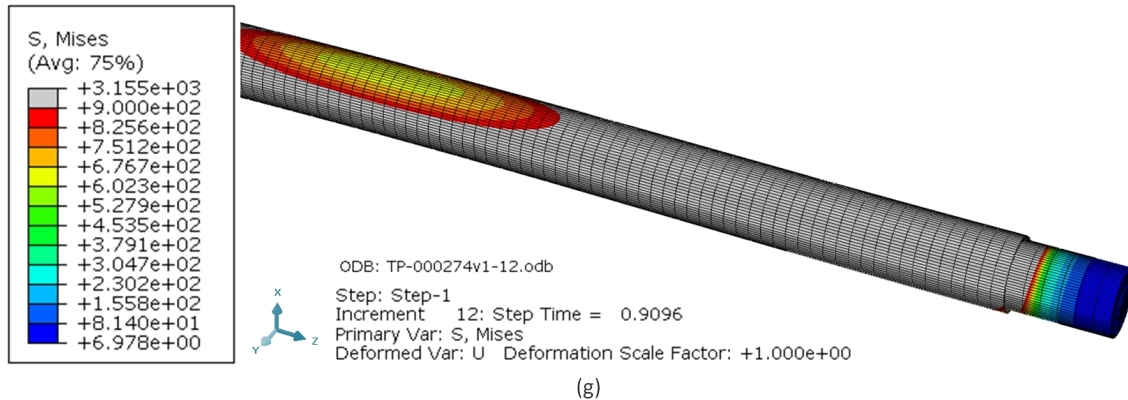


Figure 4.7: Stresses from nonlinear static large deformation buckling analysis (a) TP-000274-OD12; (b) TP-000272; (c) TP-000274-OD15; (d) TP-000274-OD15-L350; (e) TP-000274-OD18; (f) TP-000273-OD12; (g) TP-000274

4.2.3.1.2 Material Nonlinearity of Plasticity

The minimum yield criterion for 34CrNiMo6 steel is 900 MPa. For TP-000274-OD12-L350, TP-000274-OD18, TP-000273-OD12 and TP-000274 inelastic buckling occurs well above yield in the plastic range. Since the nonlinear analysis was performed in the case of ideal loading, plastification of 34CrNiMo6 steel have been introduced to the nonlinear static analysis models to get more realistic information on the buckling response.

Abaqus uses standard Mises or Hill yield surfaces with associated plastic flow in the classical metal plasticity models. Material nonlinearity is modeled in Abaqus using a standard plasticity material model which is based on an incremental plasticity formulation governed by a simple isotropic hardening rule. Stress-strain data from the uniaxial tensile test and the material certificate were used to represent the material hardening behavior. From the experimental hardening curve obtained from the uniaxial tensile tests the strain hardening coefficient should be about 0.016 for HT: 170807 and 0.008 for HT: 168232. The conversion to true stress and logarithmic plastic strain is given by:

$$\epsilon_{true} = \ln(\epsilon_{nom} + 1) \quad (23)$$

$$\ln(\sigma_{true}) = n[\ln(\epsilon_{true}) + \ln(K)] \quad (24)$$

Equation (24) is equal to a straight line, where n is the strain-hardening coefficient and K is the strength constant. The new plastic material input for this analysis is listed in Table 4.7. For simplicity the same monotonically increasing strain-hardening coefficient is considered in all the following nonlinear static large deformation analyses.

Table 4.7: Plastic strain values in the nonlinear Abaqus analysis

Yield Stress [MPa]	Plastic Strain
900	0
1450	0.008

Load-displacement curves of the nonlinear-elastic and nonlinear elastic-plastic FEM model is shown in Figure 4.9 and Figure 4.10 via a history plot of the maximum displacement node. The analysis self-aborted when the model reached plastic yield through the section. The results from the nonlinear elastic-plastic analysis show that the critical load and critical stress is considerably lower. The equivalent plastic strain in a material (PEEQ) is a scalar variable that is used to represent the material's inelastic deformation [17]. The maximum equivalent plastic strain for the reference test part when buckling occurs with imperfection 0.7 mm is 0.00326 %.

Table 4.8: Results from nonlinear static large deformation buckling analysis with elastic-plastic material.

Part Number	L_e [mm]	OD [mm]	# Elements	P_{cr} [kN]	U_{max} [mm]	S, Mises [MPa]	Imperfection Applied
TP-000274-OD12	344	12	83712	50.6	2.3	912	0.3
TP-000272	476	20	79216	200.2	1.9	894	0.5
TP-000274-OD15	344	15	62808	111.6	1.4	892	0.7
TP-000274-OD15-L350	296	15	63656	127.7	1.3	958	0.6
TP-000274-OD18	344	18	125772	180.0	1.5	952	0.7
TP-000273-OD12	216	12	84272	82.4	0.9	961	0.5
TP-000274	344	20	80432	255.4	1.6	1006	0.5

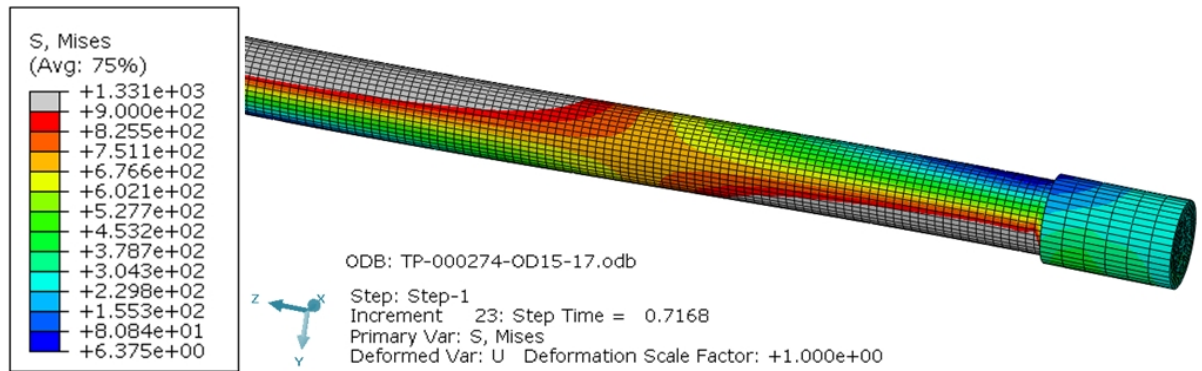


Figure 4.8: TP-000274-OD15: stresses from applied load with elastic-plastic material properties.

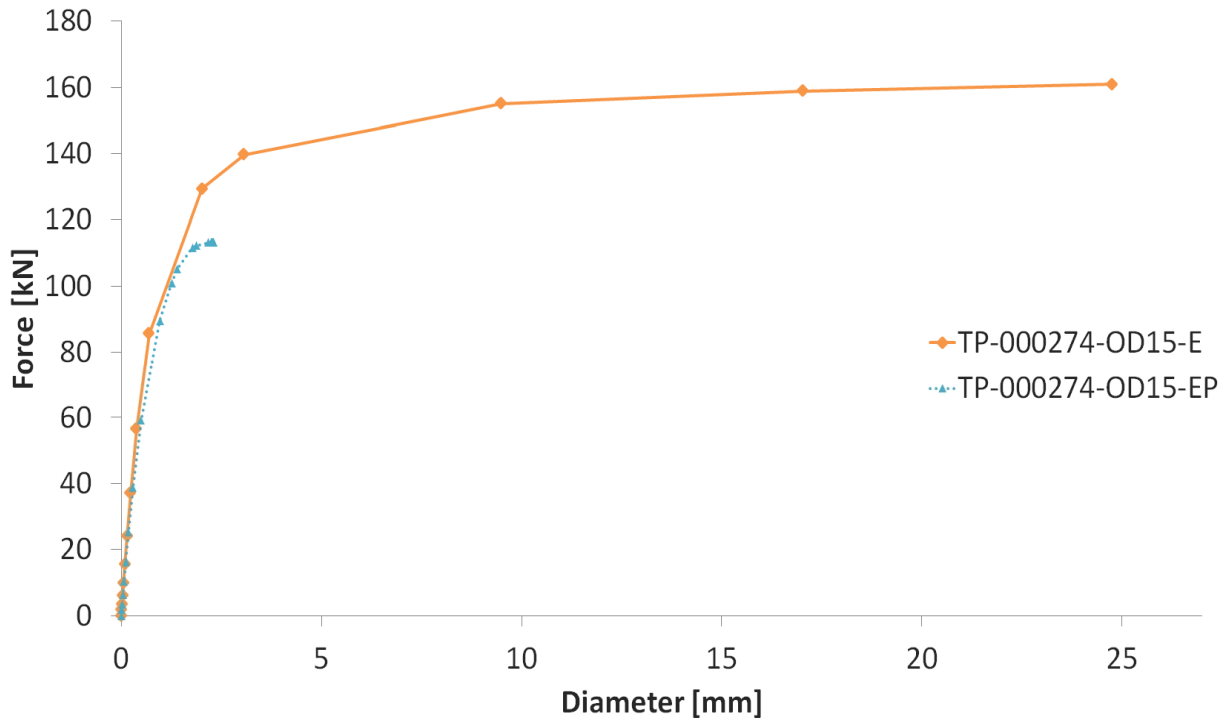


Figure 4.9: Load-displacement curves for nonlinear elastic and nonlinear elastic-plastic material for TP-000274-OD15.

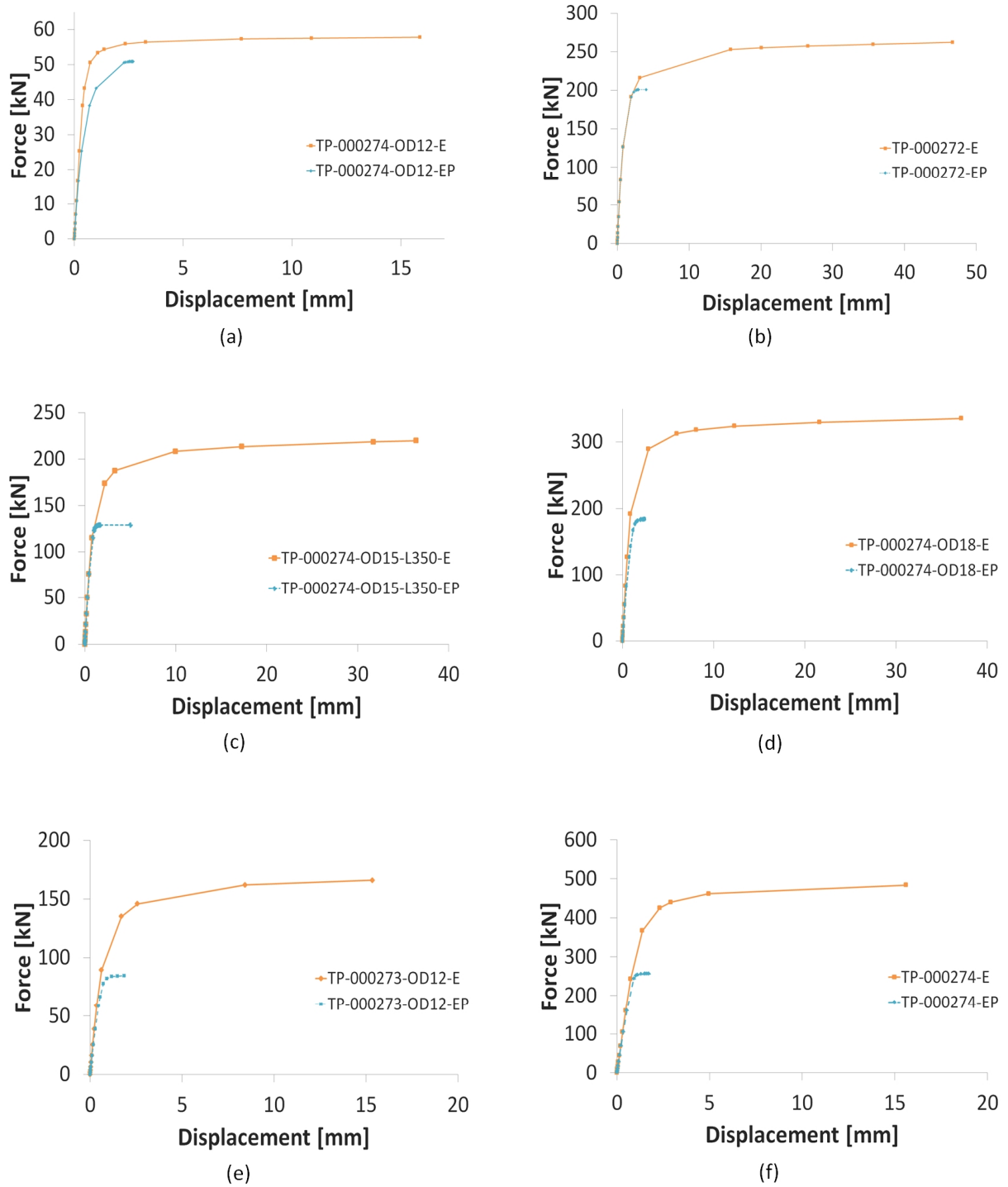


Figure 4.10: Load-displacement curves for nonlinear elastic and nonlinear elastic-plastic material for (a) TP-000274-OD12; (b) TP-000272; (c) TP-000274-OD15-L350; (d) TP-000274-OD18; (e) TP-000273-OD12; (f) TP-000274

The effect of different plasticity properties was also studied on the reference test part and the result is shown in Figure 4.11. From the figure it is evident that EP1 is more conservative, since the strain-hardening begins when the model reaches the minimum yield criteria of 900 MPa.

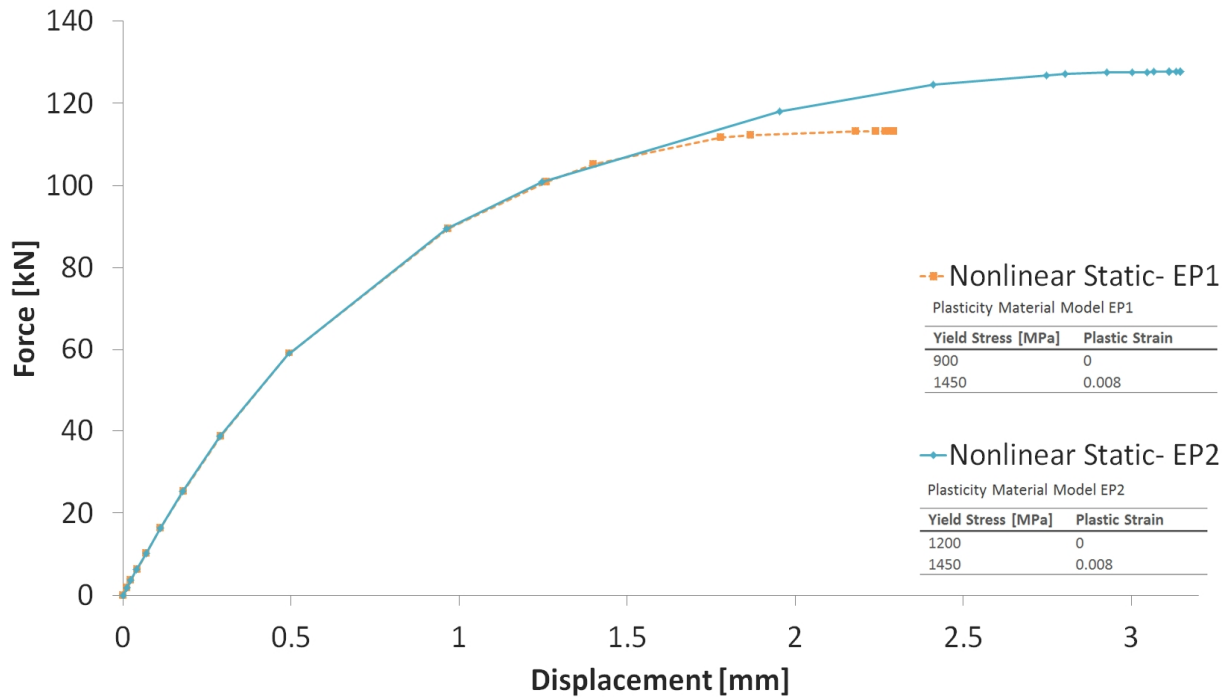


Figure 4.11: Different plasticity properties for TP-000274-OD15.

4.2.3.2 Nonlinear Static Riks Buckling Analysis

For evaluation of post-buckling response of a member and verification of the nonlinear static large deformation buckling analysis, the modified Riks method in Abaqus can be used. The essence of a nonlinear buckling analysis with modified Riks method is moving with fixed increments along the static equilibrium path in a space defined by nodal variables and the proportional loading parameter (a multiple of the applied load). The size of the fixed increments is limited by moving a given distance along the arc to the current solution point and then start searching for equilibrium in the orthogonal plane that passes through the point. This method is used for cases where load magnitudes are governed by a single scalar parameter. In this study, the scalar parameter is an axial compressive load. The arc length is a measure of deformation in Abaqus used to evaluate the progress of the solution and to give an estimate of how much the total deformation have varied throughout the analysis. The same modeling procedure as in the static general analysis was applicable for all the different models. The load step applied is Static/Riks. The maximum LPF was specified to values between 0.65 and 1.0, depending on the results from the imperfection applied, to terminate the Riks analysis.

4.2.3.2.1 Results

The key output from this Riks analysis is the load proportionality factor and displacements. The current value of the LPF will be given automatically with an output database file request. The LPF versus the arc length graph was plotted in order to see if buckling occurred or not, see Figure 4.12. Imperfections were added to the models, starting with small imperfections (0.001), increasing until buckling occurred. For the imperfection where buckling occurred, the linear part was followed by a sudden peak before flattening of the load. The graph can be viewed as a single equilibrium path in a space defined by the nodal variables and the loading parameter, and the actual load may decrease or increase as the solution progresses. The cross-sections of the models with lower slenderness undergo significant plastification of the cross-section, and the results show unrealistic high buckling stresses. Force-displacement curves comparing the nonlinear static Riks buckling analysis results for all the models can be found in Figure 4.13, Figure 4.14 shows the resulting stress distribution for TP-000274-OD15. The rest of the figures for the other models can be found in Appendix D.

For more accurate results plastic material should be added to the Riks analysis. The modified Riks method is more cost effective than nonlinear static large deformation buckling analysis in terms of total simulation time for models with high number of elements. It would not be sufficient for this study to conduct Riks analyses with plastic material added to the material specification.

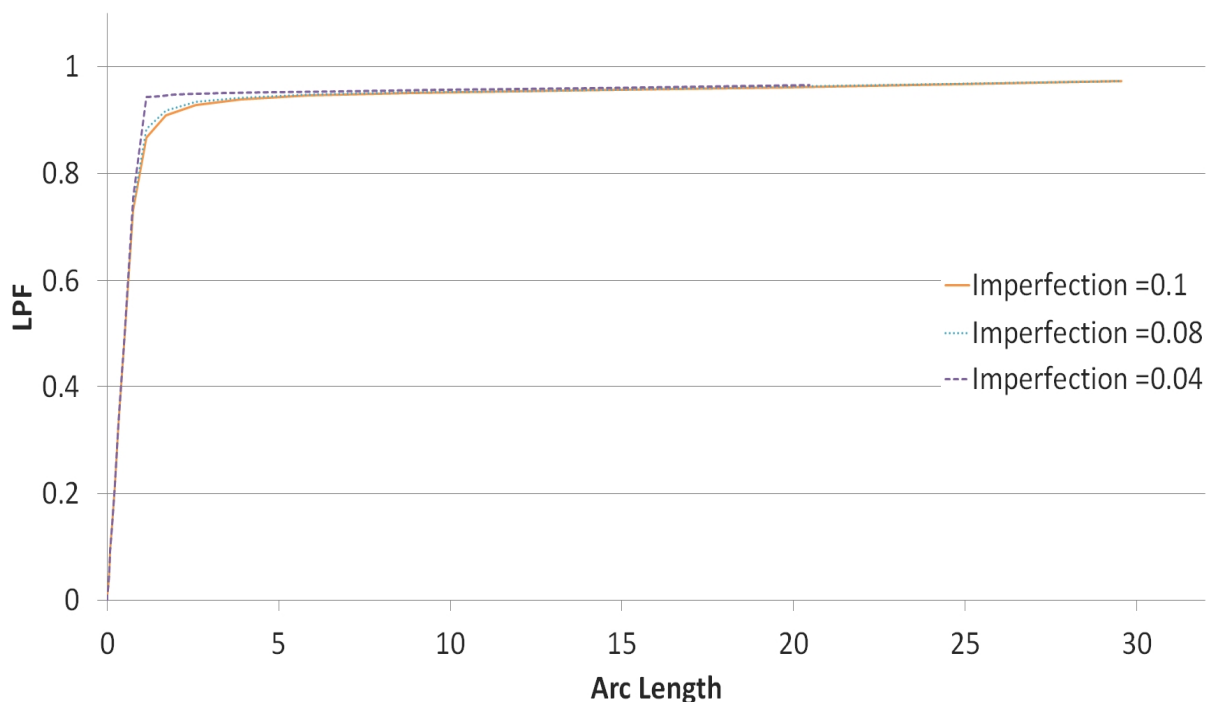


Figure 4.12: LPF-arc length curves for TP-000274-OD15.

Table 4.9: Results from the nonlinear static Riks analysis

Part Number	L_e [mm]	OD [mm]	# Elements	P_{cr} [kN]	U_{max} [mm]	S, Mises [MPa]	Imperfection Applied
TP-000274-OD12	344	12	83712	62.8	1.8	940	0.08
TP-000272	476	20	79216	228.0	2.1	1130	0.3
TP-000274-OD15	344	15	62808	155	2.1	1305	0.1
TP-000274-OD15-L350	296	15	63656	212.7	1.9	1610	0.1
TP-000274-OD18	344	18	125772	212.2	2.5	1410	0.3
TP-000273-OD12	216	12	84272	163.5	2.0	2300	0.1
TP-000274	344	20	80432	493.5	3.0	2390	0.1

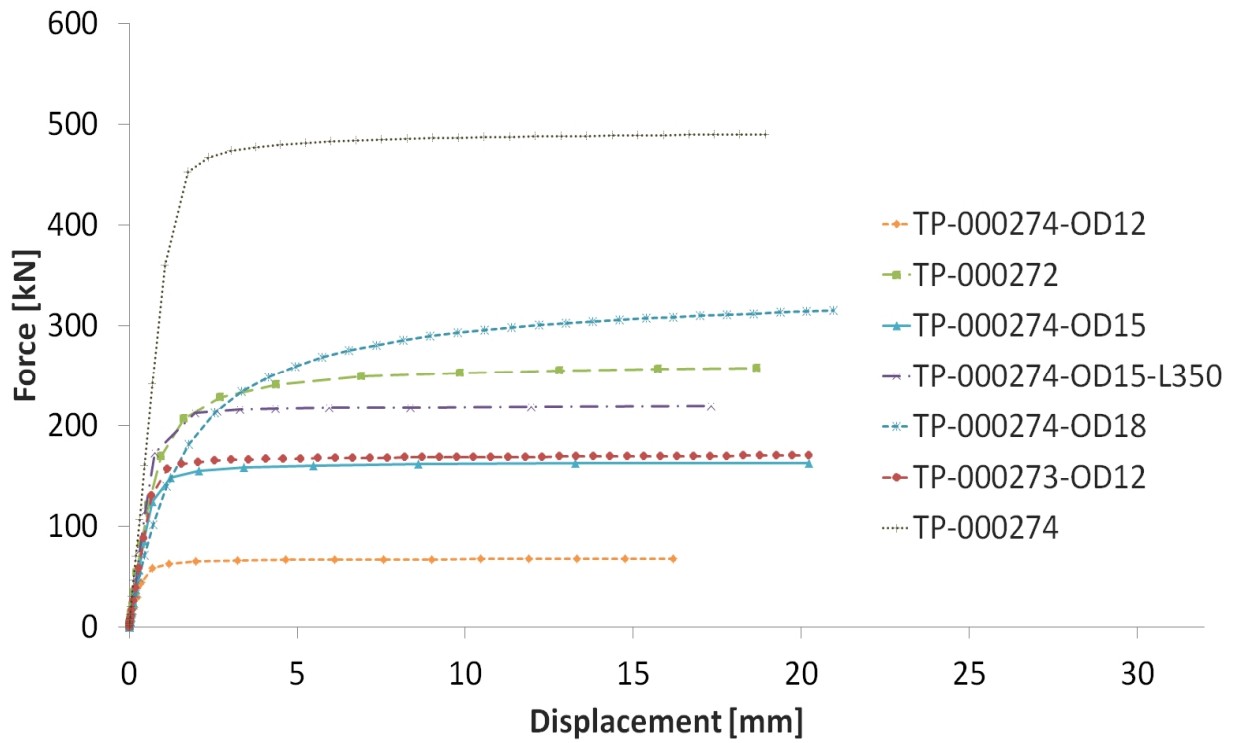


Figure 4.13: Force-displacement curves comparing the nonlinear static Riks buckling analysis results for all the models.

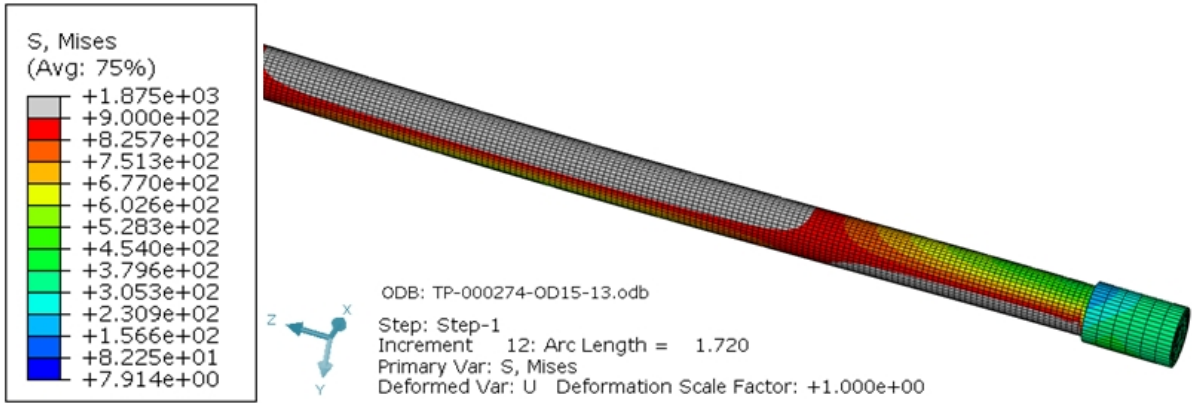


Figure 4.14: TP-000274-OD15: stresses from applied load.

CHAPTER 5

5 Experimental Studies

Although theoretical analyses are important in understanding the behavior of the Setting Chamber Mandrel, they need to be supported by well-planned and well-executed experimental investigations. The object of the compression tests was to experimentally study the behavior of the members under axial compression load and make sure that the design of the Setting Chamber Mandrel will withstand the expected loadings in a well. This chapter addresses different design situations for the Setting Chamber Mandrel using adequate structural models considering the influence of all relevant test parameters; length, diameter, material properties, temperature and effects from tool operation in well pressure. The general choice of parameter is tied up to the design and the fabrication methods whereas the value of the different parameters is determined by fabrication and/or quality control. The different parameters of the model should be documented without ambiguities. In order to enhance the structural efficiency and performance of the Setting Chamber Mandrel a systematic approach to the experimental tests has been adopted. The experimental results will be compared with the theoretical predictions started in the previous chapters.

The test equipment designed in the Specialization Project [15] for this study is called Buckling Test Equipment, BTE. The equipment is divided into two parts; Buckling Test Equipment for Test Casing and Buckling Test Equipment for Hydraulic Press. The equipment is required to simulate and establish the actual buckling loads of different geometries. In its more particular aspect, the present design is directed toward parts of an assembly for Setting Tools, such as the HSU. BTE will be used on cylindrical rods that are being exposed to axial compressive loads. The design process strived towards achieving the best possible design by utilizing the knowledge and experience from the literature study and Setting Chamber Mandrel.

Typically, the members are influenced by imperfections and thus a certain amount of scatter expected to be in the results. Imperfections are always present in the real world; i.e. loads are always applied with offsets, supports are never perfectly rigid and faces are never perfectly flat. Initial geometric-, fabrication-, load-, and support-imperfections play a defining role, but it is important to note that the effect of any imperfection will depend in the actual geometry and loading of the member. The expectation from the experiments is that the test parts will, in practice, buckle at a load lower what predicted by the FEA and higher than NS-EN 1993-1-1:2005. The results from this experiment will reveal unanticipated functionality that could be difficult to uncover by calculations and simulations alone.

5.1 Buckling with Hydraulic Press

This experimental study uses the Buckling Test Equipment for Hydraulic Press, BTEHP, to make sure that the test setup establishes the required results. The tests were conducted using Interwell's Kapema manual hydraulic press with a capacity to generate a compressive force up to 30 tons. The BTEHP is designed for testing different geometric attributes (effective length and diameter) and temperatures.

5.1.1 Preparation of test pieces

Prior to testing, preparation involved obtaining actual new specimen dimensions, mounting three strain gauges on each specimen, calibrating the load cell, setting up the BTEHP and aligning the test set-up. The work piece surface on the test specimen should be free from pits and irregularities, as well as chemically clean and totally free of contaminants before applying CN adhesive. Slight misalignment of the strain gauges and test specimen in the initial position may generate differences in strain between the opposite surfaces of the specimen, resulting in errors at low strains. However, from the proof of concept analysis it is clear that the use of strain gauges on the specimen, with independent data collection, will detect buckling and deflection rapidly. For the temperature test M-Bond 43-B and 600 adhesives were used and then cured according to manual, Appendix E.

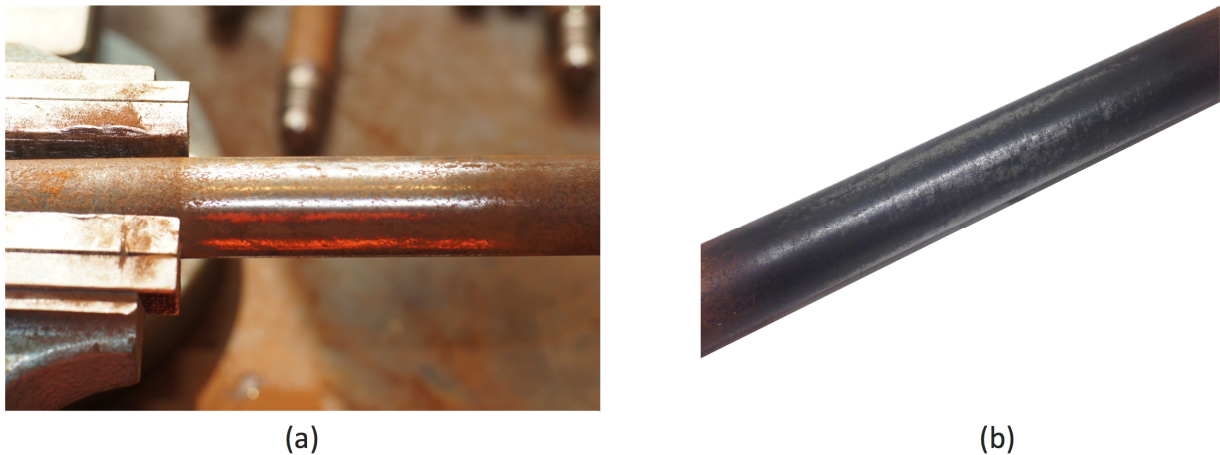


Figure 5.1: Surface preparation of strain gauge (a) test specimen in aluminum clamps; (b) cleaned surface.

5.1.2 Instrumentation

Labview Signal Express is the data logger used to record and store the experimental data, providing an extensive range of measurement. This system has precision analogue measurement facilities, control functions, digital input and output and pulse accumulating. This is the same portable system that was used in the proof of concept analysis. Strain gauges (FLA-5-11-1L) and the TC8 loadcell were directly wired to the system, which conditioned the signals to enable automatically, accurate and fast measurements. The strain-gauge configuration used in this study is a quarter-bridge with one active element leg in the

Wheatstone bridge, see Figure 5.2. Having completed soldering the circuit on the NI circuit board, the strain gauges could easily be changed.

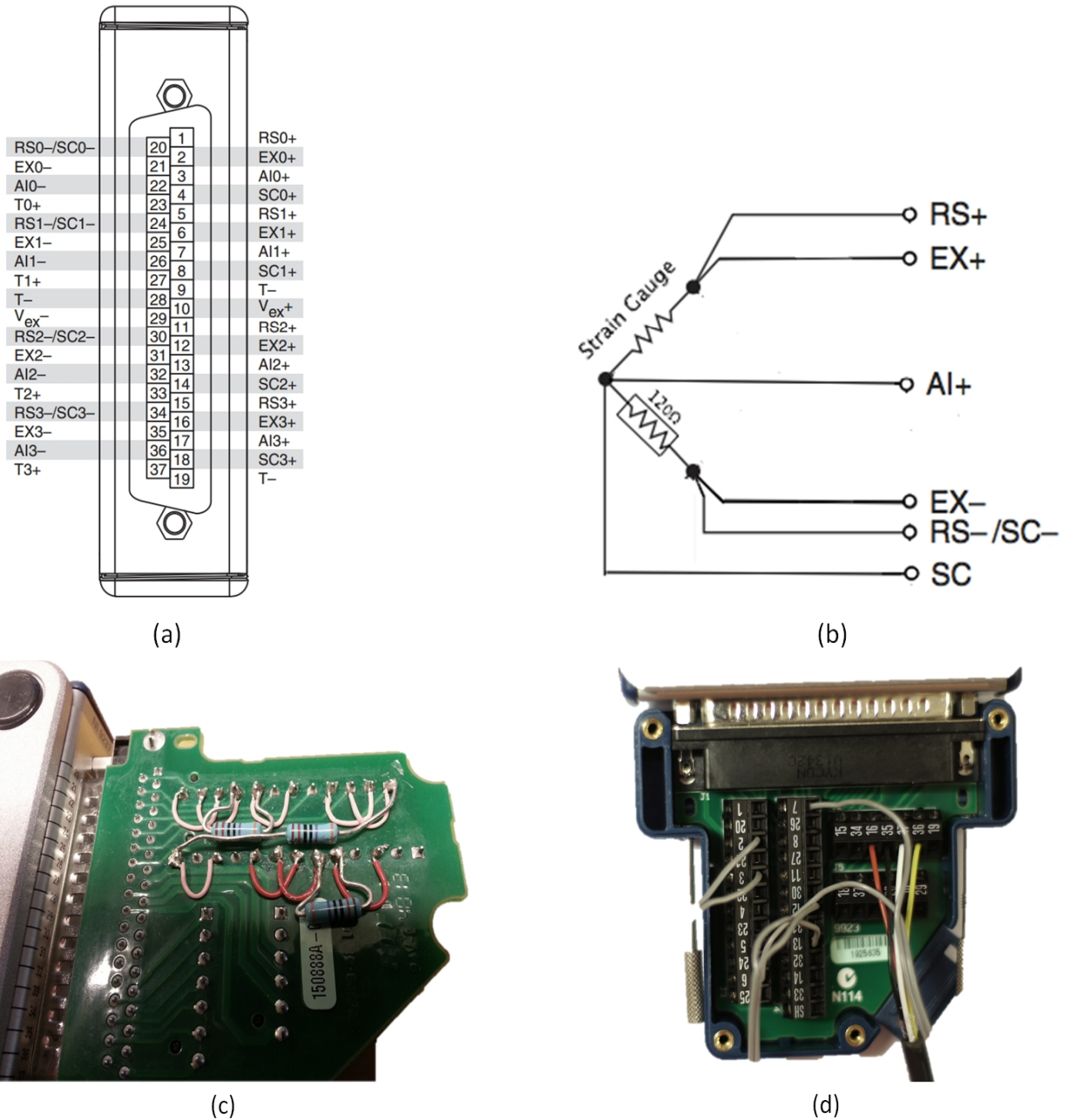


Figure 5.2: NI circuit board (a) NI 9237 with DSUB Pin Assignments; (b) Quarter-bridge circuit diagram; (c) The circuit on the NI circuit board; (d) NI 9923 37-Pin DSUB to Screw-Terminal Connector Block connected to strain gauges (grey cables) and loadcell (colored cables)

5.1.2.1 TC8 Load Cell

CTC8TM300KNI05 TC8 with 300 kN load has been chosen to be the ideal load cell for this project. This load cell gives high accuracy, hassle free installation and reliability. The accuracy class for this load cell is ISO 376. TC8 is ideal for space restricted environments and offer a high level of corrosive resistance. This load cell can be used to measure both tensile and compressive loads, where the load may come from compression to tension and vice versa, for more details see Appendix F.

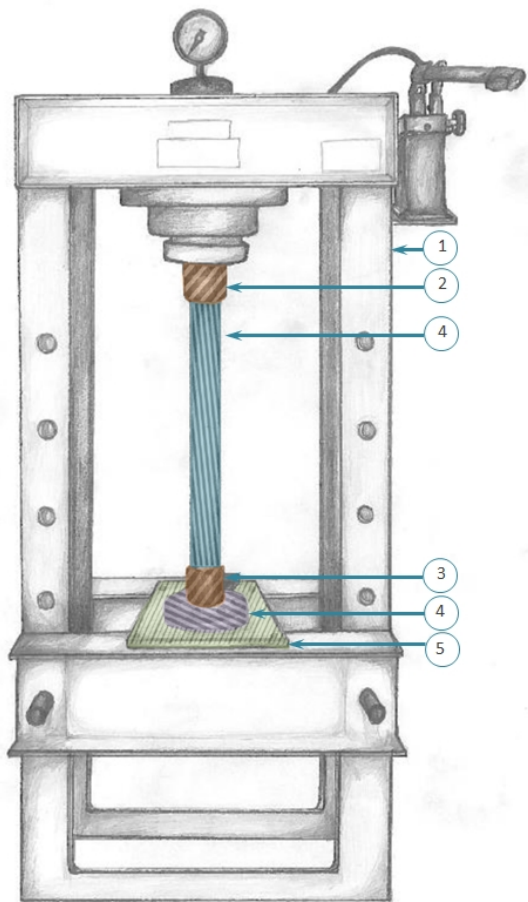
5.1.3 Test Setup and Procedure

The specimens are positioned vertically and connected to the hydraulic press by the BTEHP designed in the Specialization Project. The two ends of the specimens are connected rigidly with joints, realizing the external constraints. The upper joint has a part that can be adjusted in the horizontal plane and the required alignment with the lower one, establishing correct transmission of the load. The load should be applied to the center of the load cell and not to the external fixing rim. Test and calibrations performed in compression mode with this load cell will be mounted on a bearing support with correctly tightened clamping screws. The accuracy of the load cell performance was checked by comparing it to another load cell. The load cell performance depends considerably on inherent design features such as sensitivity to temperature, loading conditions and deflection.

After the specimen was aligned in the hydraulic press, the test was started at a loading of rate ca. 5 kN per minute. This rate was maintained well into post-buckling region until it was considered unsafe or not necessary to carry out any further deformation of the member. SignalExpress recorded load and strain with a rate of 1000 Hz at 1000 samples to read. The general view of the experimental setup is shown in Figure 5.3-Figure 5.4. Figure 5.3 shows a schematic representation of the upper and lower end joints.

5.1.3.1 Assembling of BTEHP

- I. Screw the Plate from HP (item 6) into the Hydraulic Press (item 1) with 4x set screws. This component is connected to the TC8 load cell by 42x3 mm metric threads and represents the lower end of the Setting Chamber Mandrel. This end is guided by the Sealing Cap in the HSU and allows axial rotation.
- II. Mount the load cell (item 5) upon the Plate for HP (item 6) with 2x M16 bolts, and connect the load cell (item 5) to the sensor measurement system.
- III. Screw the Test Part (item 4) into the Pinned Test Component for HP (item 2) and the Fixed Test Component for HP (item 3). Then, screw the Fixed Test Component for HP (item 3) into the load cell (item 5). Threaded ends facilitate easy installation. Ensure that the specimen is fully aligned.
- IV. Slide the Pinned Test Component for HP (item 2) onto the Hydraulic Press (item 1). Make sure that the parts are fully aligned.
- V. Make sure that the strain gauges are connected to the bridge circuit. (footnote: For test 4: The High-Temperature Strain Gauges should be used, as well as isolation is needed for the heat cable.)



- 1 Hydraulic Press
- 2 Upper Fixed Test Component for HP
- 3 Lower Fixed Test Component for HP
- 4 Test Part
- 5 Load Cell
- 6 Plate for HP

Figure 5.3: Test-setup in Interwell's premises.

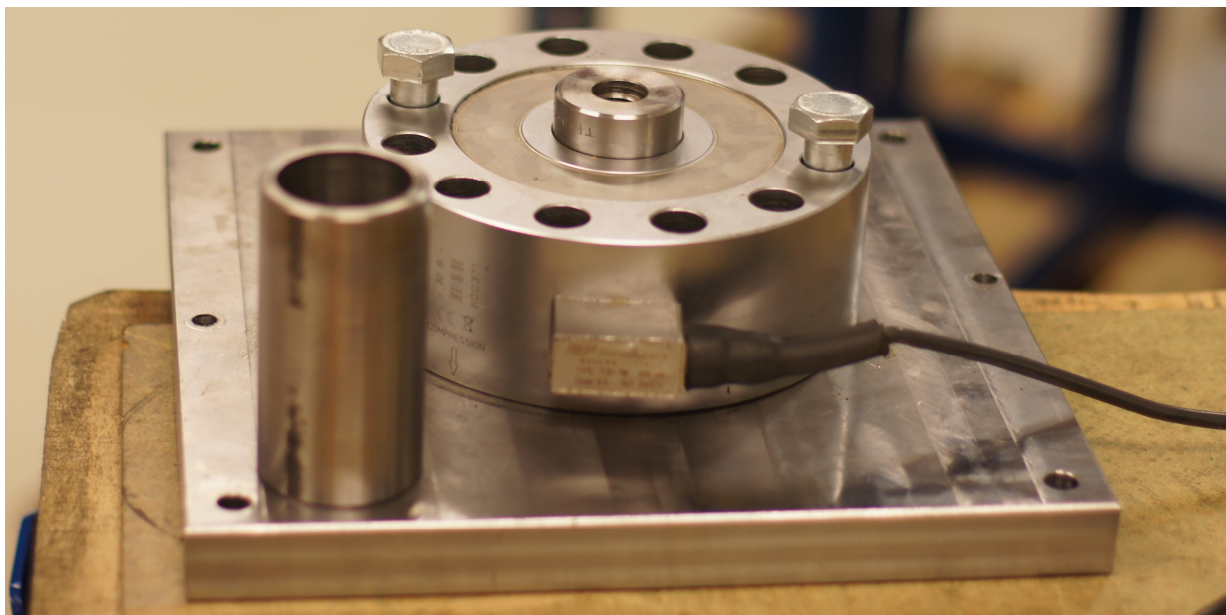


Figure 5.4: BTE connected to the load cell.

5.1.4 TEST 1: Length and Diameter

Consequently, in order to describe the inelastic buckling behavior the variation of deformation behavior following the change in slenderness ratio and the effects of deformation behavior due to buckling load must be known. Instability in the member may be defined in general terms as a condition in which the member has no tendency to return to its initial position when disturbed, even when the material is assumed to have an infinitely large yield stress. From intermediate member theory buckling will occur after the stress in the members exceeds the proportional limit of the material and before the stress reaches the ultimate strength. As it was mentioned previously the critical buckling load is associated with the state of neutral equilibrium, i.e., characterized by the stationary condition of the load with respect to displacement. The critical stress is the stress from the critical load and the critical length is the length at which the critical stress is achieved. The lengths of the test mandrels as well as the type of mounting determine the buckling length. The different effective lengths chosen for this study are respectively 476 mm, 344 mm, 296mm and 216 mm. The effective length can be considered as the length between the ends of mounting conditions where the moment is equal to zero. The influence of the diameter in the slenderness ratio is expressed by the radii of gyration, i , which takes both the minimum moment of inertia, I_{min} , and the cross-sectional area A into consideration:

$$i = \sqrt{I_{min}/A} \quad (25)$$

The geometric moment of inertia indicated the resistance against deflection resulting from cross-sectional shape of the member. The member will buckle in the direction of least resistance; hence the minimum geometric moment of inertia is the decisive factor. This experimental study focuses on four different configurations of the member with the same length but different diameters; 20 mm, 18 mm, 15 mm and 12 mm. The results are presented in Table 5.1 and Figure 5.6-Figure 5.8.

Buckling occurs suddenly with a large change in deformation but little change in loading, see Figure 5.9-Figure 5.12. The stress that causes buckling failure is substantially less than the force required for a direct compressive failure. The applied force from the hydraulic press causes compressive strain, which results in slightly shortening the member in the direction of the applied axial compressive force before buckling. For the test specimens with high slenderness-ratio the loss of stability occurs within the elastic range of the material and the axial shortening is detected only at the initial stages of loading, thus providing little warning of an impending failure. The test part with higher slenderness buckles at a significantly lower critical stress than the test parts with lower slenderness; with a failure stress closer to yield stress of the material. The manual hydraulic press makes it difficult to identify a gradual decrease in ratio of load to deflection in the loading process, which would imply that yielding occurred. The diameter has a great influence on buckling; a reduction in diameter of 33 % (20 mm to 15 mm) causes an increase in critical buckling load of about 50 %, see Figure 5.5. It is noticeable that the strength of the specimen increases as the slenderness becomes larger with increasing the diameter. A reduction in effective length of 13.9 %

from 344 mm to 296 mm (OD 15 mm) gives a decrease about 4 % in buckling force. This decrease in buckling force is about the same for the test specimen with an OD of 20 mm.

As the slenderness gets smaller, the difference in the test results obtained increases. The large deviation in the results can be traced down to four main reasons for discrepancy in the test results; measuring inaccuracy, material yielding, radial play in the test setup and initial curvature. The test specimen will probably see an eccentricity in loading, and if the load is not centered, and thus not equally distributed over the cross-sectional area, the likelihood of failure will increase. The last test of TP-000274-OD15 shows the lowest critical buckling load of the TP-000274-OD15 tests. The buckling shapes for the test parts of different geometry with the influence of an axial load are presented in Figure 5.13. The last test of TP-000274-OD15 was not conducted the same day, so the radial play between the parts in the hydraulic press could have an impact of the result, as well as the electronic instruments have reading to drift over time. The amount of drift is generally not a considerable concern, since some deviation in the test results are expected, but occasionally this source of error can be significant and should be considered. The curves in figure of TP-000272 could be explained by unattached strain gauges after buckling; hence the sudden drop in Figure 5.12c.

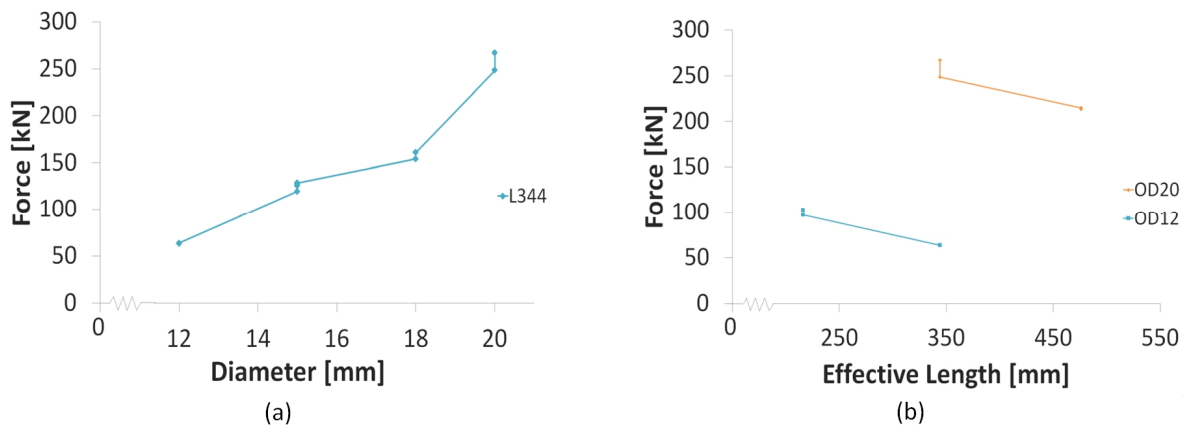
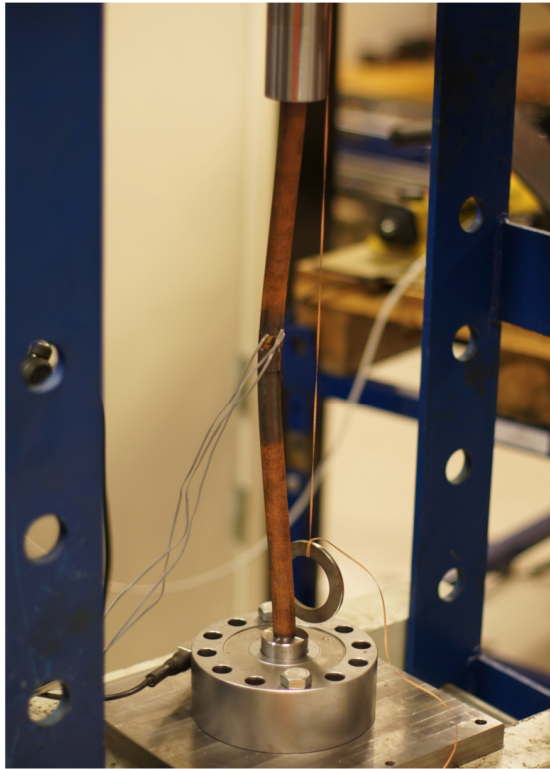


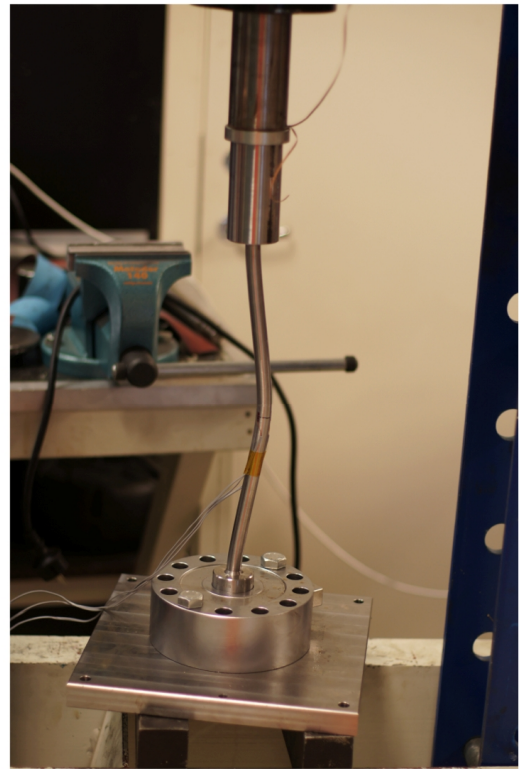
Figure 5.5: Influence of geometric attributes; diameter and effective length: (a) force-diameter curve for L_e of 344 mm (b) force-effective length curve for OD12 and OD20.

Table 5.1: Results from TEST1: length and diameter

Test Part #	L_e [mm]	OD [mm]	λ	Heat No	P_{cr} [kN]	% Deviation	σ_{cr} [MPa]
TP-000274-6-OD12	344	12	57.3	HT: 168232	63.3	0.5 %	559.7
TP-000274-7-OD12					63.6		562.3
TP-000272-1	476	20	47.6	HT: 168232	213.3	0.5 %	678.9
TP-000272-8					214.5		682.7
TP-000272-9					214.5		682.7
TP-000274-3-OD15	344	15	45.8	HT: 168232	125.4	7 %	709.6
TP-000274-4-OD15					128.4		726.7
TP-000274-5-OD15					127.4		720.9
TP-000274-10-OD15					119.4		675.6
TP-000274-16-OD15-L350	296	15	39.4	HT: 170807	121.2	0.3 %	685.5
TP-000274-17-OD15-L350					121.6		688.1
TP-000274-18-OD18	344	18	38.2	HT: 168232	160.9	4.2 %	632.3
TP-000274-19-OD18					154.1		605.6
TP-000273-11-OD12	216	12	36.0	HT: 168232	102.6	5.7 %	907.2
TP-000273-12-OD12					96.7		855.0
TP-000274-0	344	20	34.4	HT: 168232	266.9	6.9 %	849.6
TP-000274-13					248.5		791.0



(a)



(b)

Figure 5.6: Pictures from buckling in HP (a) TP-000272; (b) TP-000274-OD15.

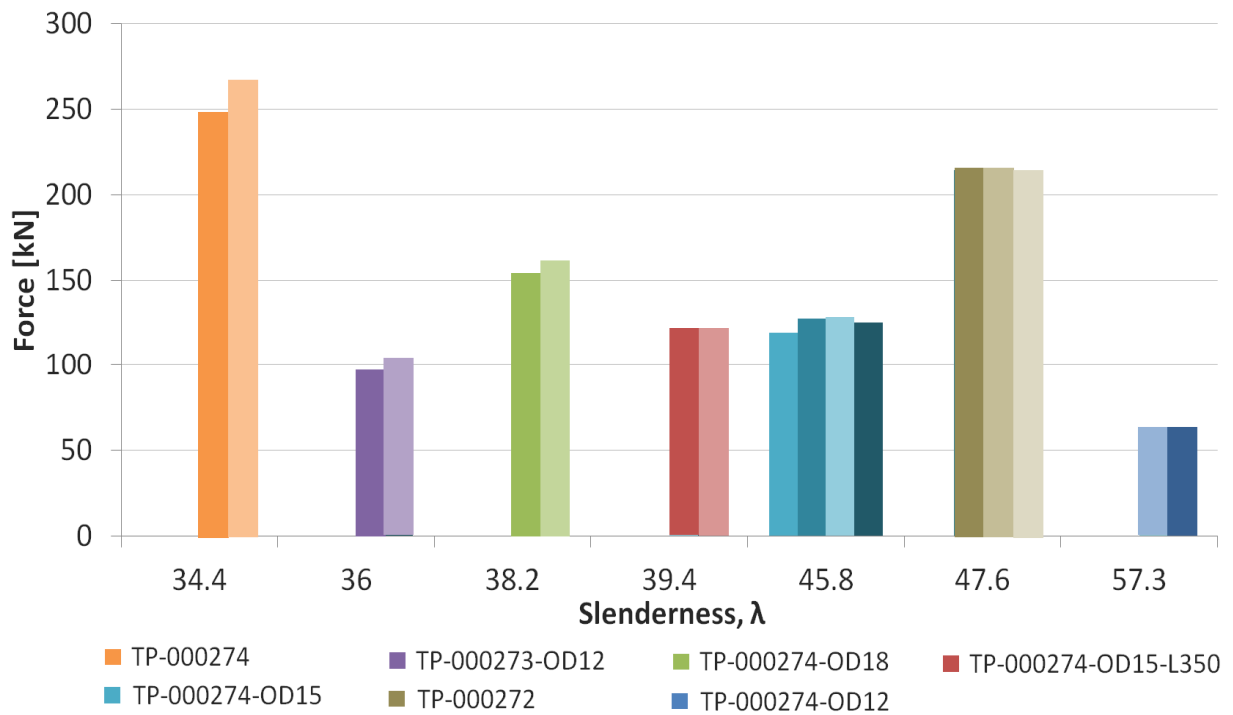


Figure 5.7: Results from TEST 1: length and diameter

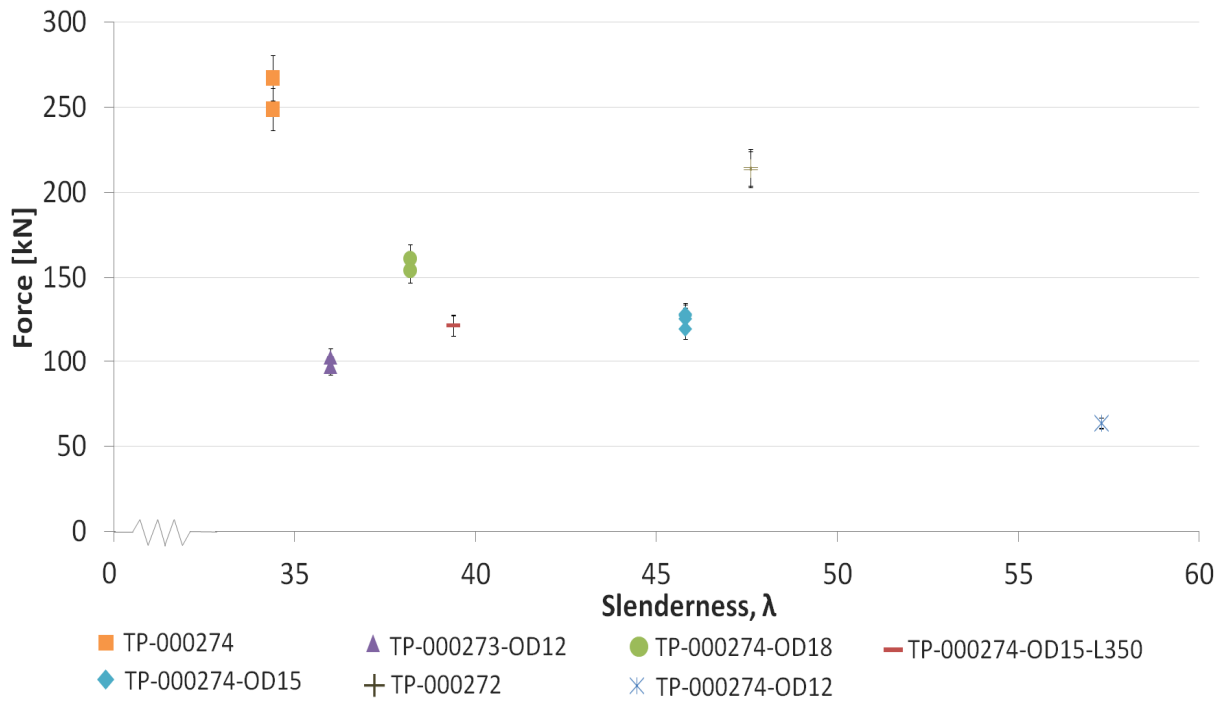


Figure 5.8: Results from TEST 1 with 5% error bars.

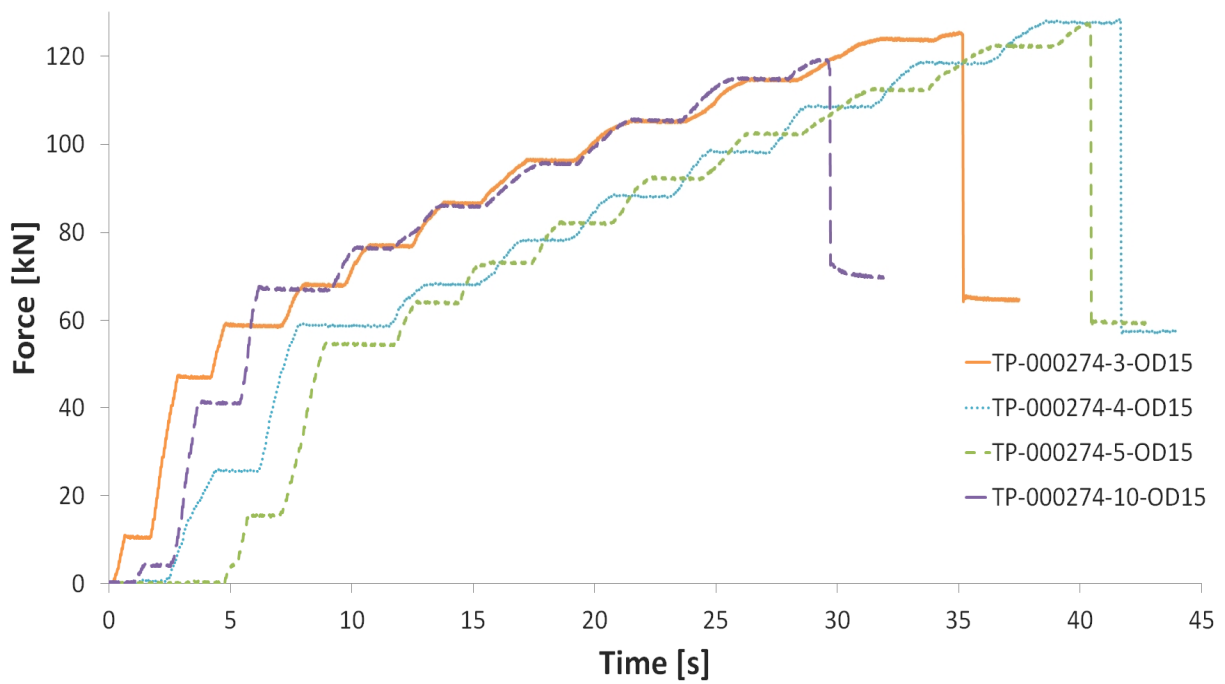


Figure 5.9: Force-time curves for TP-000274-OD15

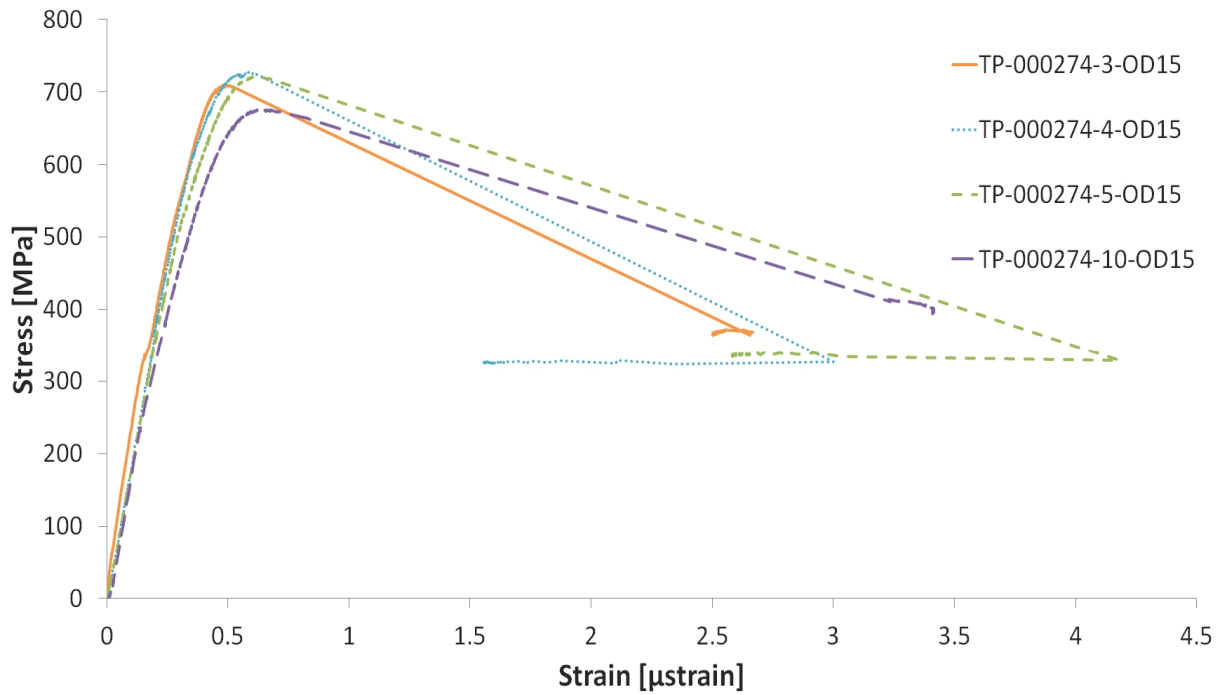


Figure 5.10: Stress-strain curves for TP-000274-OD15.

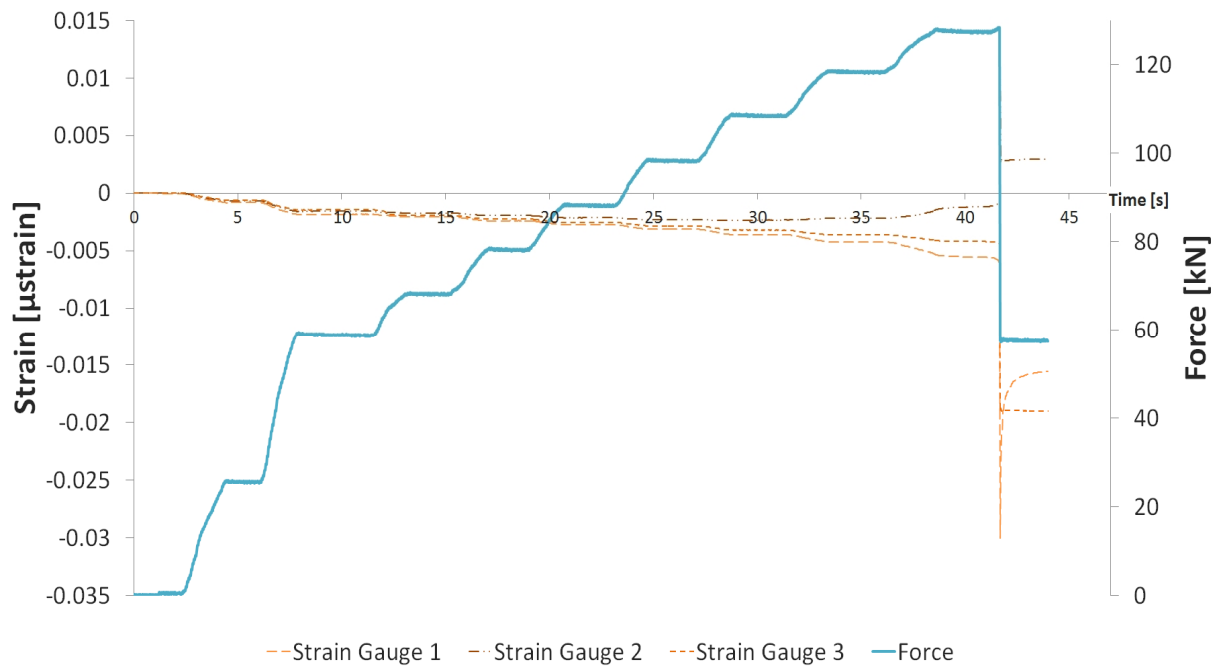
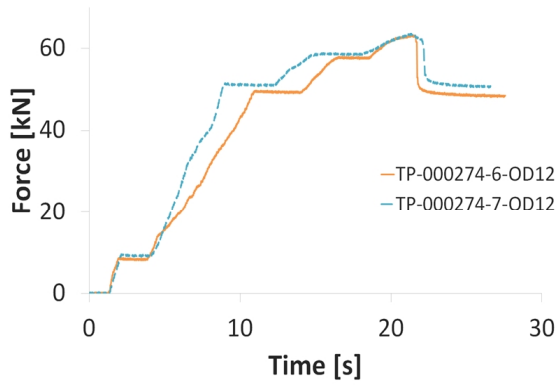
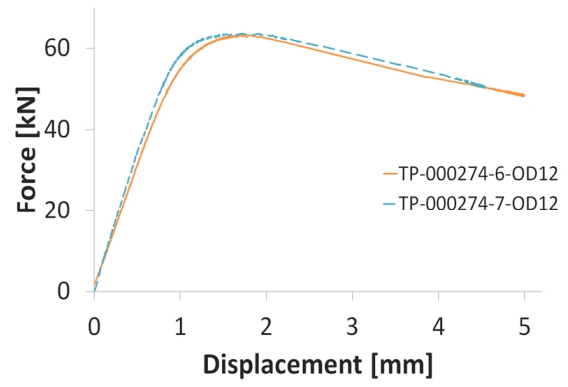


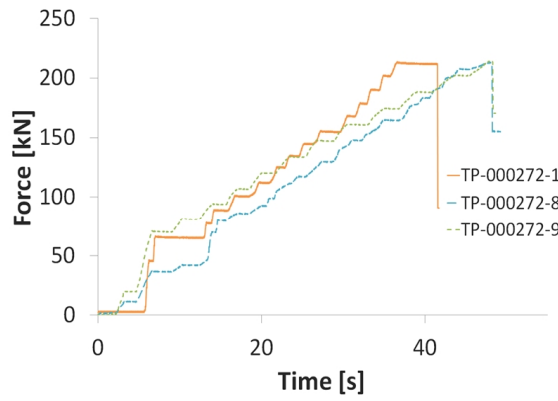
Figure 5.11. Strain-Time curves vs Force-Time curve for TP-000274-OD15



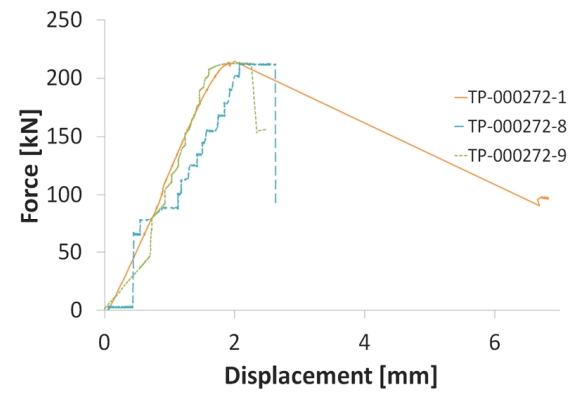
(a)



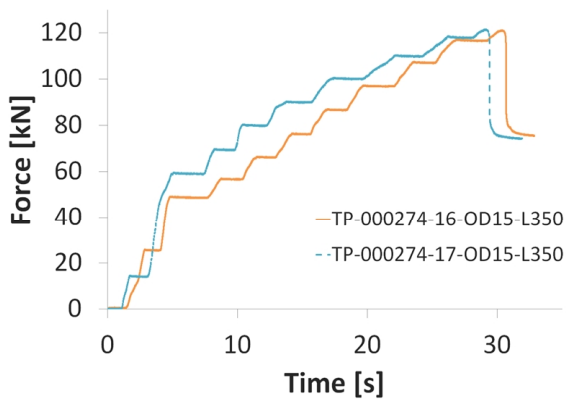
(b)



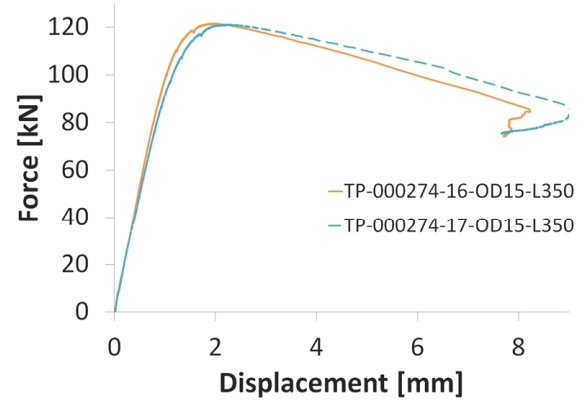
(c)



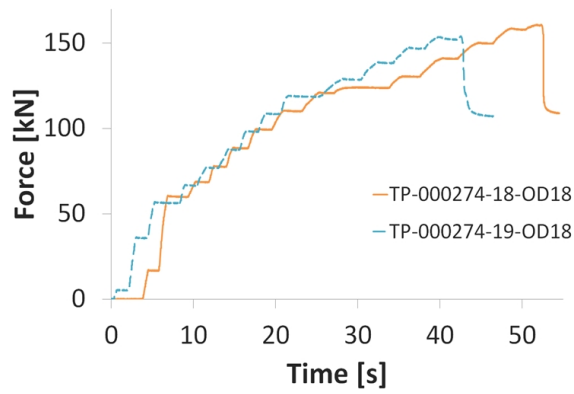
(d)



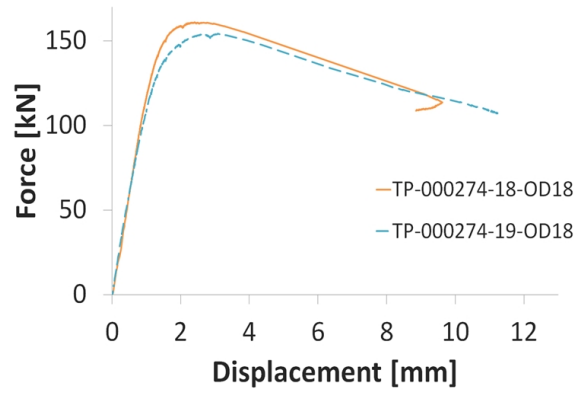
(e)



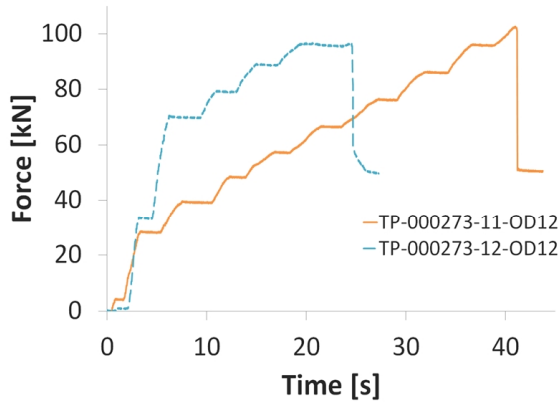
(f)



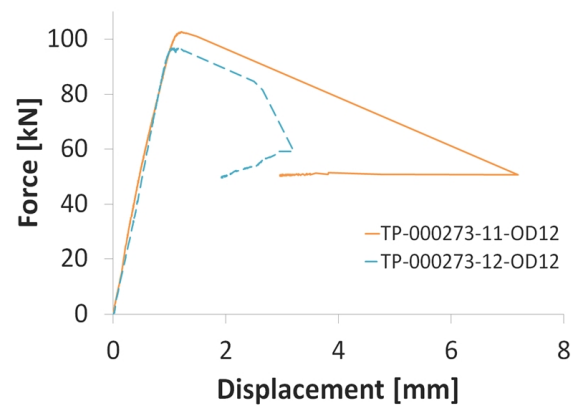
(g)



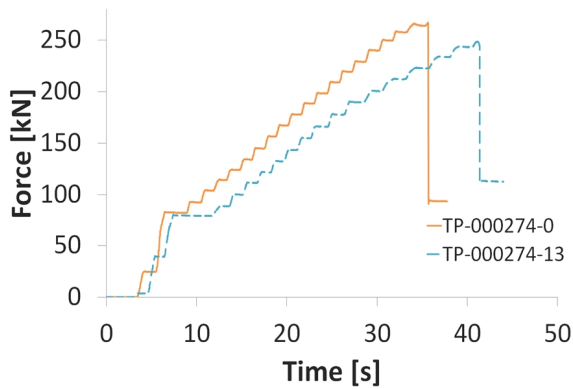
(h)



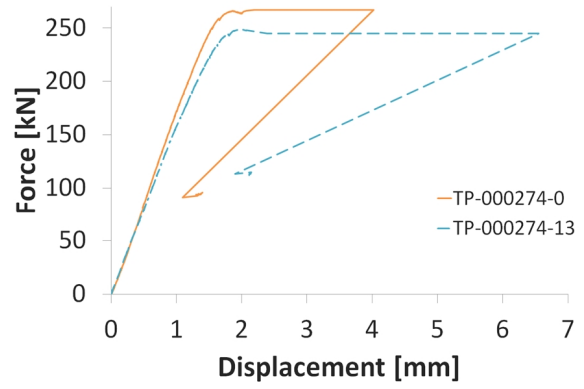
(i)



(j)



(k)



(l)

Figure 5.12: Force-time curves: (a) TP-000274-OD12; (c) TP-000272; (e) TP-000274-OD15-L350; (g) TP-000274-OD18; (i) TP-000273-OD12; (k) TP-000274. Force-displacement curves: (b) TP-000274-OD12; (d) TP-000272; (f) TP-000274-OD15-L350; (h) TP-000274-OD18; (j) TP-000273-OD12; (l) TP-000274.



(a)



(b)



(c)



(d)

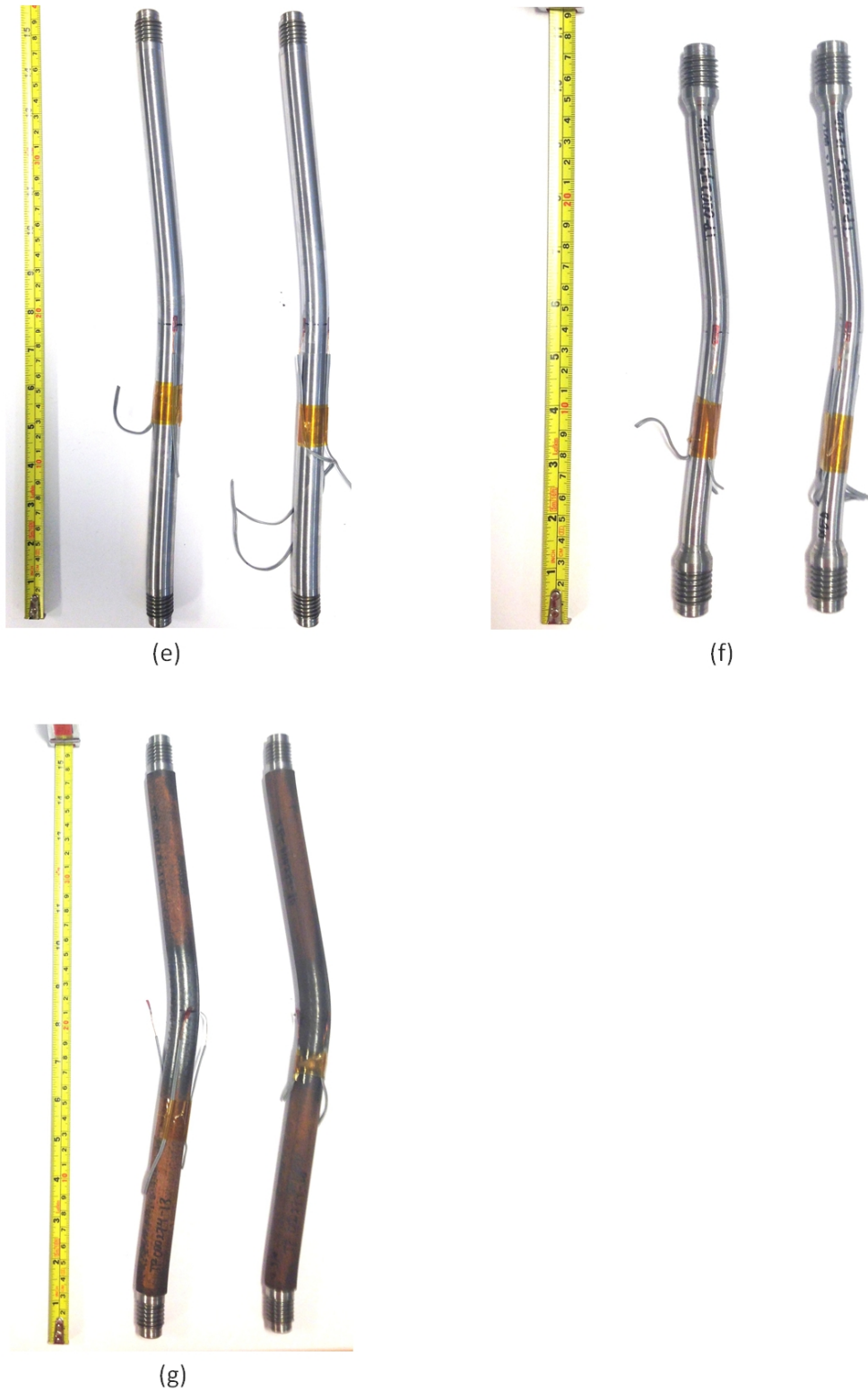


Figure 5.13: The buckling shapes for the test parts of different geometry with the influence of an axial load (a) TP-000274-OD12; (b) TP-000272; (c) TP-000274-OD15; (d) TP-000274-OD15-L350; (e) TP-000274-OD18; (f) TP-000273-OD12; (g) TP-000274.

5.1.5 TEST 2: Temperature

The Setting Chamber Mandrel should be prepared to operate in a range of temperatures, which may vary from subzero temperatures to temperature well above ambient temperature; 150 °C and 200 °C. This section is concerned with a comparison study on the influence of temperatures, and the results will be used to evaluate the influence of increased temperature on the Setting Chamber Mandrel. The material investigated is a high strength steel 34CrNiMo6 alloy. The high temperature tests were done with an electric heat cable and QFLA-5-11-6FA-1LT high temperature strain gauges. To make sure that the required temperature was reached, temperature readings with a thermometer and two steel temperature data loggers were connected to the test specimen, one at the center and one at the lower end over the load cell. The specimens were isolated with an outer jacket. The buckling test was conducted after the temperature distribution through the specimen was assumed to be linear; the thermometers showed equal values $\pm 3\%$.

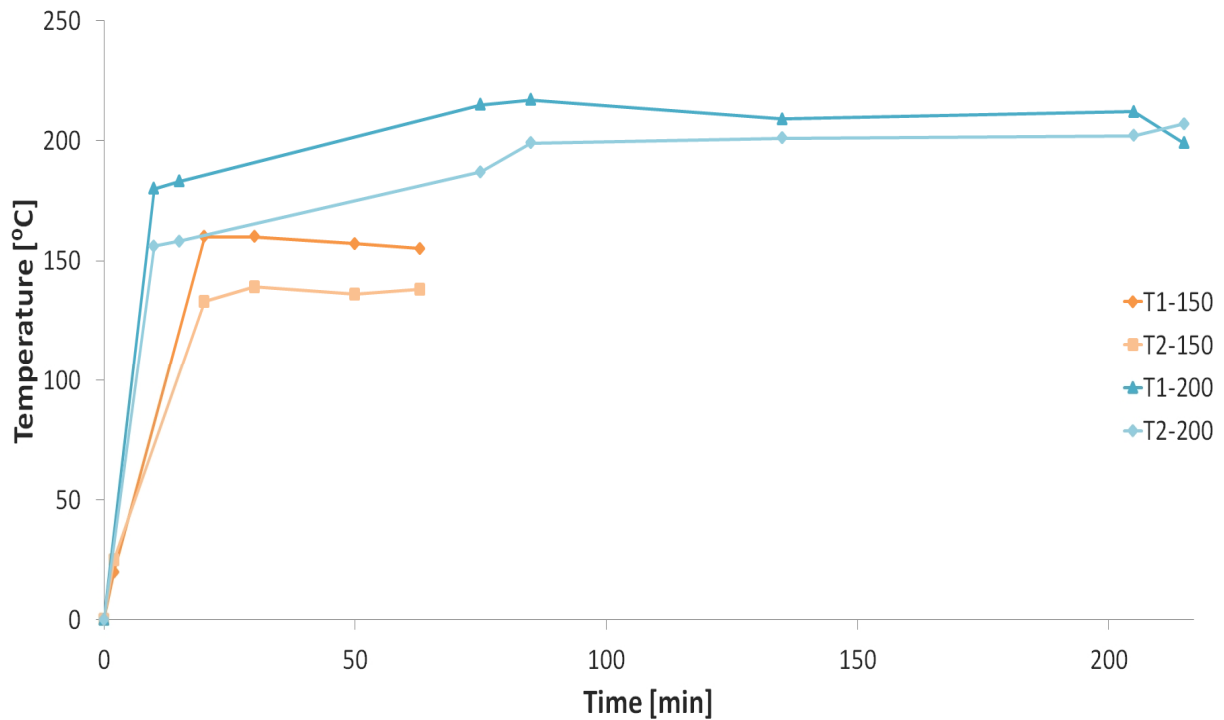


Figure 5.14: Temperature calibration: time-temperature curves for T1 and T2 sensor.

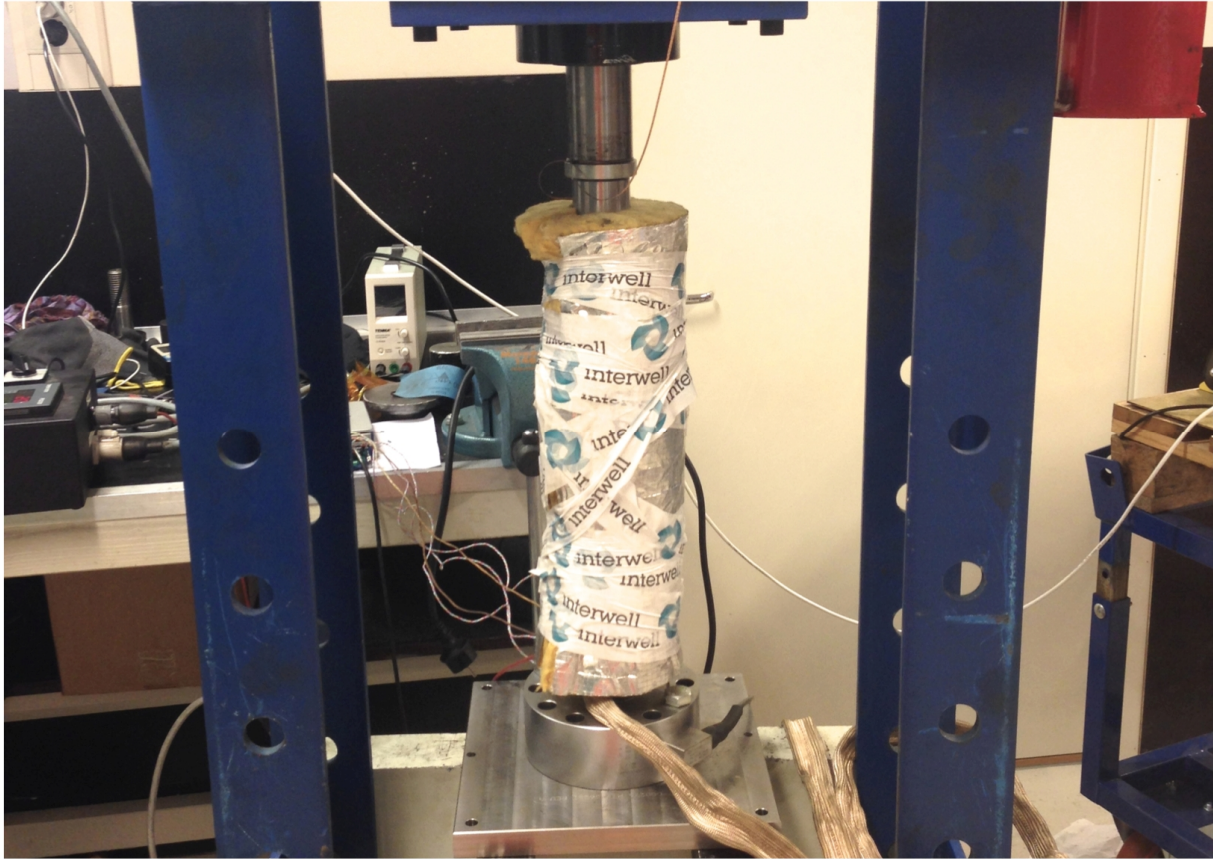
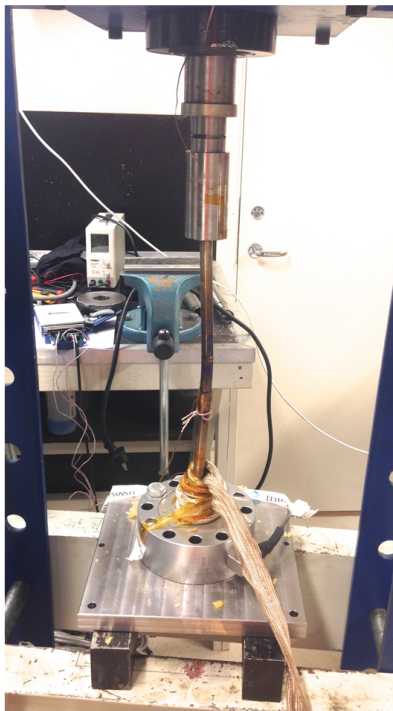


Figure 5.15: Test setup for temperature tests in Interwell's premises.

The Setting Chamber Mandrel must be designed in such way that it maintains its load bearing capability during the required temperature exposure. As the temperature of the steel increases, it expands. When a specimen is heated, the force holding the atoms together in bonds decreases as the bond length increases, causing a greater overall volume. The temperature affects the yield strength of the material, as well as the elastic modulus and tensile strength. It was expected that the critical load of the specimen would decrease when the temperature increased. From a temperature of 25 °C to 150 °C the results show a decrease of 12.2% in critical load, and from 25 °C to 200 °C there is an unexpected decrease of 8.9 % in critical buckling load, 3.3% less than the T150 test. The temperature effect on the load cell during the T200 test could be a reason for the increase in loading during the second test. The magnitude of the outcome depends not only on the load cell, but also on the test setup; i.e. isolation, strain gauge mounting, which may lead to a compromise of test specimen or system capabilities. It would be desirable to carry out more tests with temperature well above ambient temperature, but lack of time and test parts made it difficult. However, the trend from these tests show that temperature has a considerable impact on the critical load and 10 % reduction in critical buckling load from ambient temperatures should be expected and included in the global safety factor. The temperature change has no visual effect on the buckling mode shape compared to the length and diameter test results of TP-000274-OD15 with the same geometric attributes, Figure 5.16.

Table 5.2: Results from TEST 2: temperature tests compared with TP-000274-4-OD15

Part Number	L_e [mm]	OD [mm]	Heat No:	$P_{cr,T}$ [kN]	$\frac{P_{cr,T}}{P_{cr,25^\circ C}}$	σ_{cr} [MPa]
TP-000274-15-OD15-T200	344	15	HT: 168232	112.7	0.88	637.7
TP-000274-15-OD15-T200	344	HT: 168232	117.0	0.91	662.1	
TP-000274-4-OD15	344	15	HT: 168232	128.4	-	726.6



(a)



(b)

Figure 5.16: Test results from TEST 2 (a) TP-000274-OD15-T200 after buckling; (b) TP-000274-OD15-T150 to the left and TP-000274-OD15-T200 to the right

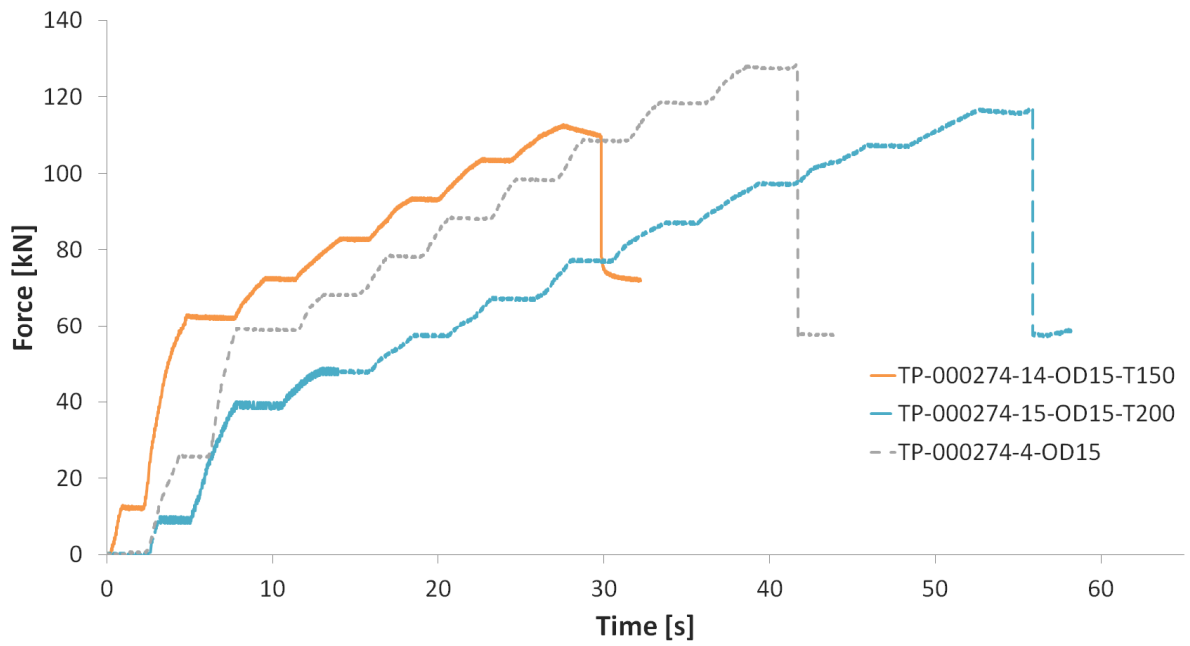


Figure 5.17: Force-time curves for TP-000274-OD15-T150, TP-000274-OD15-T200 and TP-000274-4-OD15

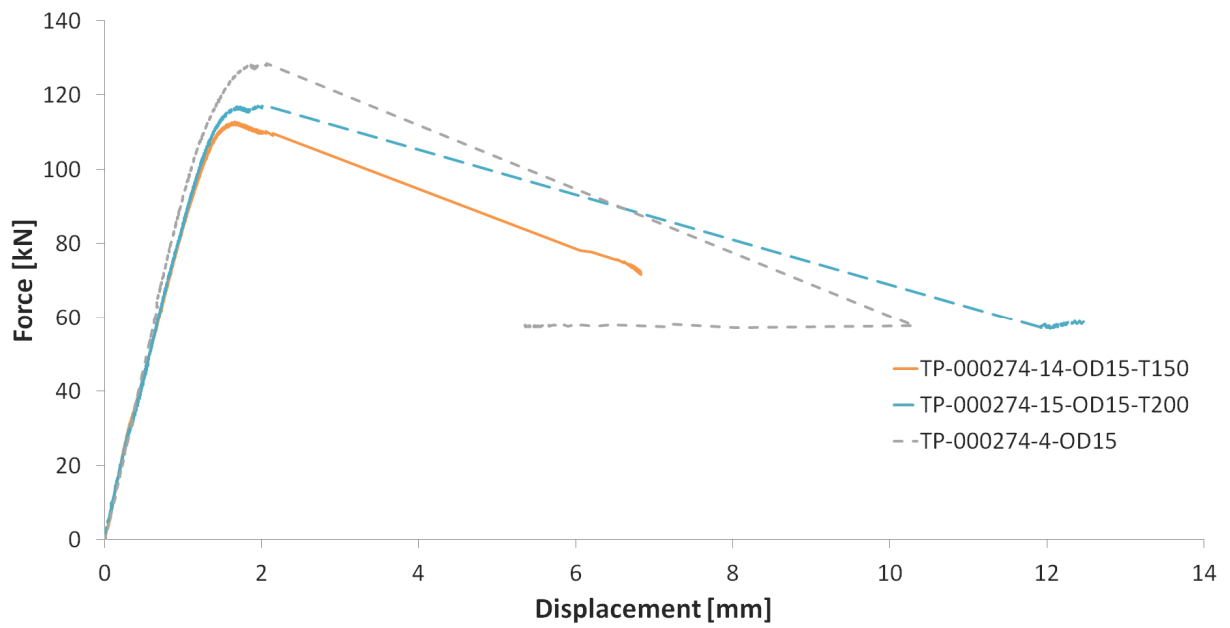


Figure 5.18: Force-displacement curves for TP-000274-OD15-T150, TP-000274-OD15-T200 and TP-000274-4-OD15

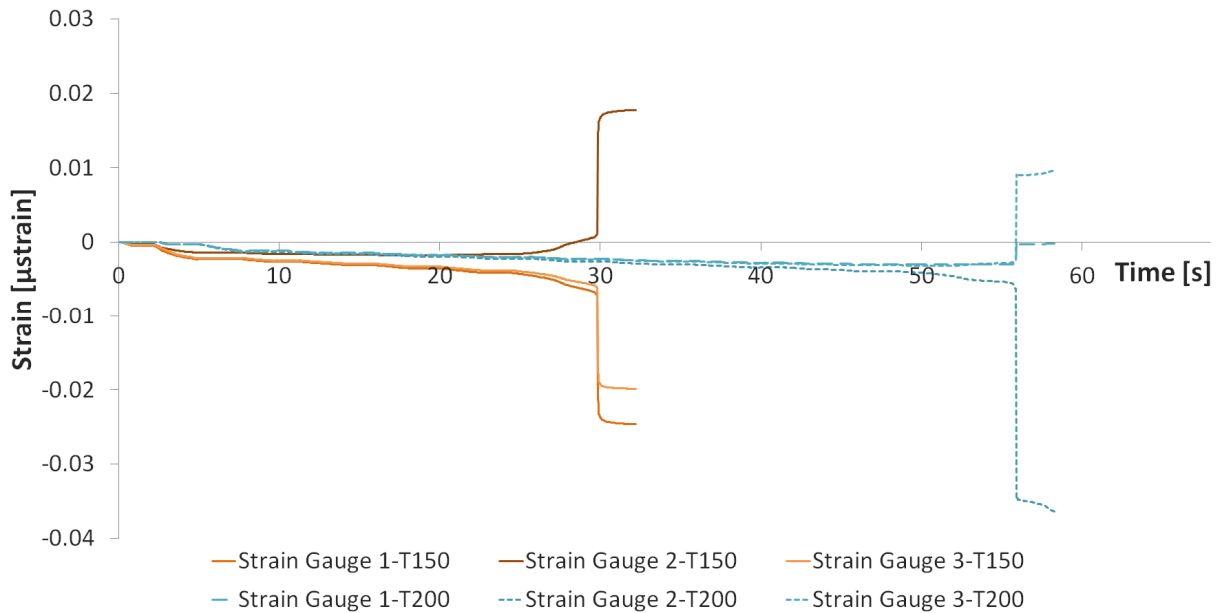


Figure 5.19: Strain-time curves for TP-000274-OD15-T150 and TP-000274-OD15-T200

5.2 Buckling in Test Casing

The Buckling Test Equipment for Test casing, BTETC, is designed for testing with simulated well pressure, see Figure 5.20. The purpose with this test is to ensure that the Setting Chamber Mandrel with requirements regarding functionality, quality and safety prior to being accepted into Interwell's tool pool and being put to use, as well as provide proper documentation. The 10,000 psi test casing enables the mechanical integrity of the Setting Chamber Mandrel to be evaluated by simulating the applied load from operation in well pressure. Two end joints were specially designed and realized in the Specialization Project in order to create the end restraints of the specimens, and at the same time connect them to the 2.70" HSU. The correct connections are utilized based on the anticipated condition to ensure that coupling integrity will not affect the overall integrity.

5.2.1 TEST 3: Well Pressure

The 2.70" HSU well test pressure was conducted in a test pit with water pressure equipment. The chamber between pressure intake cylinder and intake cylinder piston was filled with water and as much air as possible was evacuated. The 1.48" Trigger Mechanism and the 1.40" Electronics Cartridge prevented the water and pressure from entering the 2.70" HSU until being activated. Activation was done by a manually activated plunger system that triggered a timer sequence in the Electronic Cartridge. For this study the timer sequence was set to one hour. Once the 2.70" HSU was activated, an electric motor served as an actuator for the Trigger Mechanism that in turn retracted a barriers valve pin allowing water to access the tool. The 2.70" HSU was connected to the water pressure test facility and logging equipment. The

assembling of the 2.70" HSU was done accordingly to Interwell's technical manual, TM HSU270SP02XX [18].

In order to keep the 2.70" HSU intact until stroking a shear screw with a reducer fitting was connected to the sealing cap, see Figure 5.21. The calculations used to determine the cross-sectional area and diameter for the shear screw were estimated from the piston pressure; 18.85 kN/1000 psi, which gave 6650 psi for a critical buckling load at 125 kN. The value of pressure was estimated from an anticipated critical buckling load at 125 kN from static compression in the hydraulic press. The diameter of the rod of the shear screw was chosen to allow the shearing action at half the buckling load, 62.5 kN. The calculations give an area of 79.5 mm² and a diameter of 8.9 mm, so a M12 shear screw ($A_s = 84.3 \text{ mm}^2$, $\phi_D = 9.72 \text{ mm}$) was chosen. The force needed to cause the M12 shear screw to shear was conducted from the first test; 248.6 bar.

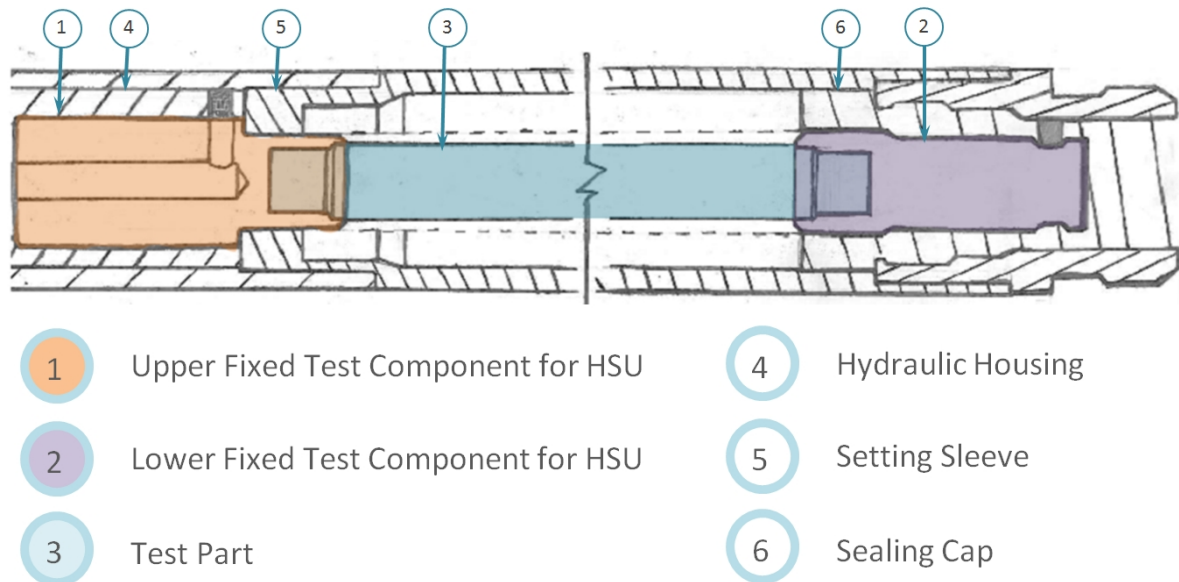


Figure 5.20: Assembly of Buckling Test Equipment for HSU

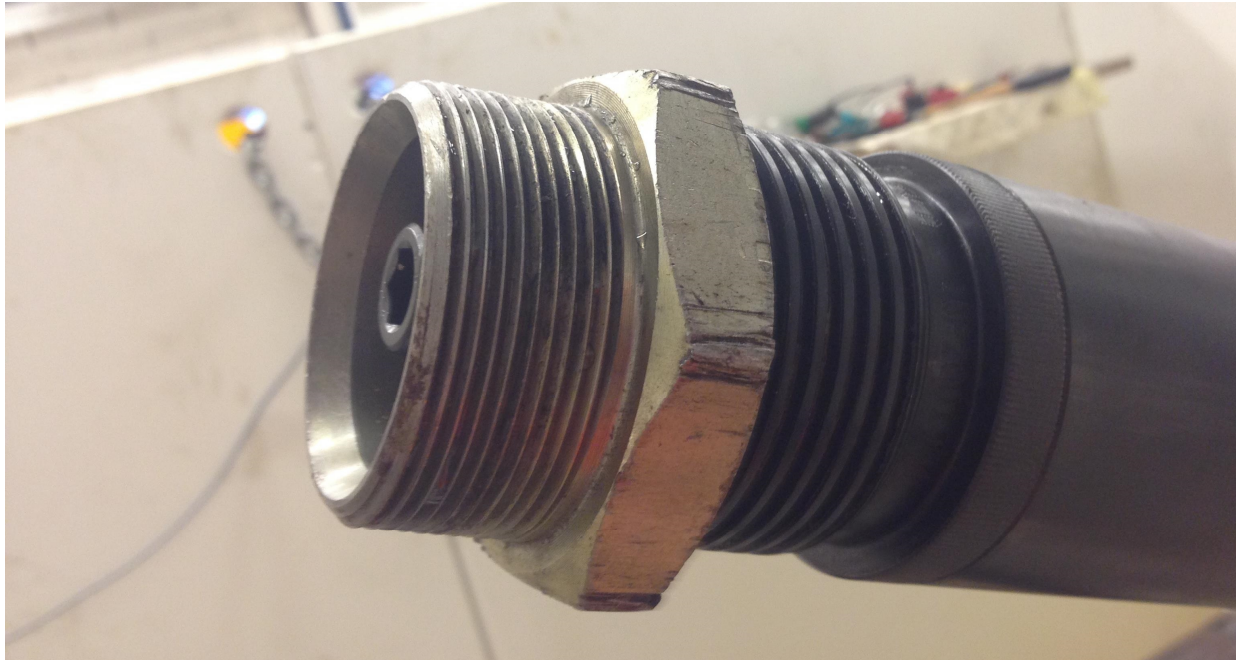


Figure 5.21: Shear screw with a reducer fitting connected to the sealing cap.



(a)



(b)

Figure 5.22: Test setup from Interwell's workshop (a) test part in 2.70"HSU; (b) 2.70" HSU to the left and test casing to the right.

The test specimen was pressurized up to a predetermined load, before isolated until the timer was done. After disassembling a visual inspection of the test specimen was done. No visual deformation could be detected, see Figure 5.25. The specimen withstood the load of 289 bar without showing signs of deformation. It is noticeable that the drop of each test is different, which made it difficult to conduct the tests with right pressure. The highest pressure applied without buckling was 389.3 bar = 106.4 kN, which is equal to 94 % of the static compression buckling load and 89 % of the critical load obtained from the TP-000275-OD15 tests in the HP. The main reason for the discrepancy in the test results obtained is not obvious, but optimized boundary condition in HSU is probably an essential factor.

Table 5.3: Results from TEST 3: Well pressure

TEST #	Pressure [bar]	Drop	P _{cr} [bar]	Static Compression Test in HSU, P _{cr}	
TP-000274-OD15-T1	266.1	17.5	248.6	-	
TP-000274-OD15-T2	321.2	26.6	294.6	-	
TP-000274-OD15-T3	354.4	31.8	322.6	-	
TP-000274-OD15-T4	391.6	51.7	339.9	-	
TP-000274-OD15-T5	436.1	46.8	389.3	-	
TP-000274-OD15-T6	437.4	55.6	381.8	-	
TP-000274-OD15-T7	459.1	84.4	374.7	-	
TP-000274-OD15-T8	405.9	3.2	402.7	412.0 bar	112 kN
TP-000274-OD15-T9	504.1	4.9	499.2	416.6 bar	113.7 kN

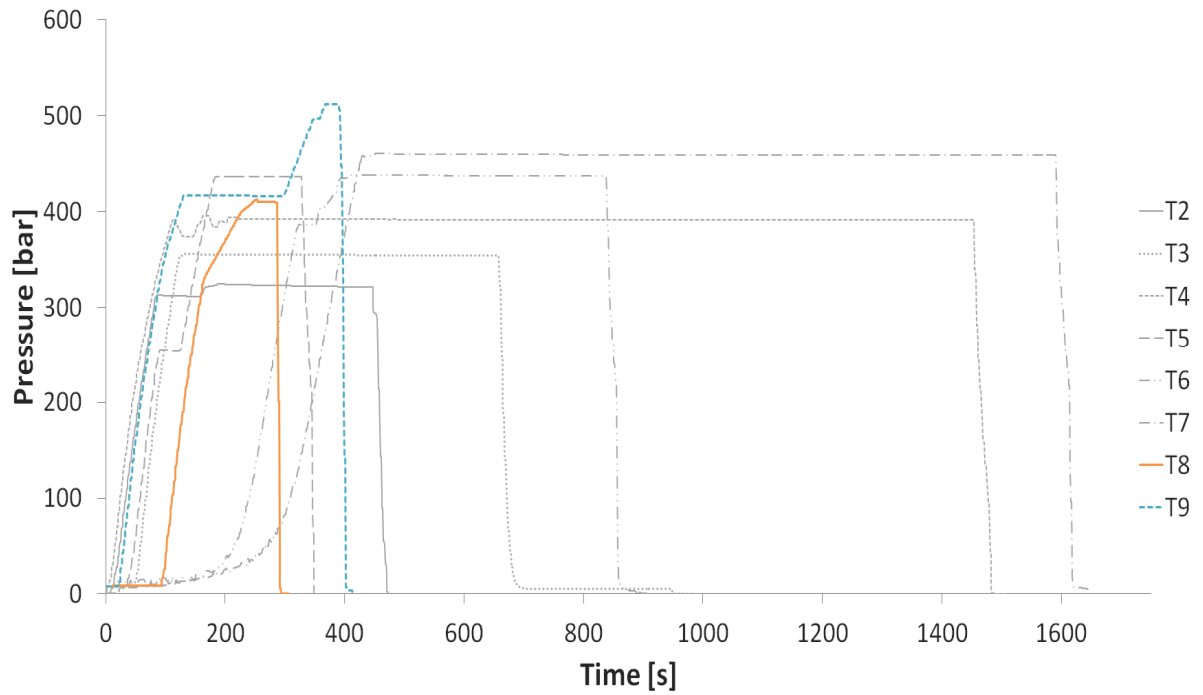


Figure 5.23: Pressure-time curves for the different tests in the 2.70'' HSU

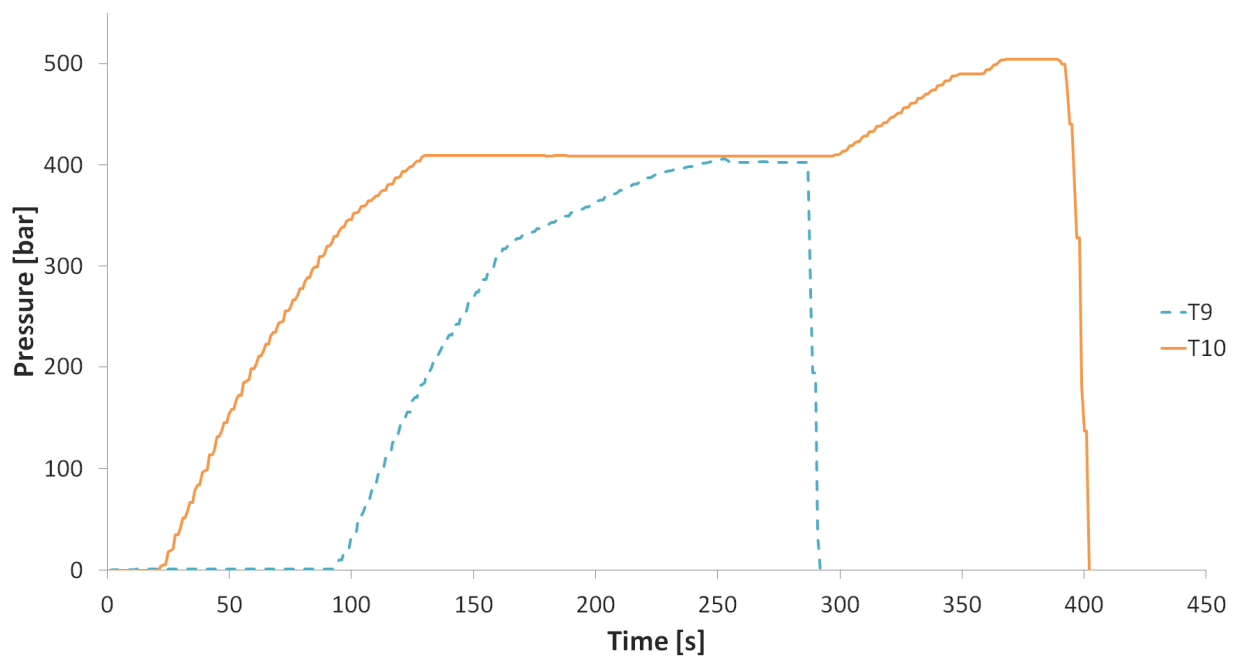
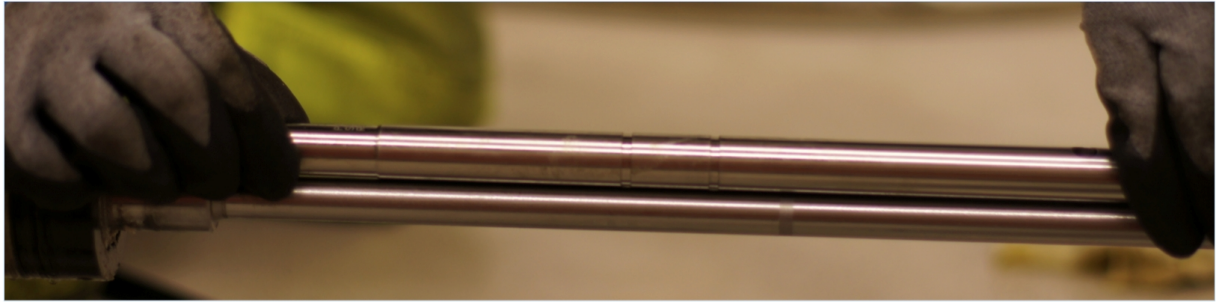
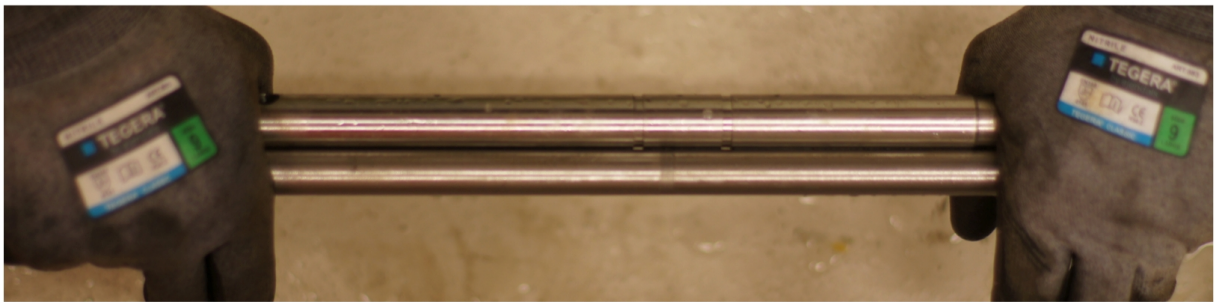


Figure 5.24: Pressure-time curves for the static compression test in 2.70'' HSU.



(a)



(b)



(c)

Figure 5.25: Before and after critical load for buckling test in test casing (a) TP-000274-OD15-T1; (b) TP-000274-OD15-T5; (c) TP-000274-OD15-T6



(a)



(b)

Figure 5.26: Results after static compression test in HSU (a) TP-000274-OD15-T9; (b) TP-000274-OD15-T8 compared with TP-000274-10-OD15.

CHAPTER 6

6 Discussion

This study introduces buckling in the context of axially compressed members and identifies the parameters governing buckling behavior. The challenge consists of a metal cylinder that is fixed-fixed and subjected to a uniaxial distributed compressive load. The buckling load of the Setting Chamber Mandrel was investigated by means of FE-analysis in Abaqus 6.12 and test performed in Interwell premises. Four kinds of buckling analyses were conducted in Abaqus; a linear elastic eigenvalue buckling analysis, a nonlinear static large deformation buckling analysis (one with elastic material properties, and one with plasticity properties added to the material) and a nonlinear Riks buckling analysis. In order to conduct the analysis, both the geometry of the Setting Chamber Mandrel, loading and support conditions and the orthotropic properties was idealized by means of a numerical model in Abaqus. The results from Abaqus were compared with the experimental results and the results from NS-EN 1993-1-1:2005. Stability of the test members have been analyzed by computing its buckling load, i.e., the load corresponding to the situation in which a perturbation of the deformation state does not disturb the equilibrium between the external and internal forces [19]. The experimental tests and analyses are a part of an optimization problem where the objective function is to minimize the gap between the numerical and the experimental results and find safety factors that can be used to optimize Interwell's Down Hole Equipment. The final results are represented in Table 6.1 (Note that the most conservative results from the experimental study is chosen).

Research from the literature study combined with the analysis has revealed some fundamental and unexpected features of the members behavior under axial compressive load. It should be noted that the terms short, intermediate and long are relative and defined by interpretation of their slenderness ratio. Based on the available data, all the FE-analysis with linear elastic material properties overestimate the load carrying capacity of the members with intermediate length. This overestimation may be of different reasons; initial curvature, accidental eccentricity, residual stresses or simplification in end restrains. The linear eigenvalue buckling theories consider the members to be ideal with no initial imperfections, while experimentally there are many parameters that will affect the critical load. The differences including variability in the Abaqus analysis are most likely related to assumed imperfections in the model. Typically, for intermediate members with higher slenderness ratio buckling occurs before the material begins to yield, hence linear elastic material properties are acceptable for such buckling analyses. However, the results for the lower slenderness member from the nonlinear buckling analysis are not in correlation with the linear theory because the critical load predicted will not be reached, since plastic

deformation or material failure takes place before this point. As a consequence, the cross-section remains elastic until it achieves deformation corresponding to the yield strength in the material. Under increasing loads, the member undergoes gradual plastification until maximum strains are achieved for compression.

A series of experimental tests on the members have been carried out to verify the theoretical results obtained from Abaqus. The experimental results obtained from the testing are in reasonable agreement with the theoretical predictions, see Table 6.1. When comparing the results from the analyses with the experimental study it is evident that the nonlinear static buckling analysis shows more agreement than linear eigenvalue buckling analysis, especially nonlinear static general analyses with plastic material properties. The nonlinear static analyses with plastic material properties estimates the results with a difference of $\pm 20\%$ compared to the experimental results, with a mean difference of 11% . The FE-results from the other FE-analysis compared to the experimental results shows high dispersion ranging from -11% to 114% , see Figure 6.1 and Figure 6.2. NS-EN 1993-1-1:2005 consequently estimates the results to be lower than the experimental result with only one exception: TP-000274-OD18, which is overestimated with a 13% difference. When excluding the results from TP-000274-OD18 NS-EN 1993-1-1:2005 estimates the results to be lower with a difference ranging from 20% to 32% and a mean difference of 25% . It is difficult to find a reasonable explanation for this discrepancy and more tests with this model should be conducted to make sure that the dimensional tolerance, load cell calibration and configuration alignment are within the exactable limit for experimental studies in Interwell's premises. The test results from TEST 1: length and diameter for TP-000274-OD18 will not be included in the calculation of safety factors. As the slenderness increases the interaction effect from imperfections and test-setup becomes more significant and the design standard NS-EN 1993-1-1:2005 become less conservative. The actual applied forces and the resulting displacement at all equilibrium states from the nonlinear static analysis are sampled and plotted against the test data as load-displacement curves, which are shown in Figure 6.4 and Figure 6.5 respectively. Further investigation of imperfection would be required to get better agreement between the experimental study and the analysis results.

The results obtained from the experimental tests shows a proportional limit well below the yield plateau obtained from the uniaxial tensile test for the specimens with low slenderness. The material of the member will diverge from a linear stress-strain behavior. The test part with higher slenderness buckles at a significantly lower critical stress than the test parts with lower slenderness; with a failure stress closer to yield stress of the material. It is clear that the critical load and critical stress are depending on geometric properties. The smaller the effective length is for member with the same OD, the smaller its danger of lateral buckling and the greater its load carrying capacity. The cross-sectional properties that are important regarding buckling are; cross-sectional area, moment of inertia and radii of gyration. From the experimental results it is shown that immediately before buckling occurs, the displacement increases with the same rate of loading until the buckling load is reached.

Table 6.1: Overview over the final results from experiment, NS-EN 1993-1-1:2005 and FE-analyses.

Part Number	Experiment HP [kN]	NS-EN 1993-1-1:2005 [kN]	Linear eigenvalue [kN]	Nonlinear Static [kN]	Nonlinear Riks [kN]	Nonlinear Static -EP [kN]
TP-000274-OD12	63.3	47	66.7	55.9	62.8	50.6
TP-000272	213.3	147	259.9	216.3	228.0	200.2
TP-000274-OD15	119.4	91	161.1	129.4	155	111.6
TP-000274-OD15-L350	121.2	102	215	173.8	212.7	127.7
TP-000274-OD18	154.1	174	329.2	298.6	212.2	180.0
TP-000273-OD12	102.6	69	165.9	135.2	163.5	82.4
TP-000274	248.5	199	482.3	439.7	493.5	255.4

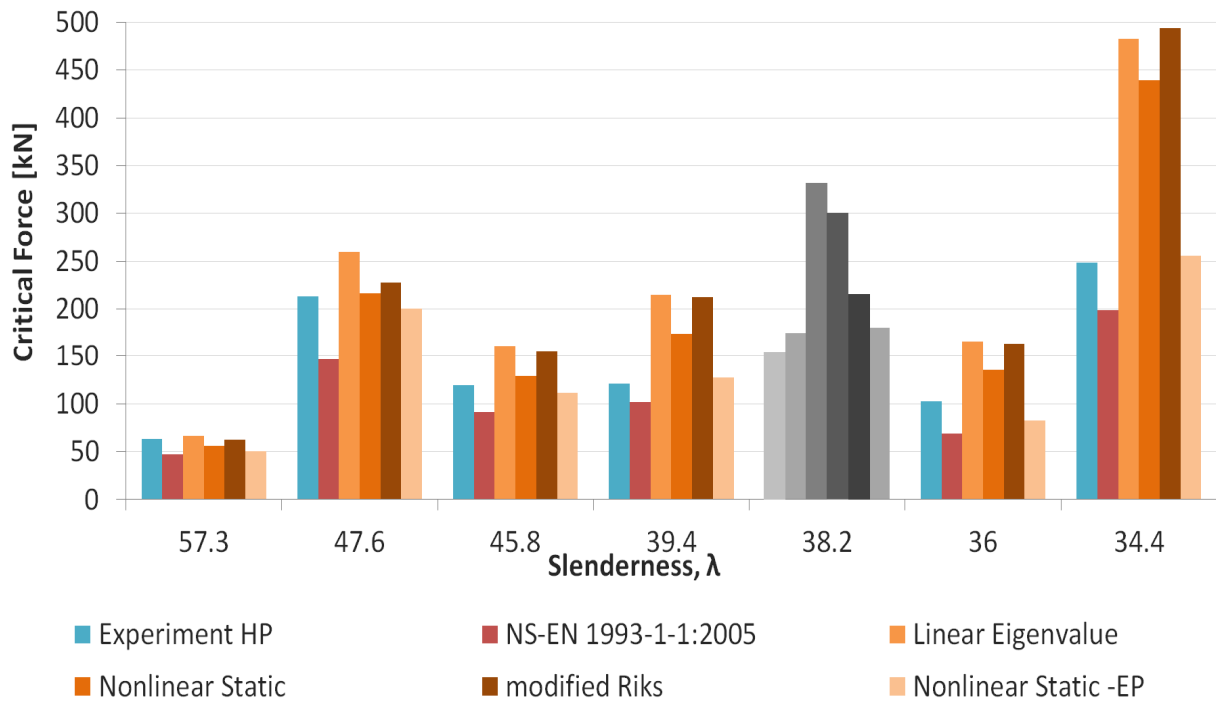


Figure 6.1: Comparison between the different critical forces obtained vs the slenderness ratio for each test part.

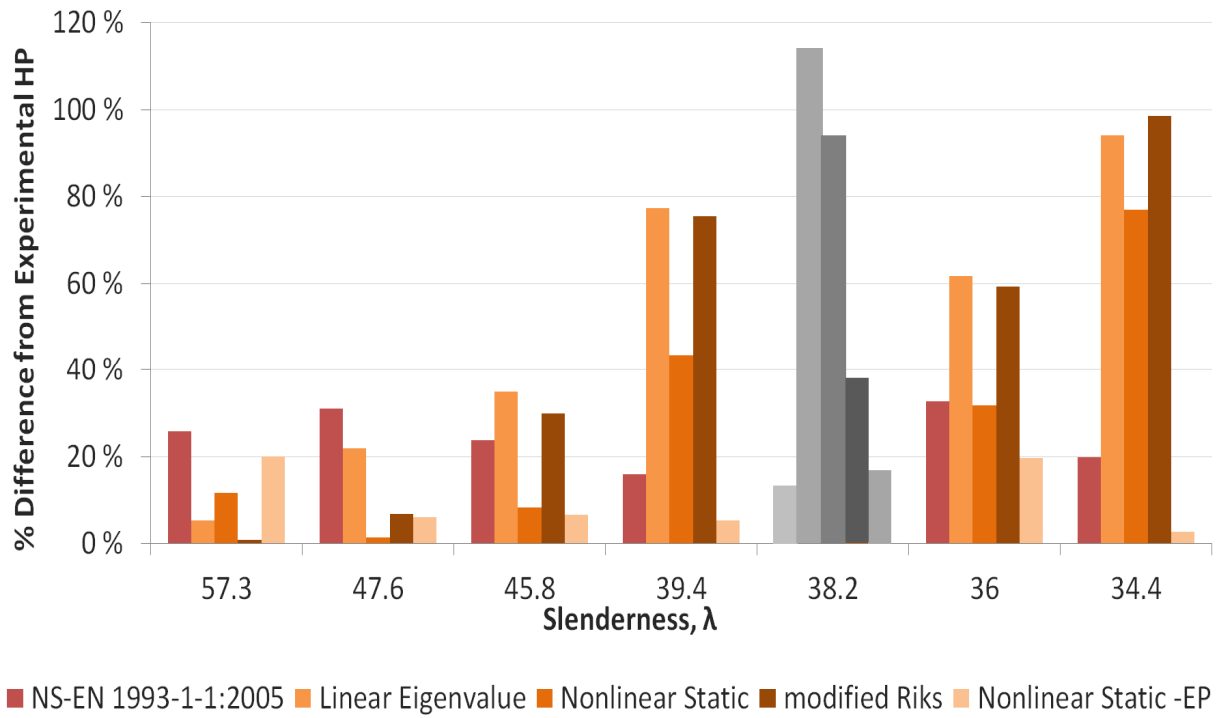


Figure 6.2: Percentage difference between the experiments and the theoretical analyses.



Figure 6.3: Buckled test parts sorted by slenderness-ratio from left; lowest to highest.

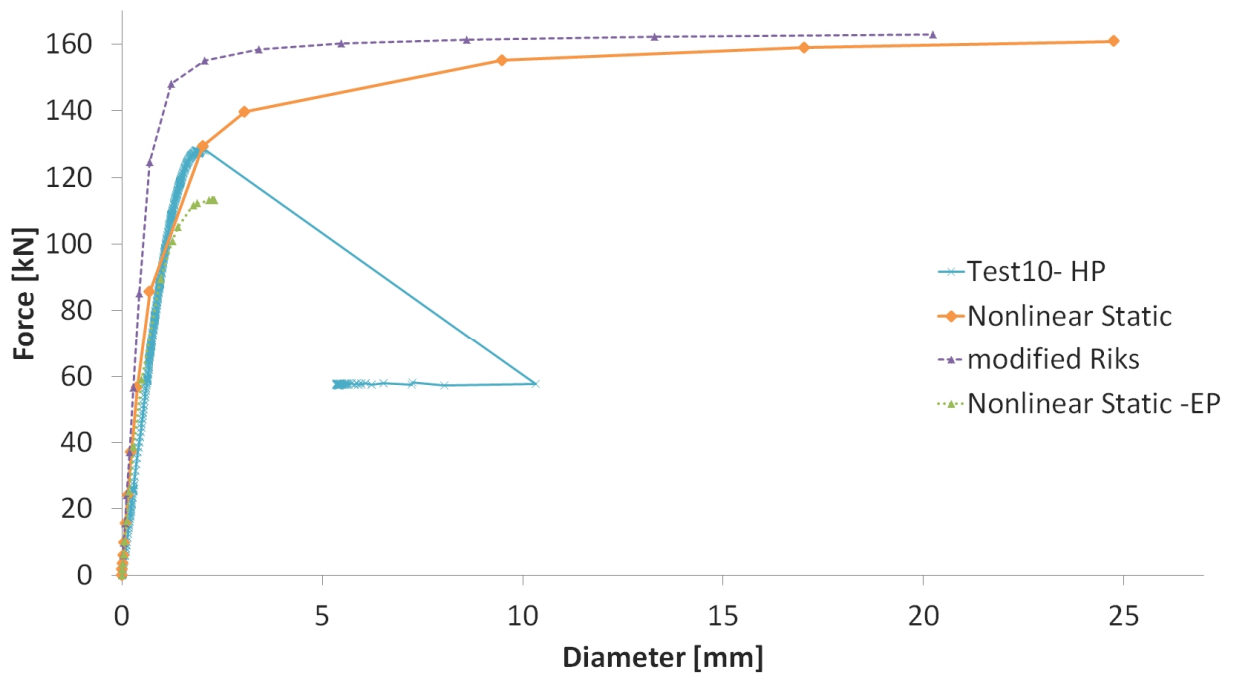
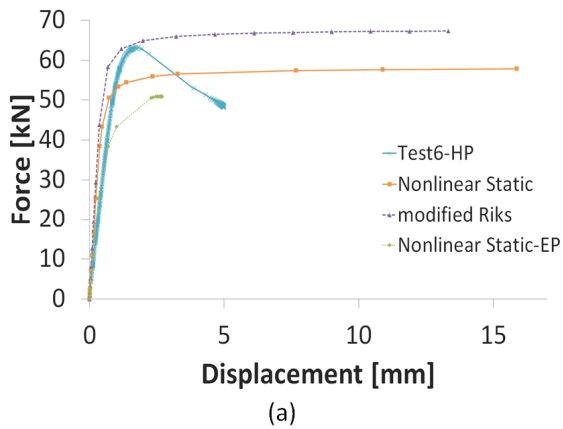
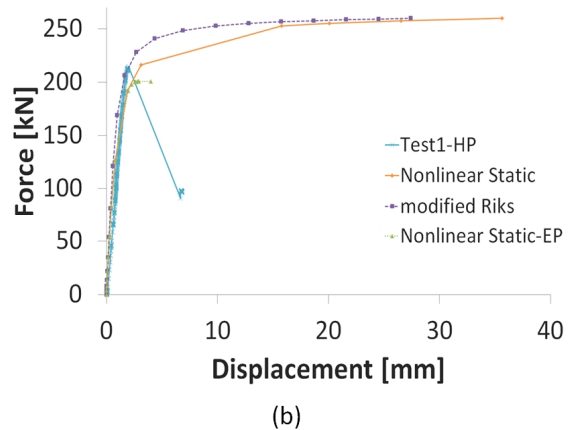


Figure 6.4: Force-displacement curves for the different results obtained from experimental study in HP and Abaqus 6.12 TP-000274-OD15 for TP-000274-OD15.



(a)



(b)

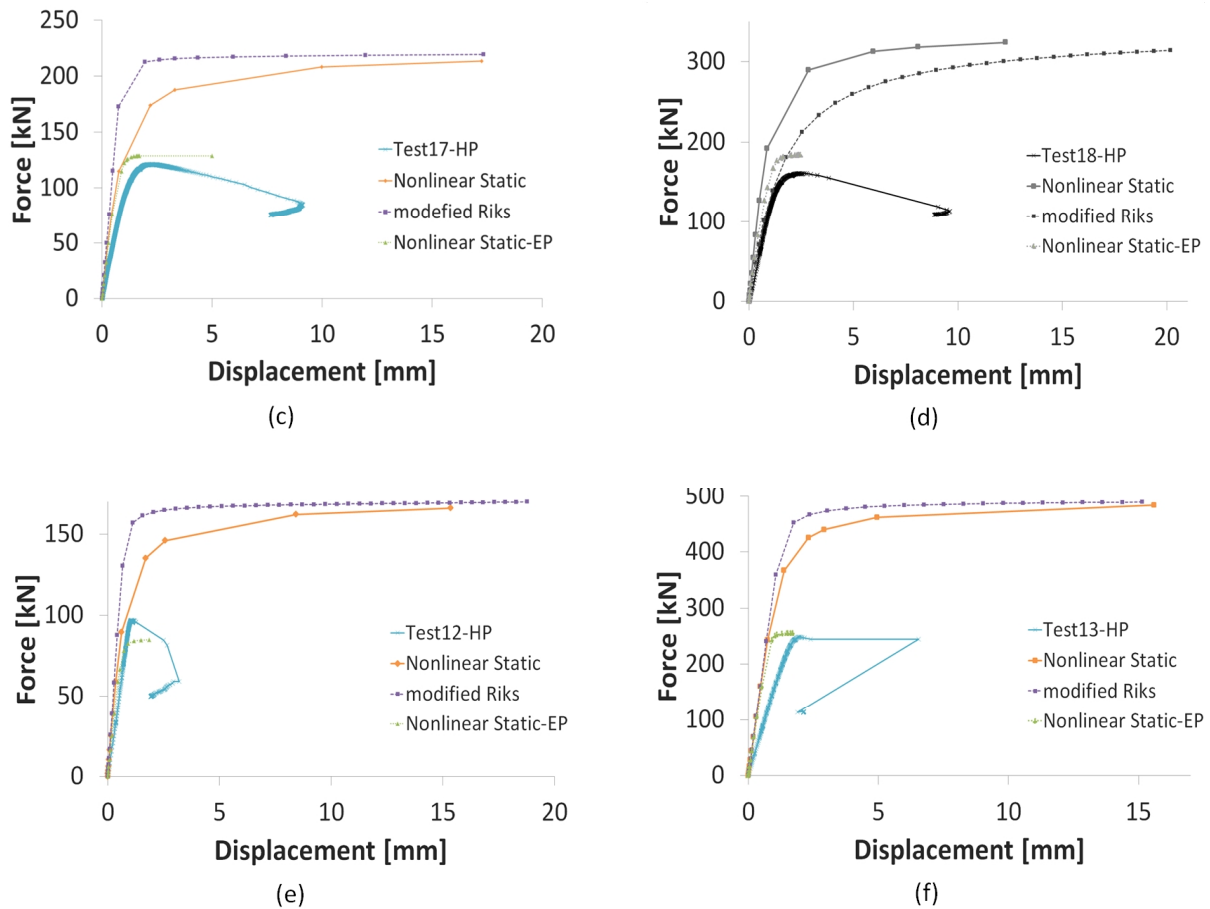


Figure 6.5: Force-displacement curves for the different results obtained from experimental study in HP and Abaqus 6.12 TP-000274-OD15 for (a) TP-000274-OD12; (b) TP-000272; (c) TP-000274-OD15-L350; (d) 000274-OD18; (e) TP-000273-OD12; (f) TP-000274.

From the temperature tests it is found that it is not only the slenderness ratio of the member, the material nonlinearity and the stiffness of restrains at support that effect the critical load, but also the temperature dependence of the material properties. Two temperature tests were conducted, one with 150°C and one with 200°C, both showing a lower critical load than the results from the hydraulic press. It is difficult to obtain a safety factor that depends on increasing temperature from these two tests, since the test with highest temperature yielded higher critical load. The difference between the lowest critical load from hydraulic press and the temperature tests is about 4 %, while the difference between the highest critical load and the temperature tests is about 13 %, which could result from optimized boundary conditions in the HSU. Simulation of in well-pressure also gives a lower critical load than the reference test part test in the hydraulic press. In the 2.70" HSU the static compression tests shows critical loads of 112 kN and 113.7 kN, which is 6 % of the lowest critical force obtained in the hydraulic press and 12.5 % of the highest critical force. The comparison between the different tests for the reference test part is shown in Figure 6.6.

The influence of the material is taken into consideration by the longitudinal rigidity of the member. The elasticity modulus is defined as the slope of its stress-strain curve in the elastic deformation region. The modulus of elasticity is a measure of stiffness of an elastic isotropic material. 34CrNiMo6 steel has high yield strength and ultimate strength compared to other standard low-alloy materials; hence compression members made of steel tend to be slender. At high slenderness where the material remains elastic until buckling the theoretical buckling load also represent the ultimate capacity of the member, because there is no reduction due to imperfections. For TP-000274-OD12 buckling occurs while stresses are significantly below the yield strength of the member and not by overstress of the models. Note that in Figure 6.7 and Figure 6.8 the highest value of critical stress for TP-000274 from the linear elastic buckling analysis was not included because it was unrealistic high.

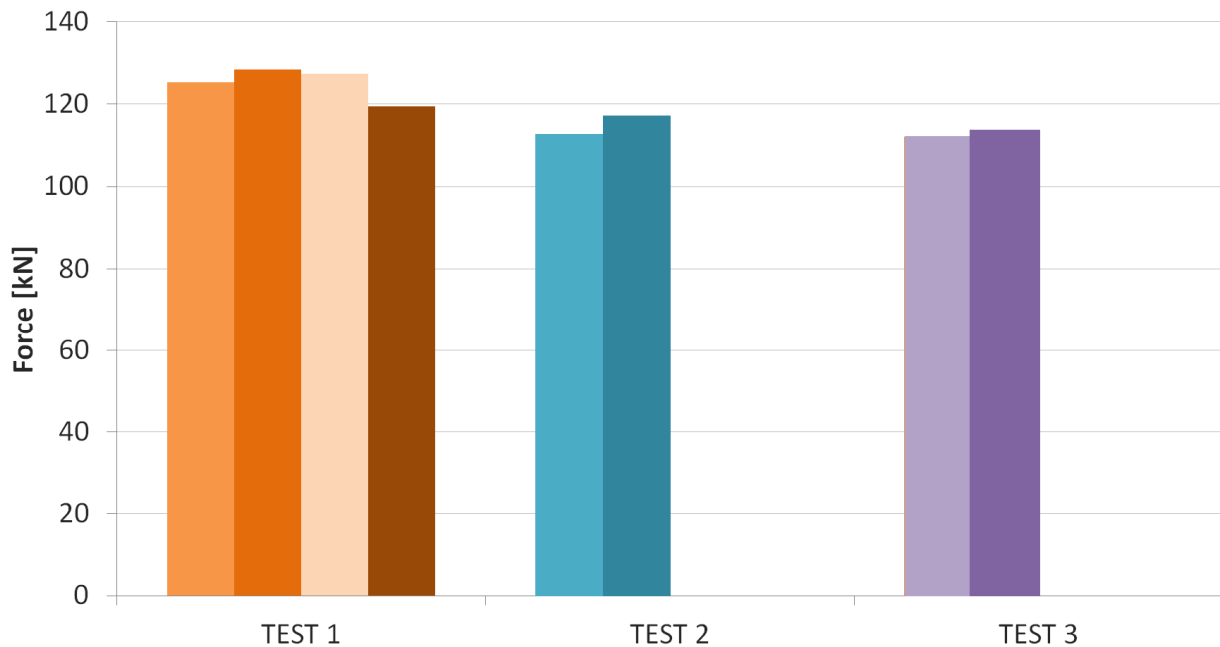


Figure 6.6: Comparison between the different tests; TEST 1= Length and Diameter, TEST 2 = Temperature, TEST 3 = Well Pressure, for TP-000274-OD15.

The calculation method chosen should reflect the real buckling behavior; hence the advantage of each theoretical approach depends on the considered problem. First eigenvalue buckling analysis is often conducted in the early phases in a design process to obtain estimates of the buckling loads and their corresponding displacement modes. The critical load P_{cr} from the eigenvalue buckling analysis, for which buckling can occur is depending on both the material used and the slenderness of the member, i.e. influence of length and diameter. The influence of the length of the member is quadratic in Eulers equation (3), thus twice the length of the admissible load is only one-fourth the original value. The critical load in J.B. Johnsons equation (15) is affected by the strength of the material in addition to its stiffness and geometry. The capacity of a model with linear-elastic properties is inversely proportional to the square of the slenderness ratio. Linear eigenvalue analyses do not take prebuckling deformation and stresses into

consideration, and its important to note that strength is not a factor for a long member when Euler equation is used. As a consequence of discretization error, eigenvalue buckling analysis overestimates the buckling load and provides non-conservative results. A typical factor of safety for an Euler column is between 2 and 4 [20], but this is not based on the yield or ultimate strength of the material, but the critical load. From this it is evident that in practice, linear eigenvalue buckling analysis can only be applied in certain regions and empirical equations are required for members of intermediate length.

Table 6.2: Euler and J.B Johnsons failure stress compared with experimental results from HP.

Part Number	λ	Critical stress, σ_{cr} [MPa]			Deviation Factor
		Euler	Johnson	Experiment HP	
TP-000274-OD12	57.3	600.3	571.4	559.7	1.02
TP-000272	47.6	871.1	673.3	678.9	0.99
TP-000274-OD15	45.8	938.2	690.0	675.6	1.02
TP-000274-OD15-L350	39.4	1267.0	744.6	685.8	1.09
TP-000274-OD18	38.2	1351.0	753.9	605	1.25
TP-000273-OD12	36	1523.5	770.3	855.0	0.90
TP-000274	34.4	1667.9	781.6	791.0	0.99

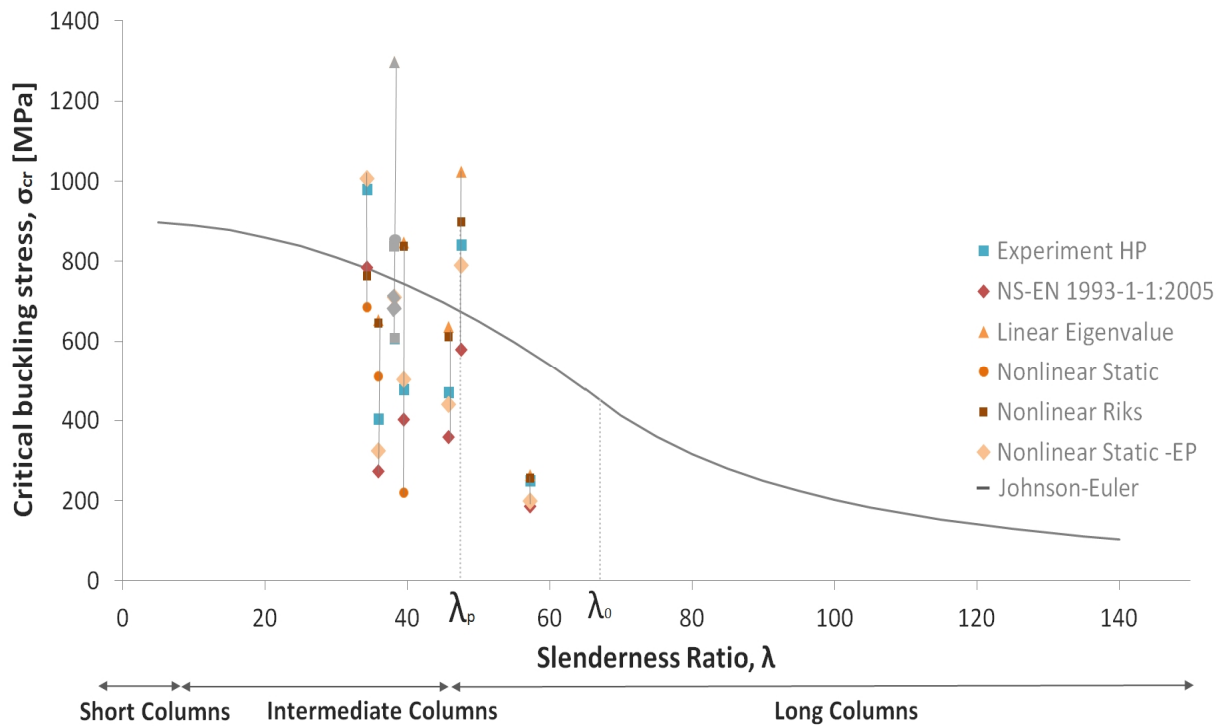


Figure 6.7: J.B. Johnson-Euler curve with the experimental and Abaqus analyses results.

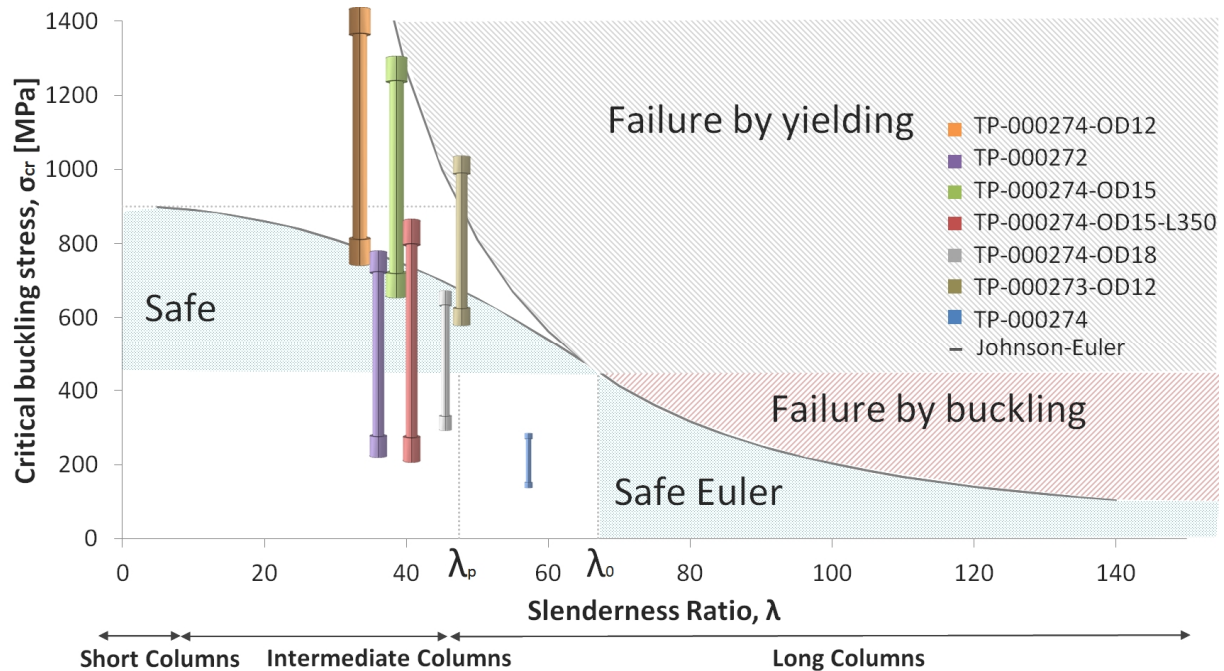


Figure 6.8: J.B. Johnson-Euler curve with the experimental and the analysis results with test parts representing the scatter in the results.

6.1.1 Safety Factor

For safe design the buckling resistance should safely exceed the applied load. Failure of intermediate members could be progressive and unpredictable, and it is therefore common practice to use large safety factors related to empirical design factors when predicting the buckling strength of an axially loaded member. The experiments were performed for specific cases, and it should be noted that only 2-4 tests were performed on each test part with the same configuration. The partial safety factors should be determined on a probabilistic basis of the corresponding quantity; i.e. more than 2-4 tests on each test part. This study allows for revisions of the partial safety factors when specific imperfections are further analyzed. The main methodology with this approach was to gather experimental results and to proceed with comparison between the theoretical analyses before calibration of safety factors. All engineering methods need to be calibrated against an empirical basis in order to obtain a safe design. Calibration was based on realistic extreme conditions and the partial factors are chosen to reflect the buckling behavior of the Setting Chamber Mandrel. This method of partial safety factors allows Interwell to use a global safety factor more proportionally reflecting the uncertainties in the design than a single uniform factor of safety on equipment with similar shape and boundary conditions as the Setting Chamber Mandrel.

A good agreement is found between the experimental results and NS-EN 1993-1-1:2005. NS-EN 1993-1-1:2005 is chosen to be the safest and most efficient analysis method for an optimum design process for Interwells Down Hole Equipment. An Interwell safe design procedure is established based on a

comparison between the experimental results and NS-EN 1993-1-1:2005 equations; see Appendix G. This design procedure is a reasonable practical estimate of the maximum buckling strength of an axially loaded member. The Interwell safe design procedure uses equations instead of determining the reduction factor from reading of the graph (Figure 2.4), hence the results from Interwells safe design procedure are more accurate than the NS-EN 1993-1-1:2005 procedure used in Mathcad, see Table 6.3. The results from the Interwell design procedure have been used to calibrate safe design against buckling. The following suggestions are based on the assumptions that the critical loads obtained from the experimental result are within reasonable agreement compared to a probabilistic basis of the same members.

The members are influenced by imperfections and a certain amount of scatter is expected to be in the results. The difference in the test results for TP-000274-OD15, TP-000273-OD12 and TP-000274 is more than 5 % and it is therefore difficult with reasonable confidence to predict the uncertainty of the variability and the effect of this uncertainty on the safety factor. The load and support partial safety factor, γ_{ls} , is estimated based on the difference in the test results obtained from TEST 1, as well as the difference between the static compression tests in the HSU. The deviation between the static compression test in the HSU and HP combined with the partial safety factor for the highest deviation in test results for the same test part (TP-000274-OD15) gives the load and support partial safety factor; $\gamma_{ls} = 1.08$. The geometric partial safety factor, $\gamma_g = 1.01$, is based on the permissible deviation of geometric attributes on the Setting Chamber Mandrel from NS-ISO 2769. Factors for temperature and static compression test in the HSU are calculated from the lowest critical force obtained in TEST 1 for the reference test part. For members exposed to temperatures well above ambient temperature (field of application: 100 °C -200 °C) a partial safety factor of $\gamma_{t,100-200} = 1.059$ should be used. From the tests in the HSU the effect of simulated well pressure gives an estimate of a partial safety factor equal to; $\gamma_p = 1.122$.

Other factors that may be included in further investigation is different boundary conditions and surface treatment of the members. QPQ (Quench Polish Quench) is a specialized type of case hardening that is applied to improve the corrosion properties and wear resistance of the HSU components. The influence of QPQ on the critical buckling load is expected to be low (case hardening does not affect the rigidity of the member), and will therefore not contribute as a partial safety factor alone, but it will be included in the partial safety factor for material strength, γ_{ms} . The partial safety factor for material strength allows for uncertainties of element behavior and possible strength and reduction due to manufacturing tolerances and imperfections in the material. The value of γ_{ms} is determined from NS-EN 1993-1-1:2005 and given as 1.10 for steel material failure by yielding or buckling [5]. The total factor of partial safety factors, SF_γ , is calculated as a product of all the partial safety factors, see Table 6.4.

The global design factor is defined as the factor of safety against buckling for intermediate members with similar shape and boundary conditions as the Setting Chamber Mandrel. It should be noted that the critical load calculated with NS-EN 1993-1-1:2005 increase with 14-18 % by increasing the yield stress to the results from the uniaxial tensile tests. The relation between the experimental results from HP divided by

the total factor of partial safety factor, SF_{γ} , and the results from NS-EN 1993-1-1:2005 implies that NS-EN 1993-1-1:2005 includes a safety factor of at least 1.4, see Table 6.7. The appropriate global safety factor for intermediate members with similar shape and boundary conditions as the Setting Chamber Mandrel is concluded to be 1.5 when calculating buckling strength with Interwell's safe design procedure. The allowed buckling load, P_{allow} , is calculated by taking the analysis result from NS-EN 1993-1-1:2005 and dividing it with a design safety factor of 1.5; see Table 6.7. The difference in the FE-analysis results compared to the experimental results in HP is shown by a deviation factor in Table 6.7 - Table 6.10. A nonlinear static large deformation buckling analysis with elastic-plastic material properties is recommended to carry out if further investigation of buckling behavior is needed. Acceptance of lower global safety factor may increase as the corresponding quantity of experimental study on the test parts increase.

Table 6.3: Interwell safe design procedure vs NS-EN 1993-1-1:2005 graph.

Part Number	λ	Experiment HP [kN]	Design procedure P_{cr} [kN]	NS-EN 1993-1-1:2005 P_{cr} [kN]	Deviation Factor
TP-000274-OD12	57.3	63.3	44	47	0.94
TP-000272	47.6	213.3	152	147	1.03
TP-000274-OD15	45.8	119.4	89	91	0.98
TP-000274-OD15-L350	39.4	121.2	101	102	0.99
TP-000274-OD18	38.2	154.1	149.7	174	0.86
TP-000273-OD12	36	102.6	69	69	1.00
TP-000274	34.4	248.5	198	199	0.99

Table 6.4: Partial safety factors obtained from experimental studies and standards.

Part Number	Results Factors	MAX	Mean	SF_{γ}
Load and support, γ_{ls}	1.08			1.08
Geometric, γ_g	1.01			1.01
Material strength, γ_{ms}	1.1			1.1
Temperature, $\gamma_{t,100-200}$	1.059	1.059	1.040	1.06
	1.021			
Well Pressure, γ_p	1.122	1.122	1.058	1.1
Total SF_{γ}:				1.4

Table 6.5: Validation of global safety factor.

Part Number	Experiment HP [kN]	NS-EN 1993-1-1:2005 [kN]	Experiment HP / SF _r	Experiment HP / 1.4 NS-EN 1993-1-1:2005
TP-000274-OD12	63.3	44	45.2	0.96
TP-000272	213.3	152	152.3	1.03
TP-000274-OD15	119.4	89	85.3	0.93
TP-000274-OD15-L350	121.2	101	86.5	0.86
TP-000274-OD18	154.1	149.7	110.0	0.63
TP-000273-OD12	102.6	69	73.3	1.06
TP-000274	248.5	198	117.5	0.89

Table 6.6: Allowed buckling load

Part Number	TP-000274-OD12	TP-000272	TP-000274-OD15	TP-000274-OD15-L350	TP-000274-OD18	TP-000273-OD12	TP-000274
P _{allow}	31	98	61	68	116	46	113

Table 6.7: Correlation factor for a linear elastic eigenvalue buckling analysis.

Part Number	Experiment HP [kN]	Linear Eigenvalue [kN]	Deviation Factor	Correlation Factor
TP-000274-OD12	63.3	66.7	0.949	2.1
TP-000272	213.3	259.9	0.820	2.6
Minimum slenderness ratio, $\lambda_p = 47.5$				
TP-000274-OD15	119.4	161.1	0.741	2.6
TP-000274-OD15-L350	121.2	215	0.564	3.2
TP-000274-OD18	154.1	329.2	0.468	2.8
TP-000273-OD12	102.6	165.9	0.618	3.6
TP-000274	248.5	482.3	0.515	3.6
			MEAN SF for $\lambda_p < 47.5$	2.6
			MEAN SF for $\lambda_p \geq 47.5$	3.2

Table 6.8: Correlation factor for a nonlinear static large deformation buckling analysis.

Part Number	Experiment HP [kN]	Nonlinear Static [kN]	Deviation Factor	Correlation Factor
TP-000274-OD12	63.3	55.9	1.132	1.8
TP-000272	213.3	216.3	0.986	2.2
Minimum slenderness ratio, $\lambda_p = 47.5$				
TP-000274-OD15	119.4	129.4	0.922	2.1
TP-000274-OD15-L350	121.2	173.8	0.697	2.5
TP-000274-OD18	154.1	298.6	0.516	2.6
TP-000273-OD12	102.6	135.2	0.758	2.9
TP-000274	248.5	439.7	0.565	3.3
			MEAN SF for $\lambda_p < 47.5$	1.9
			MEAN SF for $\lambda_p \geq 47.5$	2.7

Table 6.9: Correlation factor for a nonlinear Riks buckling analysis.

Part Number	Experiment HP [kN]	Nonlinear Riks [kN]	Deviation Factor	Correlation Factor
TP-000274-OD12	63.3	62.8	1.008	2.0
TP-000272	213.3	228.0	0.935	2.3
Minimum slenderness ratio, $\lambda_p = 47.5$				
TP-000274-OD15	119.4	155	0.770	2.5
TP-000274-OD15-L350	121.2	212.7	0.569	3.1
TP-000274-OD18	154.1	212.2	0.726	1.8
TP-000273-OD12	102.6	163.5	0.627	3.5
TP-000274	248.5	493.5	0.503	3.7
			MEAN SF for $\lambda_p < 47.5$	2.1
			MEAN SF for $\lambda_p \geq 47.5$	2.9

Table 6.10: Correlation factor for a nonlinear static large deformation buckling analysis-EP

Part Number	Experiment HP [kN]	Nonlinear Static-EP [kN]	Deviation Factor	Correlation Factor
TP-000274-OD12	63.3	50.6	1.251	1.6
TP-000272	213.3	200.2	1.065	2.0
Minimum slenderness ratio, $\lambda_p = 47.5$				
TP-000274-OD15	119.4	111.6	1.069	1.8
TP-000274-OD15-L350	121.2	127.7	0.949	1.8
TP-000274-OD18	154.1	180.0	0.856	1.6
TP-000273-OD12	102.6	82.4	1.245	1.8
TP-000274	248.5	255.4	0.973	1.9
			MEAN SF for $\lambda_p < 47.5$	1.8
			MEAN SF for $\lambda_p \geq 47.5$	1.8

CHAPTER 7

7 Conclusion

Failure of intermediate members could be progressive and unpredictable, and it is therefore common practice to use large safety factors when predicting the buckling strength. A safe design approach has been suggested for predicting the critical load and critical stresses of intermediate members by comparing experimental results to existing literature. The critical buckling load is associated with the state of neutral equilibrium, i.e., characterized by the stationary condition of the load with respect to displacement. The results presented in this study introduce options to supplement the safe design of axially loaded members, focusing mainly on the Setting Chamber Mandrel. The conclusions are supported by detailed literature survey of references drawn from research material published over the two past centuries bringing together equations predicting the strength of intermediate members. Global safety factors used to optimize Interwell's Down Hole Equipment have been identified and provide the basis for minimizing the gap between the numerical and experimental results. The effect on all parts of the Setting Chamber Mandrel by various analysis methods have been identified by checking the ultimate capacity and limit states. In general the choice of parameter is tied up to the design and the fabrication methods whereas the value of the different parameters is determined by fabrication or quality control. The partial safety factors in the global safety factor are utilized based on the anticipated conditions to ensure that build in functionality and constructional integrity of the Setting Chamber Mandrel will not affect the overall integrity of the 2.70" HSU.

The structural members in this study have been characterized into three general types depending on their proneness to buckling; short, intermediate and long. The dividing lines between short, intermediate and long members have not been accurately defined; furthermore the maximum load-carrying capacity of a member in each category is based upon different types of mechanical failure scenarios. The Setting Chamber Mandrel is classified as an intermediate member with inelastic buckling behavior.

The experimental studies consist of three different experimental tests; TEST 1: length and diameter, TEST 2: temperature and TEST 3: well pressure. The results from the experimental studies were compared with NS-EN 1993-1-1:2005, FE-analyses and an established linear buckling theory; Euler and J.B. Johnsons equations. Linear elastic eigenvalue buckling analysis and nonlinear static buckling analyses were performed with Abaqus 6.12. The linear elastic eigenvalue buckling analysis provided the buckling mode shape for the Setting Chamber Mandrel. Theoretically, it is possible to calculate as many buckling modes as the number of freedom in the FEA model. The first buckling mode is of highest importance since the higher buckling modes have less probability of taking place. In reality, imperfections and nonlinear

behavior keep the member from achieving this theoretical buckling strength, leading the linear eigenvalue analysis to consequently over-predict the critical load. Following the linear analysis in Abaqus, two nonlinear analysis techniques were carried out; a nonlinear static large deformation buckling analysis and a nonlinear Riks buckling analysis of members with influence of imperfections. The nonlinear large deformation buckling analysis was also conducted with elastic-plastic material properties to take into account the possible plastification of the material. Results indicate that NS-EN 1993-1-1:2005 and the nonlinear analysis techniques are suitable to accurately predict the critical buckling load of an axially loaded compression member. The results from nonlinear static large deformation buckling analysis with elastic-plastic material properties are most comparable with the experimental studies. However, nonlinear FE-analyses in Abaqus are more time consuming and the difference between NS-EN 1993-1-1:2005 and the nonlinear static large deformation analysis with elastic-plastic material properties is not significant enough to justify a much more complicated procedure. When excluding the results from TP-000274-OD18 NS-EN 1993-1-1:2005 estimates the results to be lower with a difference ranging from 20 % to 32 % and a mean difference of 25 %. Keeping in mind the limitations of linear eigenvalue analyses, linear eigenvalue analysis is nevertheless considered a powerful tool, and the advantage of analytical approach chosen depends on the specific problem.

Interwell is currently using NS 3472:2001 (replaced by NS-EN 1993-1-1:2005) with a global safety factor between 1.5-2.0 to calculate buckling of members. From the results obtained in this study NS-EN 1993-1-1:2005 is an acceptable method for predicting the critical load and critical stresses due to axial compression. The most accurate prediction of the buckling behavior of axially loaded members has been obtained by combining experimental studies and theoretical analyses in an Interwell safe design procedure. The appropriate global design factor of safety for intermediate members with similar shape and boundary conditions as the Setting Chamber Mandrel is concluded to be 1.5 when calculating buckling strength with Interwell safe design procedure. It should be noted that the partial safety factors obtained from this study were not determined from a probabilistic basis of the corresponding quantity and more tests should be conducted to get safety factors with less uncertainty. The deviations in safety margins from the different results obtained in this study make it difficult to estimate the partial safety factor with high confidence in accuracy. In order to obtain a high degree of confidence in the design of axially loaded compression members it is recommended that follows the complete methodology provided in this study.

References

- [1] El Naschie “Stress, Stability, and Chaos in Structural Engineering: An Energy Approach”. London: McGraw-Hill, 1990
- [2] Euler, Leonhard: "De curvis elasticis" (The Elastic Curve). Lausanne and Geneva, 1744
- [3] NS 3472:2001, Prosjektering av stålkonstruksjoner – Beregnings- og konstruksjonsregler: 12-13, 36-44, 2001
- [4] Interwell, Hydrostatic Setting Unit; Available (15.12.2013): http://www.interwell.com/getfile.php/Dokumenter/HSU_Rev_3.pdf
- [5] NS-EN 1993-1-1:2005, Eurocode 3: Design of steel structures - Part 1-1: General rules and rules for buildings, 2005
- [6] ABAQUS Analysis User’s Manual, 6.2.3 Eigenvalue Buckling prediction
- [7] Larsen, Per Kr “Dimensjonering av stålkonstruksjoner“, 1. utgave, Tapir Akademisk Forlag, ISBN 978-82-519-2285-2: 186 – 187, 1990
- [8] Ayrton, W.W and Perry, j. “On struts”, The Engineer, 62, 464-465, 513-515, 1886
- [9] ABAQUS Analysis User’s Manual, 6.2.4 “Unstable collapse and postbuckling analysis”
- [10] Engesse, F., “Zeitschrift für Architektur und Ingenieurwesen”, 1889
- [11] Johnson, J. B., “The Materials of Construction”. 1st ed. Wiley, New York , NY, 1897
- [12] Stanley, F. R. “The column paradox”. J. Aeronaut. Sci. 13, 1946
- [13] National instruments, Strain Gauge Principles; Available (15.12.2013): <http://zone.ni.com/devzone/cda/ph/p/id/257>
- [14] Tokyo Sokki Kenkyujo Co., Ltd., Products; Available (05.06.2014) http://www.tml.jp/e/product/strain_gauge/gauge_list/flead_list.html
- [15] Lund, J. “Buckling of Cylindrical members with respect to axial load”, Trondheim, NTNU, 2013
- [16] NS-EN ISO 6892, Metallic materials - Tensile testing - Part 1: Method of test at room temperature, 2009
- [17] ABAQUS Analysis User’s Manual, 23.2.1 Classical metal plasticity
- [18] Grande, E, “TM HSU270SP02XX”, Stavanger, 2013
- [19] Silva, V. D. Mechanics and Strength of Materials. Springer, Netherland, 2006
- [20] Budynas-Nisbett., “Shingle’s Mechanical Engineering Design, Eight Edition” 170-190, 2008

Acknowledgement

The author would like to thank for the cooperation with Eirik Grande and his colleagues at Interwell and supervisor Prof. Nils Petter Vedvik and for the support from NTNU.

Appendix

List of Appendix

Appendix A	Material Certificate for 34CrNiMo6
Appendix B	Derivation of Euler and J.B. Johnsons equation
Appendix C	Buckling Calculations according to NS-EN 1993-1-1:2005
Appendix D	Results from Nonlinear Riks analysis
Appendix E	M-Bond Adhesives Manual
Appendix F	Data Sheet TC8.212.R4
Appendix G	Buckling Calculation
Appendix H	Uniaxial tensile test
Appendix I	Risk Assessment

Appendix A: Material Certificate for 34CrNiMo6

ArcelorMittal Warszawa Sp. z o.o. 132 Kasprzowicza Street 01-949 Warsaw Poland fax: (022) 8354222 - 8340952 tlx: 82-53-51		ŚWIADCTWO ODBIORU INSPECTION CERTIFICATE ABNAHMEPRÜFZEUGNIS ACCORDING TO PN-EN 10204:2006 3.1.		Certificate No. Date 17740/2011(144) 2011-07-11					
Contract dated 2011-03-18 PL/010592085/11-0254				Confirmation No. 884425/2011 **1/*10					
				Department: P48					
Purchaser/Käufer Order No/Bestell-Nr 313-5402232752 dated/Datum 2011-03-17	Purchaser/Käufer (020003514) THYSSENKRUPP MATERIAL NEderland BV TAYLORWEG 7 5466AA VEGHEL NETHERLANDS-NIDERLANDY								
Hereby we declare that the product is conforming with the standards and other records contented in this document. Wir bestätigen hiermit, dass das Erzeugnis mit den Normen und anderen im Text dieses Belegs erwähnten Unterlagen gerecht ist.									
Article Gegenstand Hot Rolled Round Bars Rundstange warmgewalzt	Delivery conditions (SPO) Lieferzustand Quenched and Tempered Vergütet	Material destination (+QT) Materialverwendung for mechanical working zur mechanische Bearbeit.							
Material Werkstoff 34CrNiMo6	standard normen EN 10083-1:1991+A1:1996	Heat No Schmelze-Nr 170807							
Dimensions Abmessungen [mm] Durchmesser. 25 Length tolerance[+/-]:	Diameter Durchmes. 25	Exact length: Feinlänge: 5,500 [m] Längstoleranz[+/-]: 100,0 [mm] -100,0 [mm]							
Weight[kg] Gewicht[kg]	Bundles 5.816 Bunde 3	Standards Normen EN 10060:2003	+						
Ladle chemical analysis [%] Schmelze chemische Zusammensetzung [%]									
C	Mn	Si	P	S	Cr	Ni	Cu	Mo	Al
0,35	0,70	0,24	0,016	0,006	1,70	1,43	0,19	0,16	0,020
-Mechanical properties/Impact test -mechanische Eigenschaften/Kerbschlagzähigkeit					according to entsprechend EN 10002-1 / EN 10045				
Direction Richtung					Impact test temperature Kerbschlagzähigkeitprüftemperatur				
L	Re [N/mm ²]	Rm [N/mm ²]	A5 [%]	Z[%]	KV	[J]			
L	1004	1107	15,0	56,5	64,0-	62,0-	61,0	20,0°C	
-Impact test in temperature -Kerbschlagzähigkeit Prüftemperatur -40,0 °C					according to entsprechend DIN 50115/91				
Direction Richtung									
L	ISO-V [J]		= 25,0 - 26,0 - 27,0						
-Hardness -Härte					surface Fläche according to entsprechend EN ISO 6506-1:1999				
					HBW = 341,0 - 352,0				
-Austenitic grain size -Austenit Korngröße					7 - 7 according to entsprechend EN 103/71				
-Non-metallic inclusions K -nichtmetallische Einschlüsse K					-0- K4 = 1,0 according to entsprechend DIN 50602/85				
Responsible: Quality Management Department Verantwortlicher: Qualitätssicherungsabteilung					Manager M.Sc.Eng. Leiter Dipl.Ing. B. Dorota Pietrzyk				
ArcelorMittal					1/2				

ArcelorMittal Warszawa Sp. z o.o. 132 Kasprzowicza Street 01-949 Warsaw Poland fax: (022) 8354222 - 8340952 tlx: 82-53-51	ŚWIADCTWO ODBIORU INSPECTION CERTIFICATE ABNAHMEPRÜFZEUGNIS ACCORDING TO PN-EN 10204:2006 3.1.	Certificate No. Date 17740/2011(144) 2011-07-11 Confirmation No. 884425/2011 **1/*10 Department: P48
Contract dated 2011-03-18 PL/D10592085/11-0254		

Purchaser/Käufer Order No/Bestell-Nr 313-5402232752 dated/Datum 2011-03-17	Purchaser/Käufer (020003514) THYSSENKRUPP MATERIAL NEDERLAND BV TAYLORWEG 7 5466AE VEGHEL NETHERLANDS-NIDERLANDY
--	--

Hereby we declare that the product is conforming with the standards and other records contained in this document.
Wir bestätigen hiermit, dass das Erzeugnis mit den Normen und anderen im Text dieses Belegs erwähnten Unterlagen gerecht ist.

Article Gegenstand Hot Rolled Round Bars Rundstange warmgewalzt	Delivery conditions (SPO) Lieferzustand Quenched and Tempered (Vergütet)	Material destination (+QT) Materialverwendung (Pwm) for mechanical working zur mechanische Bearbeit.
--	---	---

Material Werkstoff 34CrNiMo6	standard normen EN 10083-1:1991+A1:1996	Heat No Schmelze-Nr 170807
---------------------------------	--	---------------------------------

Dimensions Abmessungen [mm] Durchmesser: 25 Length tolerance [+/-]:	Diameter Durchmes.	Exact length: Feinlänge: 5,500 [m] Längstoleranz [+/-]: 100,0 [mm] -100,0 [mm]
---	-----------------------	--

Weight [kg] Gewicht [kg]	Bundles 5.816 Bunde	Standards Normen EN 10060:2003	*
-----------------------------	------------------------	-----------------------------------	---

Ladle chemical analysis [%]

Schmelze chemische Zusammensetzung [%]

C	Mn	Si	P	S	Cr	Ni	Cu	Mo	Al
0,35	0,70	0,24	0,016	0,006	1,70	1,43	0,19	0,16	0,020

-Mechanical properties/Impact test -mechanische Eigenschaften/Kerbschlagzähigkeit	according to entsprechend EN 10002-1	/ EN 10045 Impact test temperature Kerbschlagzähigkeitprüftemperatur
Direction Richtung	Re [N/mm2] Rm [N/mm2] A5 [%] Z [%] KV [J]	
L	1004 1107 15,0 56,5 64,0- 62,0- 61,0	20,0°C

-Impact test in temperature -Kerbschlagzähigkeit Prüftemperatur -40,0 °C	according to entsprechend DIN 50115/91
---	---

Direction Richtung	ISO-V [J]	= 25,0 - 26,0 - 27,0
L		

-Hardness -Härte	surface Fläche HBW = 341,0 - 352,0	according to entsprechend EN ISO 6506-1:1999
---------------------	--	---

-Austenitic grain size -Austenit Korngröße	7 - 7	according to entsprechend EN 103/71
---	-------	--

-Non-metallic inclusions K -nichtmetallische Einschlüsse K	-O- K4 = 1,0	according to entsprechend DIN 50602/85
---	-----------------	---

Responsible: Quality Management Department
Verantwortlicher: Qualitätssicherungsabteilung

Manager M.Sc.Eng.
Leiter Dipl.Ing. B. Dorota Pietrzyk

Appendix B: Derivation of Euler and J.B. Johnsons equation

Eulers equation for long columns

Consider an axially loaded pinned-pinned column, Figure (B.1), which is subjected to an axial load P . This load P produces a deflection z at a distance x from one end.

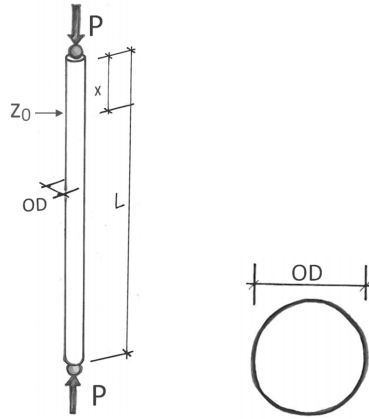


Figure B.1: Load case; initially straight column with Euler load

$$M = -Pz \quad (B.1)$$

For columns the bending moment is proportional to the curvature of the column, which for small deflection can be expressed as:

$$\frac{M}{EI} = \frac{d^2z}{dx^2} \quad (B.2)$$

Substetuting equation (B.1) into equation (B.2) gives:

$$\frac{d^2z}{dx^2} + \frac{P}{EI}z = 0 \quad (B.3)$$

This is a second order diffirential equation, which has a general solution form of;

$$z = A \cos\left(\sqrt{\frac{P}{EI}}x\right) + B \sin\left(\sqrt{\frac{P}{EI}}x\right) \quad (B.4)$$

In order to evaluate the constants A and B the boundary conditions $z=0$ at $x=0$, and $z=0$ at $x=L$ must be applied. Applying the first boundary condition yields $A=0$, while applying the second boundary condition gives $B \sin(L\sqrt{P/EI}) = 0$.

$$\sin\left(\sqrt{\frac{P}{EI}}L\right) = 0 \rightarrow \sqrt{\frac{P}{EI}}L = \pi \quad (\text{B.5})$$

$$P = \frac{\pi^2 EI}{L^2} \quad (\text{B.6})$$

For column with fixed ends:

$$\frac{M}{EI} = \frac{d^2 z}{dx^2} + \frac{P}{EI} \quad (\text{B.7})$$

The general solution form for equation (B.7) is given by;

$$z = B\cos(nx) + A\sin(nx) + \frac{M}{P} \quad (\text{B.8})$$

where $n^2=P/EI$. For this case the boundary conditions relevant are $z=0$ at $x=0$ and $z=0$ at $x=L$, which gives $B=-M/P$ and also at $x=0$; $dy/dx=0$, hence $A=0$. Therefore

$$z = -\frac{M}{P}\cos(nx) + \frac{M}{P} \quad (\text{B.9})$$

Further, when $z=0$ at $x=L$;

$$\frac{M}{P}(1 - \cos(nL)) = 0 \rightarrow \cos(nL) = 1 \rightarrow nL = 2\pi \quad (\text{B.10})$$

$$P = \frac{4\pi^2 EI}{L^2} \quad (\text{B.11})$$

J.B. Johnsons equation for intermediate members

The general form for the parabolic equation is given by equation (B.12).

$$\frac{P_{cr}}{A} = a - b\lambda^2 \quad (\text{B.12})$$

Boundary conditions:
$$\begin{cases} \frac{P}{A} = \sigma_y & \text{at } \lambda = 0 \\ \frac{P}{A} = \frac{\sigma_y}{2} & \text{at } \lambda = \lambda_0 \end{cases} \quad (\text{B.13})$$

Applying the boundary conditions in equation (B.13) gives $a = \sigma_y$ and $b = \frac{\sigma_y/2}{\lambda_0}$, where the tangent point between the Euler hyperbola and the Johnsons curve is given by λ_0 . Substituting the values for a and b gives J.B. Johnsons equation (B.15). Notice that the factor of safety is not included.

$$\lambda_0 = \sqrt{\frac{2\pi^2 E}{\sigma_y}} \quad (\text{B.14})$$

$$\frac{P_{cr}}{A} = \sigma_y - \left(\frac{\sigma_y^2}{4\pi^2 E} \right) \cdot \lambda^2 \quad (\text{B.15})$$

Appendix C: Buckling Calculations according to NS-EN 1993-1-1:2005

Buckling calculations according to NS-EN 1993-1-1:2005 for the reference test part TP-000274-OD15. The rest of the models were calculated in the same way, only changing the length and the outer diameter.

Defining Parameters:

Euler case no.:	Case := 4	
Length of beam:	$L_b := 344\text{mm}$	
Outer Diameter:	OD := 15mm	D := 55mm
Inner Diameter:	ID := 0mm	P := 20000psi
Modulus of elasticity: (@200°C)	$E := 2.05 \cdot 10^5 \text{MPa}$	
Yield stress: (@200°C)	$\sigma_y := 900\text{MPa}$	AISI4140/45 30-36HRC
Design Load:	$F_{\text{des}} := P \cdot \frac{\pi}{4} \cdot D^2 = 327.615 \cdot \text{kN}$	(C.1)
Required Safety factor:	SF := 1.5	

Load Case Selection:

Buckling length:

$$L_k := \text{if} \left(\text{Case} = 1, \frac{L_b}{0.5}, \text{if} \left(\text{Case} = 2, \frac{L_b}{1}, \text{if} \left(\text{Case} = 3, \frac{L_b}{\sqrt{2}}, \text{if} \left(\text{Case} = 4, \frac{L_b}{2}, \text{"False"} \right) \right) \right) \right)$$

$$L_k = 0.172 \text{ m}$$

Geometry:

Second moment of inertia:	$I := \pi \cdot \frac{\left[\left(\frac{\text{OD}}{2} \right)^4 - \left(\frac{\text{ID}}{2} \right)^4 \right]}{4}$	$I = 2485 \cdot \text{mm}^4$	(C.2)
---------------------------	---	------------------------------	-------

Cross section area:	$A_1 := \frac{\pi}{4} \cdot (\text{OD}^2 - \text{ID}^2)$	$A_1 = 177 \cdot \text{mm}^2$	(C.3)
---------------------	--	-------------------------------	-------

Slimness Calculations:

Radii of gyration: $i := \sqrt{\frac{I}{A_1}}$ $i = 3.75 \cdot \text{mm}$ (C.4)

Slimness: $\lambda := \frac{L_k}{i}$ $\lambda = 45.867$ (C.5)

Material Slimness Factor: $\lambda_F := \pi \cdot \sqrt{\frac{E}{\sigma_y}}$ $\lambda_F = 47.414$ (C.6)

Relative Slimness: $\lambda_{\text{red}} := \frac{\lambda}{\lambda_F} = 0.967$ (C.7)

Buckling Factor: $\chi := 0.499$ (C.8)

Buckling Stress: $\sigma_k := \chi \cdot \sigma_y$ $\sigma_k = 449 \cdot \text{MPa}$ (C.9)

Buckling Load: $F_{\text{buckling}} := A_1 \cdot \sigma_k$ $F_{\text{buckling}} = 79 \cdot \text{kN}$ (C.10)

Allowed Buckling Load : $F_{\text{max}} := \frac{F_{\text{buckling}}}{\text{SF}}$ $F_{\text{max}} = 53 \cdot \text{kN}$ (C.11)

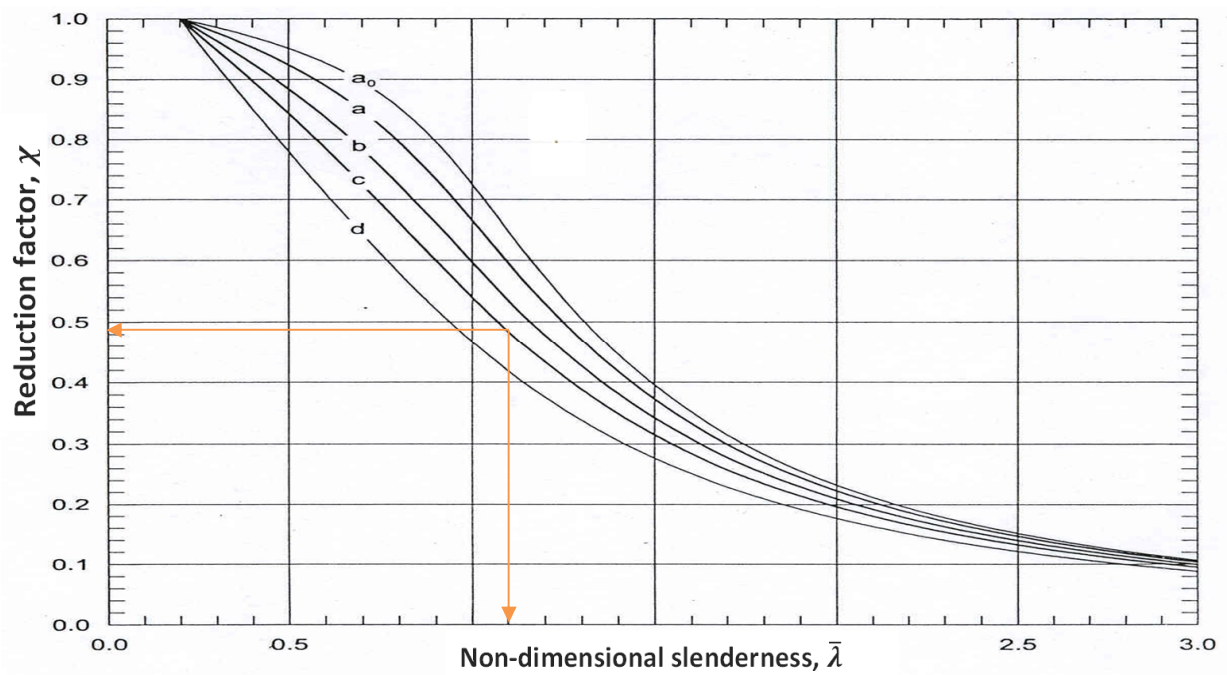
Actual Safety Factor: $SF_{act} := \frac{F_{buckling}}{F_{des}}$ $SF_{act} = 0.155$ (C.12)

Calculated Design Validation:

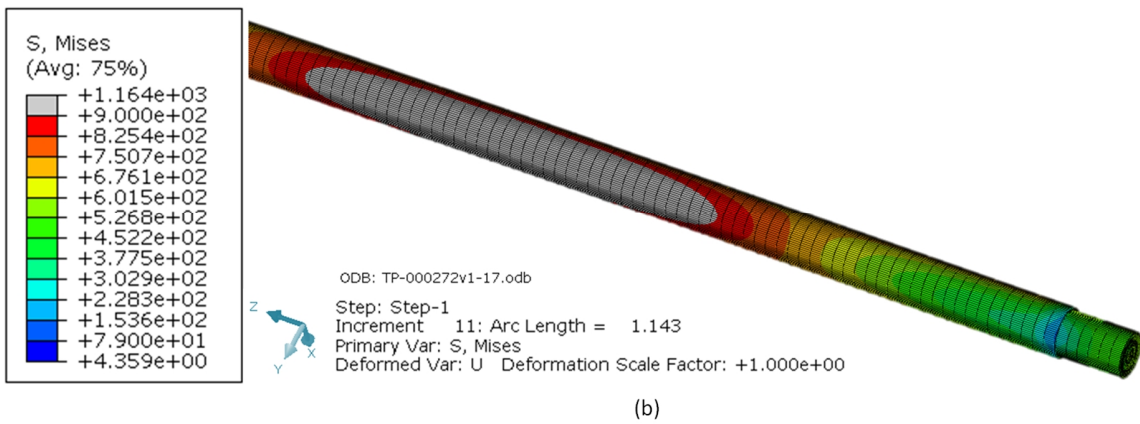
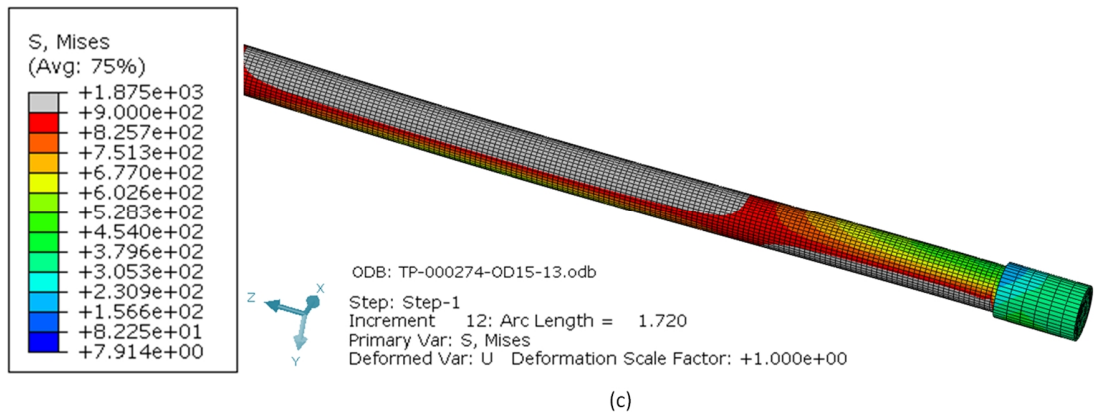
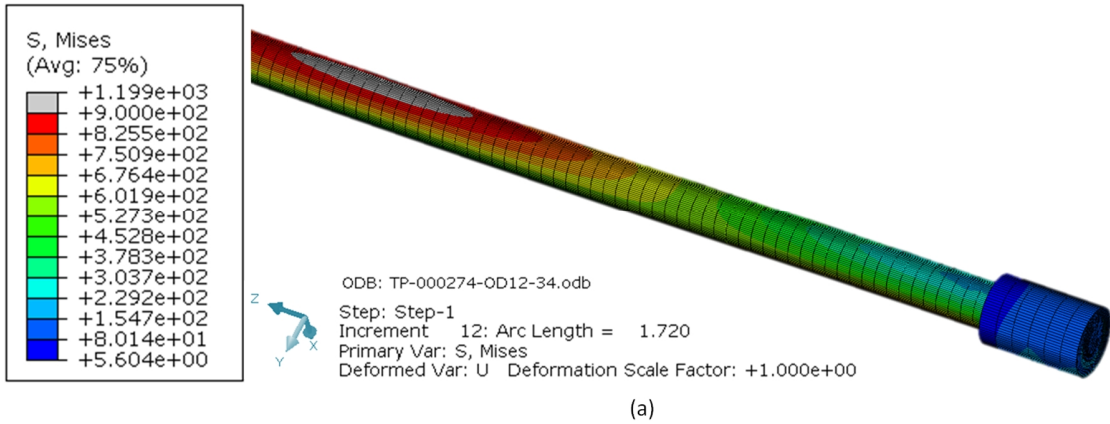
Recommended Safety factor: $1.5 \leq SF \leq 2$

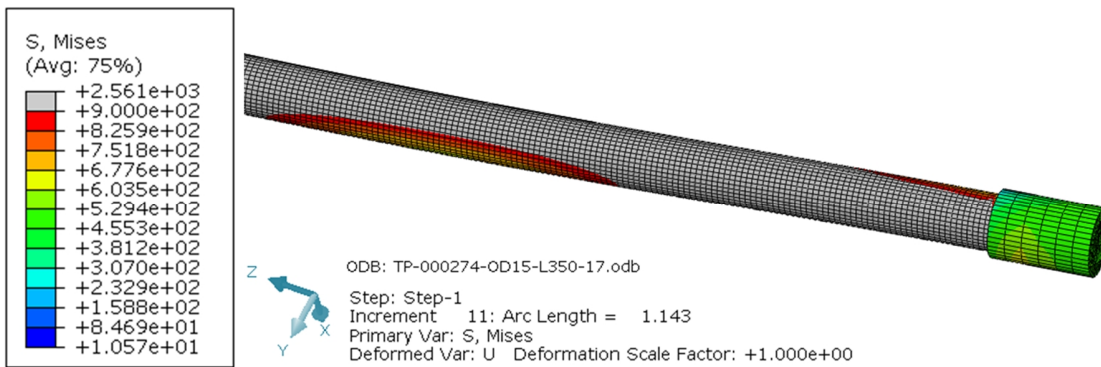
$SF_{valid} := \text{if}(SF_{act} \geq SF, \text{"OK"}, \text{"Not OK"})$ (C.13)

$SF_{valid} = \text{"Not OK"}$

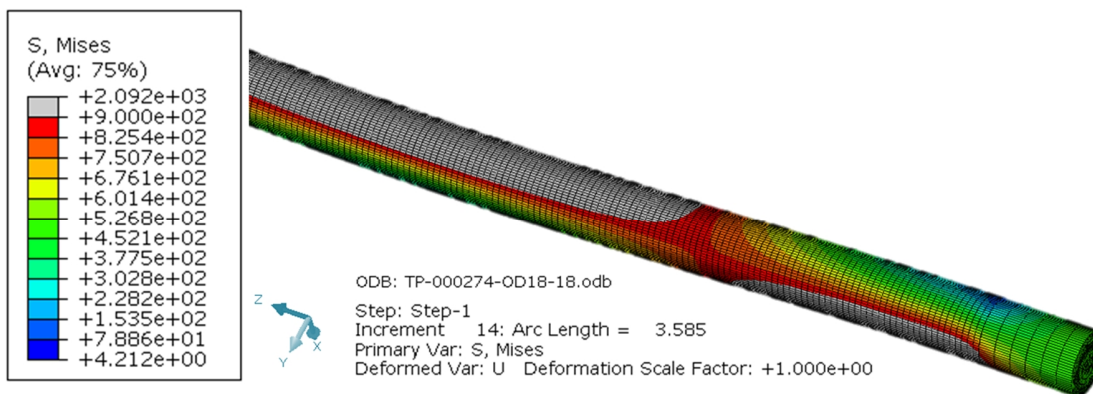


Appendix D: Results from Nonlinear Riks analysis

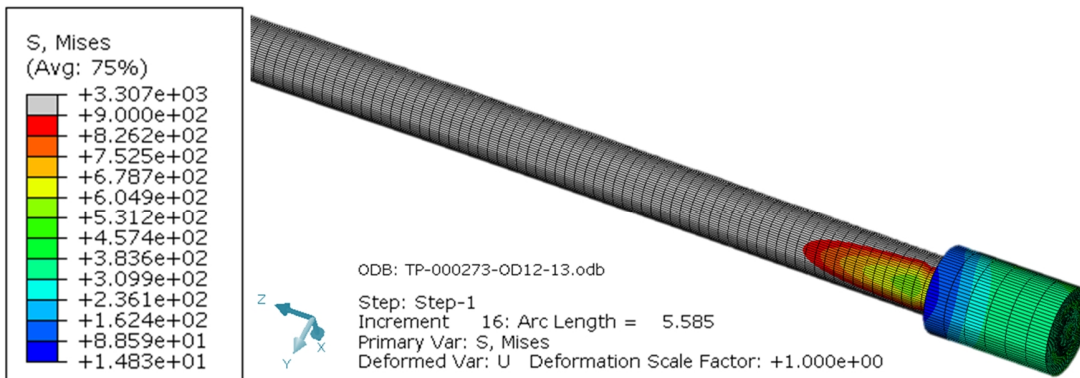




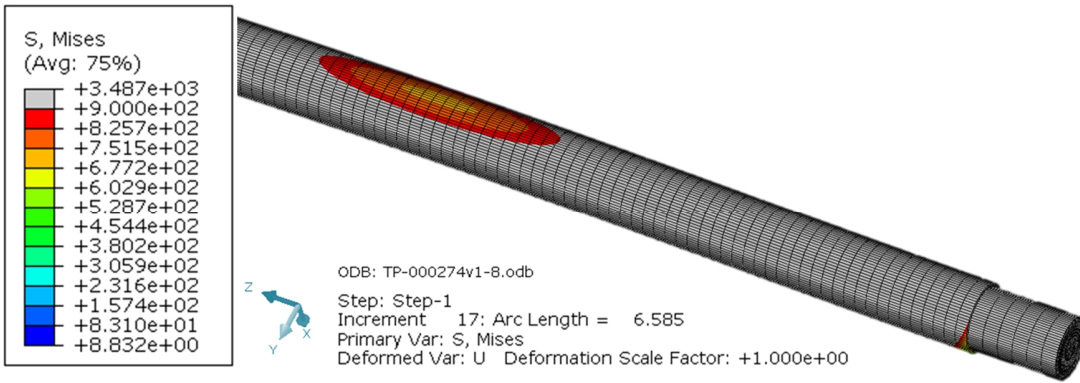
(d)



(e)



(f)



(g)

Figure D.1: Stresses from nonlinear static Riks analysis (a) TP-000274-OD12; (b) TP-000272; (c) TP-000274-OD15; (d) TP-000274-OD15-L350; (e) TP-000274-OD18; (f) TP-000273-OD12; (g) TP-000274

Appendix E: M-Bond Adhesives Manual



Instruction Bulletin B-130

Micro-Measurements



Strain Gage Installations with M-Bond 43-B, 600, and 610 Adhesive Systems

INTRODUCTION

Micro-Measurements M-Bond 43-B, 600, and 610 adhesives are high-performance epoxy resins, formulated specifically for bonding strain gages and special-purpose sensors. When properly cured, these adhesives are useful for temperatures ranging from -452° to +350°F [-269° to +175°C] with M-Bond 43-B, and to +700°F [+370°C] for short periods with M-Bond 600 and 610. In common with other organic materials, life is limited by oxidation and sublimation effects at elevated temperatures. M-Bond 43-B is particularly recommended for transducer applications up to +250°F [+120°C], and M-Bond 610 for transducers up to +450°F [+230°C].

For proper results, the procedures and techniques presented in this bulletin should be used with qualified Micro-Measurements installation accessory products (refer to Micro-Measurements Strain Gage Accessories Databook). Accessories used in this procedure are:

CSM Degreaser or GC-6 Isopropyl Alcohol	CSP-1 Cotton Applicators
Silicon-Carbide Paper	MJG-2 Mylar® Tape
M-Prep Conditioner A	TFE-1 Teflon® Film
M-Prep Neutralizer 5A	HSC-X Spring Clamp
GSP-1 Gauze Sponges	GT-14 Pressure Pads and Backup Plates

MIXING INSTRUCTIONS

Since M-Bond 43-B is a solvent-thinned, pre-catalyzed epoxy mixture, it is applied at room temperature directly as received. The M-Bond 600 and 610, on the other hand, are two-component systems. These must be mixed as follows:

1. Resin and curing agent bottles must be at room temperature before opening.
2. Using the disposable plastic funnel, empty contents of bottle labeled "Curing Agent" into bottle of resin labeled "Adhesive". Discard funnel.
3. After tightening the brush cap (included separately), thoroughly mix contents of this "Adhesive" bottle by vigorously shaking it for 10 seconds.
4. Mark bottle with date mixed in space provided on the label.

Allow this freshly mixed adhesive to stand for at least one hour before using.

SURFACE PREPARATION

The extensive subject of surface preparation techniques is covered in Application Note B-129. Metal surface cleaning procedures usually involve solvent degreasing with either CSM Degreaser or GC-6 Isopropyl Alcohol, abrading, and cleaning with M-Prep Conditioner A, followed by application of M-Prep Neutralizer 5A. When practical, these preparation procedures should be applied to an area significantly larger than that occupied by the gage. Surfaces should be free from pits and irregularities. Porous surfaces may be pre-coated with a filled epoxy, such as M-Bond GA-61, which is then cured and abraded.

SHELF LIFE AND POT LIFE

At room temperature, M-Bond 600 has a minimum storage life of three months, while M-Bond 43-B and M-Bond 610 will last a minimum of nine months.

Once opened and mixed, M-Bond 600 and 610 have room-temperature pot lives of two weeks and six weeks, respectively. Since M-Bond 43-B is supplied already mixed, its pot life is about the same as its shelf life when kept in a tightly closed container.

These periods of adhesive usefulness can be increased by refrigeration at +30° to +40°F [0° to +5°C]. Check individual adhesive kit labels for details. Never open a refrigerated bottle until it has reached room temperature.

GAGE INSTALLATION

The basic steps for bonding gages using M-Bond 43-B, 600, and 610 adhesives are given on the following pages.

HANDLING PRECAUTIONS

Epoxy resins and hardeners may cause dermatitis or other allergic reactions, particularly in sensitive persons. The user is cautioned to: (1) avoid contact with either the resin or hardener; (2) avoid prolonged or repeated breathing of the vapors; and (3) use these materials only in well-ventilated areas. If skin contact occurs, thoroughly wash the contaminated area with soap and water immediately. In case of eye contact, flush immediately and secure medical attention. Rubber gloves and aprons are recommended, and care should be taken not to contaminate working surfaces, tools, container handles, etc. Spills should be cleaned up immediately. For additional health and safety information, consult the Material Safety Data Sheet, which is available upon request.

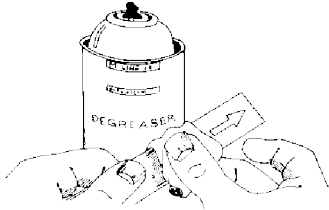


Instruction Bulletin B-130

Micro-Measurements

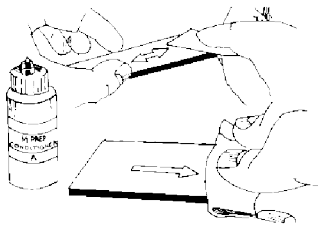


Step 1



Thoroughly degrease the gaging area with solvent, such as CSM Degreaser or GC-6 Isopropyl Alcohol. The former is preferred, but there are some materials (e.g., titanium and many plastics) that react with CSM. In these cases, GC-6 Isopropyl Alcohol should be considered. All degreasing should be done with uncontaminated solvents—thus the use of “one-way” containers, such as aerosol cans, is highly advisable.

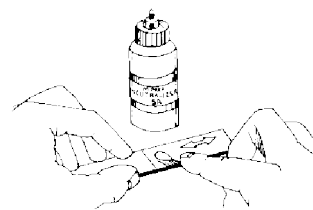
Step 2



Preliminary dry abrading with 220- or 320-grit silicon-carbide paper is generally required if there is any surface scale or oxide. Final abrading is done by using 320- or 400-grit silicon-carbide paper on surfaces thoroughly wetted with M-Prep Conditioner A; this is followed by wiping dry with a gauze sponge.

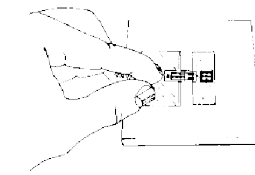
With a 4H pencil (on aluminum) or a ballpoint pen (on steel), burnish (do not scribe) whatever alignment marks are needed on the specimen. Repeatedly apply Conditioner A and scrub with cotton-tipped applicators until a clean tip is no longer discolored. Remove all residue and Conditioner by again slowly wiping through with a gauze sponge. Never allow any solution to dry on the surface because this invariably leaves a contaminating film and reduces chances of a good bond.

Step 3



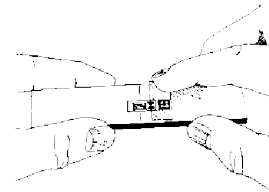
Now apply a liberal amount of M-Prep Neutralizer 5A and scrub with a cotton-tipped applicator. With a single, slow wiping motion of a gauze sponge, carefully dry this surface. Do not wipe back and forth because this may allow contaminants to be redeposited on the cleaned surface.

Step 4



Remove a gage from its mylar envelope with tweezers, making certain not to touch any exposed foil. Place the gage, bonding side down, onto a chemically clean glass plate or empty gage box. If a solder terminal is to be incorporated, position it next to the gage. While holding the gage in position with a mylar envelope, place a short length of MJG-2 mylar tape down over about half of the gage tabs and the entire terminals.

Step 5

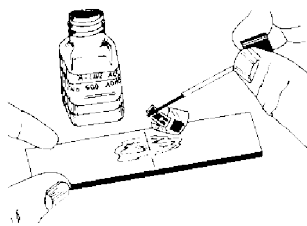


Remove the gage/tape/terminal assembly by peeling tape at a shallow angle (about 30°) and transferring it onto the specimen. Make sure gage alignment marks coincide with specimen layout lines. If misalignment does occur, lift the end of the tape at a shallow angle until assembly is free. Realign and replace. Use of a pair of tweezers often facilitates this handling.

Strain Gage Installations with M-Bond 43-B, 600, and 610 Adhesive Systems

Note: A “hot-tack” method of positioning can be used, which eliminates need for taping. This method is explained after Step 9.

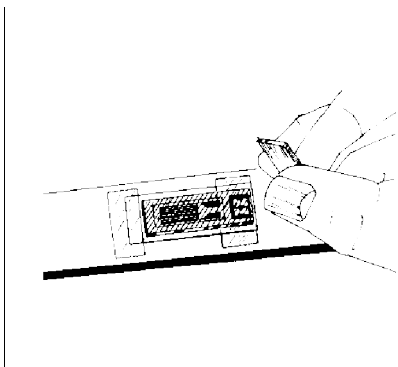
Step 6



Now, by lifting at a shallow angle, peel back one end of the taped assembly so as to raise both gage and terminal. By curling this mylar tape back upon itself, it will remain in position, ready to be accurately repositioned after application of adhesive.

Coat the gage backing, terminal, and specimen surface with a thin layer of adhesive. Also coat the foil side of open-faced gages. Do not allow the adhesive applicator to touch the tape mastic. Permit adhesive to air-dry, by solvent evaporation, for 5 to 30 minutes at +75°F [+24°C] and 50% relative humidity. Longer air-drying times are required at lower temperatures and/or higher humidities. **Note: An additional drying step with 43-B is beneficial for large gages. Place the unclamped installation in an oven for 30 minutes at +175°F [+80°C] following the air-dry step above.**

Step 7

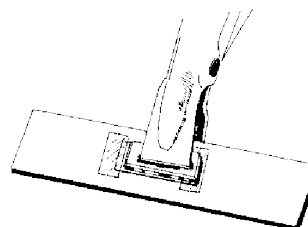


Return the gage/terminal assembly to its original position over the layout marks. Use only enough pressure to allow the assembly to be tacked down. Overlay the gage/terminal area with a piece of thin Teflon sheet (TFE-1). If necessary, anchor the Teflon in position across one end with a piece of mylar tape.

Cut a 3/32-in [2.5-mm] thick silicone gum pad and a metal backup plate (GT-14) to a size slightly larger than the gage/terminal areas, and carefully center these. Larger pads may restrict proper spreading of adhesive, and entrap residual solvents during cure process.

Note: Steps 6, 7, and 8 must be completed within 30 minutes with M-Bond 600, 4 hours with M-Bond 610, and 24 hours with M-Bond 43-B.

Step 8



Either spring clamps or deadweight can be used to apply pressure during the curing cycle. For transducers, 40 to 50 psi [275 to 350 kN/m²] is recommended and 10 to 70 psi [70 to 480 kN/m²] for general work. Place the clamped gage/specimen into a cool oven and raise temperature to the desired level at a rate of 5° to 20°F [3° to 11°C] per minute. Air bubbles trapped in the adhesive, uneven gluelines, and high adhesive film stresses often result from starting with a hot oven. Time-versus-temperature recommendations for curing each adhesive are given on the next page.

Step 9

Upon completion of the curing cycle, allow oven temperature to drop at least 100°F [55°C] before removing the specimen. Remove clamping pieces and mylar tape. It is advisable to wash off the entire gage area with either RSK Rosin Solvent or toluene. This should remove all residual mastic and other contamination. Blot dry with a gauze sponge.

“Hot-Tack” Method of Gage Installation

This procedure eliminates all need for taping to prevent movement of the gage during mounting, and is especially suited to M-Bond 43-B and M-Bond 600.

1. After completing the preceding Steps 1, 2, and 3, remove a gage from its mylar envelope using clean tweezers.
2. Coat the bonding side of gage and gaging area of the specimen with adhesive, and set each aside to air-dry for at least 15 minutes. M-Bond 43-B may dry for up to 24 hours.
3. Using tweezers, position gage onto the specimen. A properly cleaned dental probe may help.



Instruction Bulletin B-130

Micro-Measurements



4. To anchor the gage, use a 15- to 25-watt soldering iron with a new conical tip. This is usually done by hot-tack-setting the adhesive at two spots (such as opposite gage-alignment marks) while temporarily holding the gage down with a mylar envelope. A little experimentation may be required to learn the correct iron temperature and hot tip contact time. These depend upon type of adhesive used and thermal conductivity of the base material.

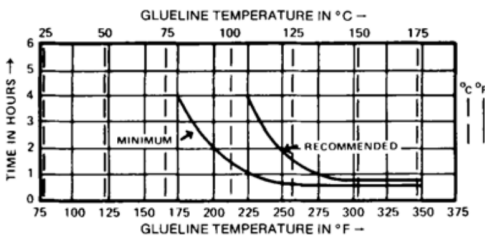
5. If the gage is open-faced, apply a thin coating of adhesive to its face and allow to dry for at least five minutes before overlaying with a Teflon sheet (as described in Step 7). Proceed with Steps 8 and 9.

RECOMMENDED CURE SCHEDULE

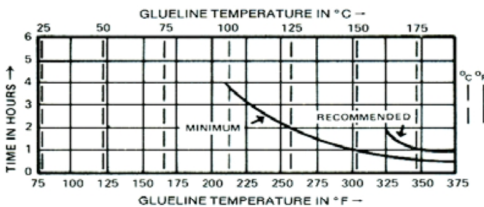
It should be noted that the following curves represent a range of time-versus-temperature; however, the upper limits of both time and temperature should be employed whenever possible, while keeping in mind the possible effect on the heat treat condition of the substrate material.

M-Bond 43-B: 2 hours at +375°F [+190°C], or as an alternate cure for aluminum alloy transducers 2 ½ hours @ +300°F [+150°C].

M-Bond 600: Cure at temperature for time period specified by graph below.



M-Bond 610: Cure at temperature for time period specified by graph below.



POSTCURING

Postcures with the clamping fixture removed are usually required for stable transducer applications. Postcuring can be done following Step 9 above, or after wiring the transducer (subject to temperature limits of solder and wire insulation).

M-Bond 43-B: 2 hours at +400°F [+205°C], or as an alternate postcure for aluminum alloy transducers 2 ½ hours @ +350°F [+175°C].

M-Bond 600: 1 to 2 hours at 50°F [30°C] above maximum operating or curing temperature, whichever is greater.

M-Bond 610: 2 hours at 50° to 75°F [30° to 40°C] above maximum operating or curing temperature, whichever is greater.

FINAL INSTALLATION PROCEDURES

1. Refer to Strain Gage Accessories Databook to select an appropriate solder, and attach leadwires. Be sure to remove solder flux with Rosin Solvent. Gage tabs and terminals can be cleaned prior to soldering by light abrading with pumice to remove the adhesive film. This pumicing is not required with gages having integral leads (Options L and LE) or pre-attached solder dots. See Application Note TT-606, "Soldering Techniques for Lead Attachment to Strain Gages with Solder Dots." General soldering instructions are discussed in Application Note TT-609, "Strain Gage Soldering Techniques."

2. Select and apply protective coatings according to recommendations given in Strain Gage Accessories Databook.

ELONGATION CAPABILITIES

M-Bond 43-B:
1% at -452°F [-269°C]; 4% at +75°F [+24°C]; 2% at +300°F [+150°C].

M-Bond 600 & 610:
1% at -452°F [-269°C]; 3% from room temperature to 500°F [+260°C].

Mylar and Teflon are Registered Trademarks of DuPont.

Appendix F: Data Sheet TC8.212.R4

Data Sheet: TC8.212.R4

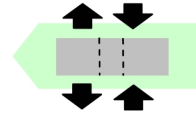
www.aep.it

TC8

Dinamometro
Dynamometer

Accessori Accessories

A



CE

RoHS
COMPLIANCE

ISO 376

Norme di riferimento *Reference standards:*
ISO 376 • ASTM E74

JTC

Certificato SIT a richiesta
SIT certificate on request

Dinamometro a basso profilo **Alta stabilità a lungo termine** **Interamente saldata al LASER** **Per applicazioni dinamiche**
Low profile Dynamometer *Long term high stability* *Completely LASER welded* *For dynamic applications*

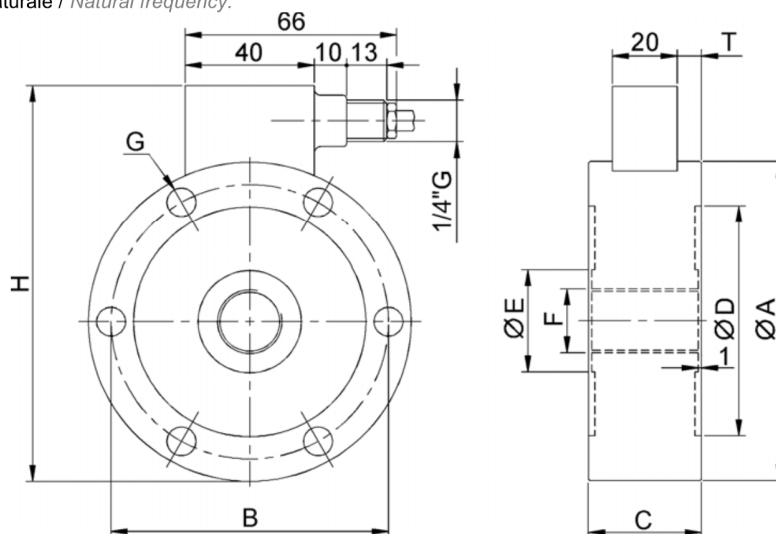
Dimensioni *Dimensions*

[mm]



CODE (Class 0.5)	CODE (Class 1)	LOAD	ØA	B	C	ØD	ØE	F	G	n°G	H	T	kHz ⁽¹⁾
CTC8TM5KNI05	CTC8TM5KNI15	5 kN	127	110	35	92	47	M30X2	10.5	8	149	7.5	2.5
CTC8TM10KNI05	CTC8TM10KNI15	10 kN											2.5
CTC8TM25KNI05	CTC8TM25KNI15	25 kN											4.8
CTC8TM50KNI05	CTC8TM50KNI15	50 kN											3.8
CTC8TM100KNI05	CTC8TM100KNI15	100 kN	165	138	60	110	62	M42X3	17	12	188	15	22.1
CTC8TM200KNI05	CTC8TM200KNI15	200 kN											22.1
CTC8TM300KNI05	CTC8TM300KNI15	300 kN											22.1
CTC8TM500KNI05	CTC8TM500KNI15	500 kN											18.2
CTC8TM750KNI05	CTC8TM750KNI15	750 kN	230	185	80	147	96	M60X3	25	12	254	30	18.2
CTC8TM1MNI05	CTC8TM1MNI15	1000 kN											18.2

⁽¹⁾ Frequenza naturale / *Natural frequency.*



Applicazioni Applications

COMPRESSIONE <i>COMPRESSION</i>	TRAZIONE <i>TENSION</i>																				
<p>ATTENZIONE: Verificare che le viti di fissaggio e gli accessori siano correttamente serrati.</p>	<p>WARNING: Check that the fixing screws and the accessories are correctly tightened.</p>																				
<table border="1" style="width: 100%; border-collapse: collapse;"> <tr> <td style="width: 30%;">Viti di fissaggio:</td> <td style="text-align: center;">Acciaio</td> </tr> <tr> <td>diámetro</td> <td style="text-align: center;">M8 M10 M16 M24</td> </tr> <tr> <td>coppia di serraggio (Nm)</td> <td style="text-align: center;">40 70 368 460</td> </tr> <tr> <td>classe di resistenza</td> <td style="text-align: center;">12.9</td> </tr> <tr> <td>Materiale accessori: da 5 a 200 kN da 300 a 1000 kN</td> <td style="text-align: center;">Acciaio inox Rm ≥90 kg/mm² Rm ≥130 kg/mm²</td> </tr> </table>	Viti di fissaggio:	Acciaio	diámetro	M8 M10 M16 M24	coppia di serraggio (Nm)	40 70 368 460	classe di resistenza	12.9	Materiale accessori: da 5 a 200 kN da 300 a 1000 kN	Acciaio inox Rm ≥90 kg/mm ² Rm ≥130 kg/mm ²	<table border="1" style="width: 100%; border-collapse: collapse;"> <tr> <td style="width: 30%;">Fixing Screws:</td> <td style="text-align: center;">Steel</td> </tr> <tr> <td>diameter</td> <td style="text-align: center;">M8 M10 M16 M24</td> </tr> <tr> <td>tightening torque (Nm)</td> <td style="text-align: center;">40 70 368 460</td> </tr> <tr> <td>resistance class</td> <td style="text-align: center;">12.9</td> </tr> <tr> <td>Accessories material: from 5 to 200 kN from 300 to 1000 kN</td> <td style="text-align: center;">Stainless Steel Rm ≥90 kg/mm² Rm ≥130 kg/mm²</td> </tr> </table>	Fixing Screws:	Steel	diameter	M8 M10 M16 M24	tightening torque (Nm)	40 70 368 460	resistance class	12.9	Accessories material: from 5 to 200 kN from 300 to 1000 kN	Stainless Steel Rm ≥90 kg/mm ² Rm ≥130 kg/mm ²
Viti di fissaggio:	Acciaio																				
diámetro	M8 M10 M16 M24																				
coppia di serraggio (Nm)	40 70 368 460																				
classe di resistenza	12.9																				
Materiale accessori: da 5 a 200 kN da 300 a 1000 kN	Acciaio inox Rm ≥90 kg/mm ² Rm ≥130 kg/mm ²																				
Fixing Screws:	Steel																				
diameter	M8 M10 M16 M24																				
tightening torque (Nm)	40 70 368 460																				
resistance class	12.9																				
Accessories material: from 5 to 200 kN from 300 to 1000 kN	Stainless Steel Rm ≥90 kg/mm ² Rm ≥130 kg/mm ²																				

Dimensioni Dimensions [mm]

TC8:	A	B	C	D	E	F	G	H	L	M
5, 10, 25, 50 kN	110	37	35	38	∅ 76	∅ 127	∅ 100	M 30 X 2	∅ 47	~ 200
100, 200, 300 kN	158	60	50	48	∅ 76	∅ 165	∅ 100	M 42 X 3	∅ 62	~ 224
500, 750, 1000 kN	253	85	80	88	∅ 126	∅ 230	∅ 180	M 60 X 3	∅ 96	/

Accessori Accessories

TC8:	CODE		ACCESSORIES (optional):	ACCESSORI (opzionali):
5, 10, 25, 50 kN	CTIC28	①	Loading head.	Testa di carico.
	CTC445M30	②	Spherical loading head M30X2.	Testa di carico sferica M30X2.
	CPBTC4D127	③	Mounting plate ∅ 127 mm.	Piastra base ∅ 127 mm.
	CACCEM30	④	Knuckle joints.	Teste a snodo sferico.
100, 200, 300 kN	CTIC35	①	Loading head.	Testa di carico.
	CTS62M42	②	Spherical loading head M42X3.	Testa di carico sferica M42X3.
	CPBTC4D165	③	Mounting plate ∅ 165 mm.	Piastra base ∅ 165 mm.
	CACCEM42	④	Knuckle joints.	Teste a snodo sferico.
500, 750, 1000 kN	CTIC60	①	Loading head.	Testa di carico.
	CTS96M60	②	Spherical loading head M60X3.	Testa di carico sferica M60X3.
	CPBTC4D230	③	Mounting plate ∅ 230 mm.	Piastra base ∅ 230 mm.



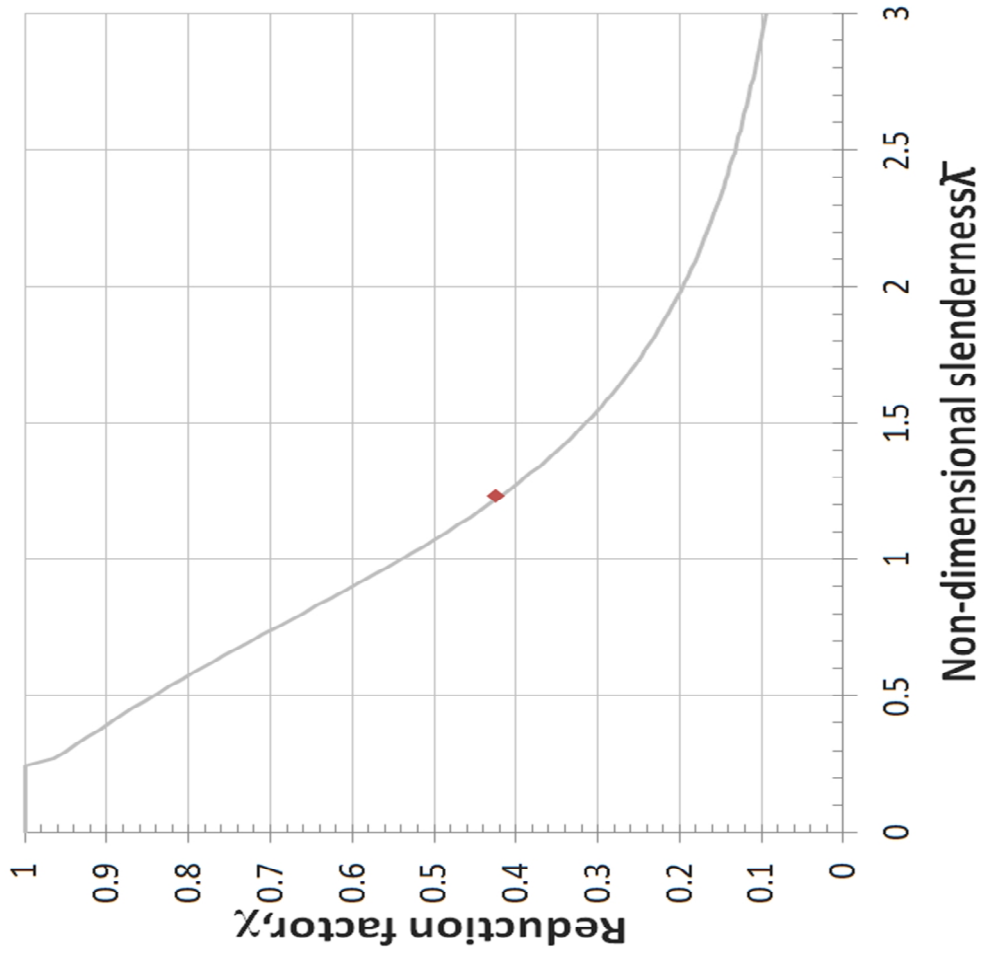
41010 Cognento (MODENA) Italy Via Bottego 33/A Tel:+39-(0)59-346441 Fax:+39-(0)59-346437 E-mail: aep@aep.it

Al fine di migliorare le prestazioni tecniche del prodotto, la società si riserva di apportare variazioni senza preavviso.
In order to improve the technical performances of the product, the company reserves the right to make any dynamometer without notice.

Appendix G: Interwell safe design procedure

Interwell Safe Design Procedure

Defining Parameters	
Effective length	Le 344 mm
Buckling case (Euler)	4
Buckling length	Lk 172 mm
Outer Diameter	OD 15 mm
Inner Diameter	ID mm
Modulus of Elasticity	E 205000 Mpa
Yield stress	σ 1456 MPa
Pressure applied on diameter	D 55 mm
Pressure applied	p 20000 psi
Design Load	P _{des} 327.62 kN
Required Safety Factor	SF 1.5
Geometry	
Second moment of inertia	I 2485.05 mm ⁴
Cross-section area	A 176.71 mm ²
Slenderness Calculations	
Radii of gyration	i 3.75 mm
Slenderness	λ 45.87
Minimum slenderness	λ_p 37.28
Relative slenderness	$\bar{\lambda}$ 1.23041343
Buckling Factor	χ 0.42411418
Buckling stress	σ_{cr} 617.51 Mpa
Buckling Load	P _{cr} 109.12 kN
Design Validation	
Allowed Buckling Load	P _{allow} 72.75 kN
Actual Safety Factor	S _{Factual} 0.3330829
Recommended Safety Factor	1.5 ≤ SF ≤ 2 NOT OK



Interwell Safe Design Procedure: Table

	σ	1456			
Yield stress,					
Minimum slenderness ratio	λp	37.28			
Imperfection Factor	α	0.49			
Robertson constant	R	0.2			
	Non-dimensional Slel Imperfection Parameter, η		Capacity Reduction Factor, Φ	Reduction factor, χ	
0	0	-0.098	0.451	1	1
1	0.026825874	-0.084855322	0.457932153	1	1
2	0.053651748	-0.071710643	0.465583933	1	1
3	0.080477623	-0.058565965	0.473955341	1	1
4	0.107303497	-0.045421286	0.483046377	1	1
5	0.134129371	-0.032276608	0.49285704	1	1
6	0.160955245	-0.01913193	0.503387331	1	1
7	0.18778112	-0.005987251	0.514637249	1	1
8	0.214606994	0.007157427	0.526606794	1	1
9	0.241432868	0.020302105	0.539295968	1	1
10	0.268258742	0.033446784	0.552704768	0.965303478	
11	0.295084617	0.046591462	0.566833197	0.951654875	
12	0.321910491	0.059736141	0.581681252	0.937939116	
13	0.348736365	0.072880819	0.597248936	0.92412136	
14	0.375562239	0.086025497	0.613536246	0.910170093	
15	0.402388114	0.099170176	0.630543185	0.896057187	
16	0.429213988	0.112314854	0.648269751	0.881758066	
17	0.456039862	0.125459532	0.666715944	0.867251949	
18	0.482865736	0.138604211	0.685881765	0.852522154	
19	0.509691611	0.151748889	0.705767214	0.837556451	
20	0.536517485	0.164893568	0.72637229	0.82234743	
21	0.563343359	0.178038246	0.747696993	0.806892863	
22	0.590169233	0.191182924	0.769741324	0.791196018	
23	0.616995108	0.204327603	0.792505283	0.775265885	
24	0.643820982	0.217472281	0.815988869	0.759117297	

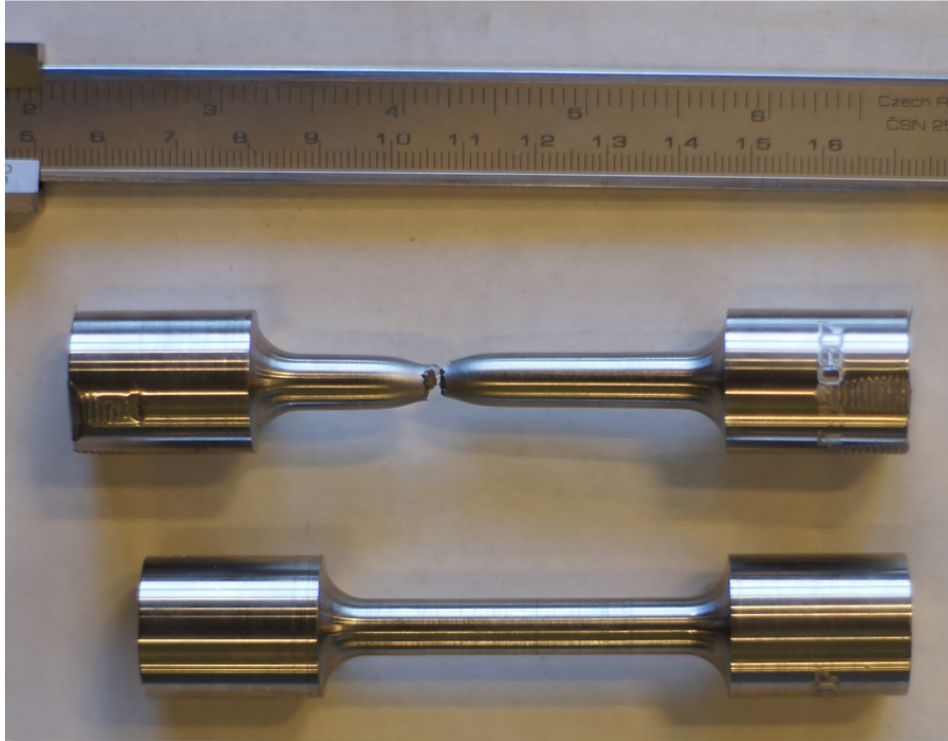
Interwell Safe Design Procedure: Check-List

Interwell Safe Design Procedure: Table	
Safe design procedure for axially loaded compression members with NS-EN 1993-1-1:2005	Check
Select steel grade and section properties of the member	
Compute the minimum moment of inertia, I and radius of gyration, i	
Find the desired design strength	
Estimate the effective length for the appropriate end conditions.	
Compute the non-dimensional slenderness for the relevant axis.	
Select the imperfection factor from table or formula	
Calculate the reduction factor using graph	
Calculate the buckling resistance	

Interwell Safe Design Procedure: Partial Safety Factors

Partial safety factors from experimental results and standards.				
Part Number	Results Factors	MAX	Mean	SF _y
Load and support, γ_{ls}	1.08			1.08
Geometric, γ_g	1.01			1.01
Material strength, γ_{ms}	1.1			1.1
Temperature, $\gamma_t, 100-200$	1.059	1.059	1.04	1.06
	1.021			
Well Pressure, γ_p	1.122	1.122	1.058	1.1
			Total SF _y :	1.4
			Total SF _y <SF	OK

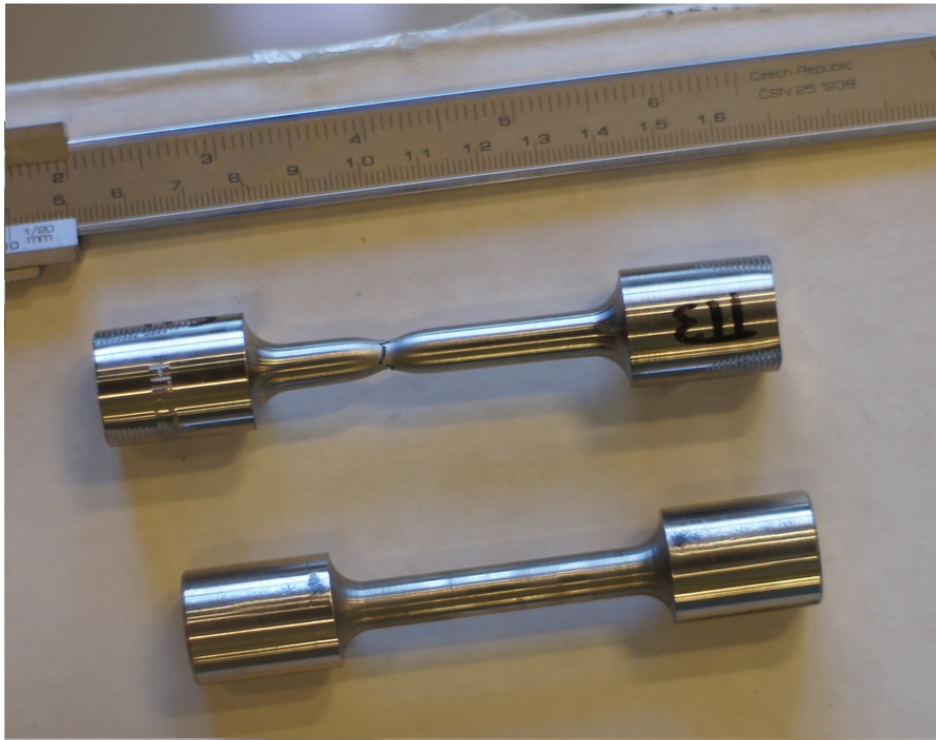
Appendix H: Uniaxial tensile test



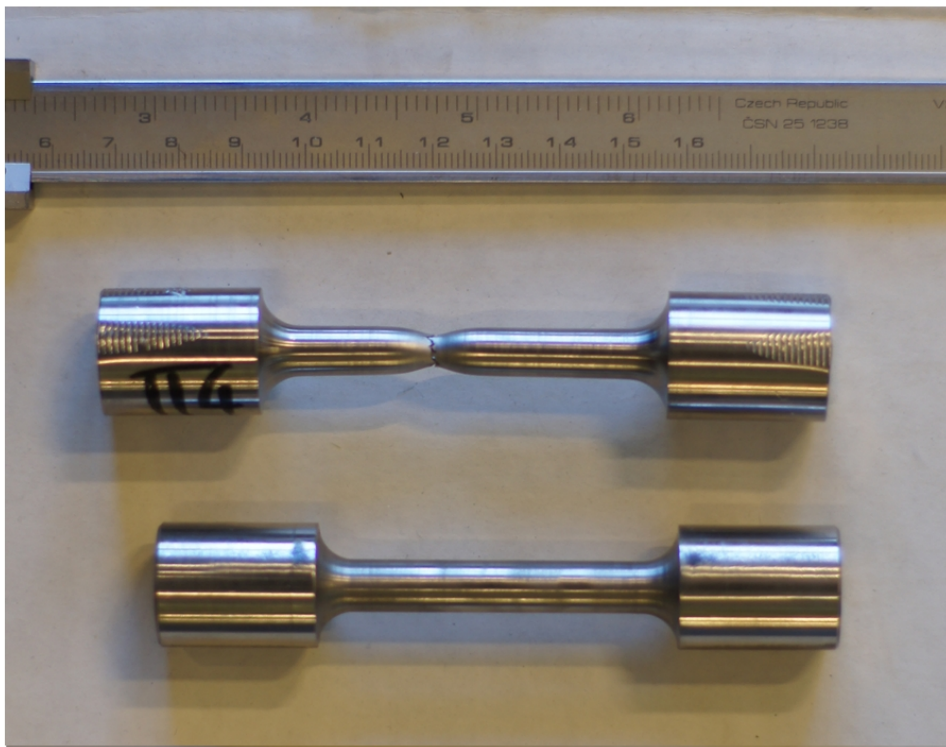
(a)



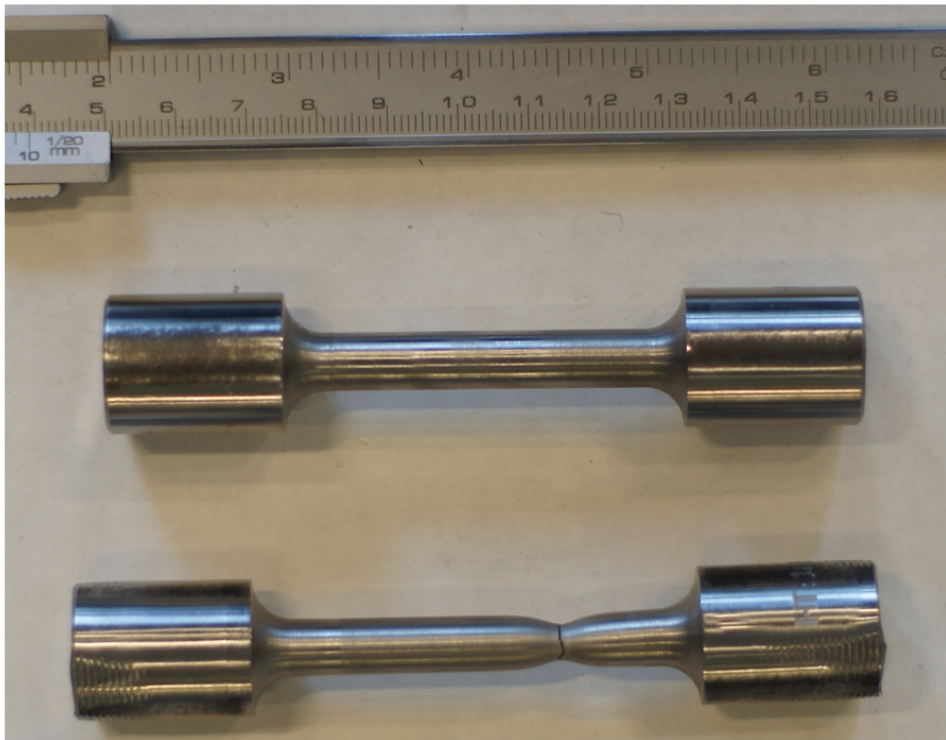
(b)



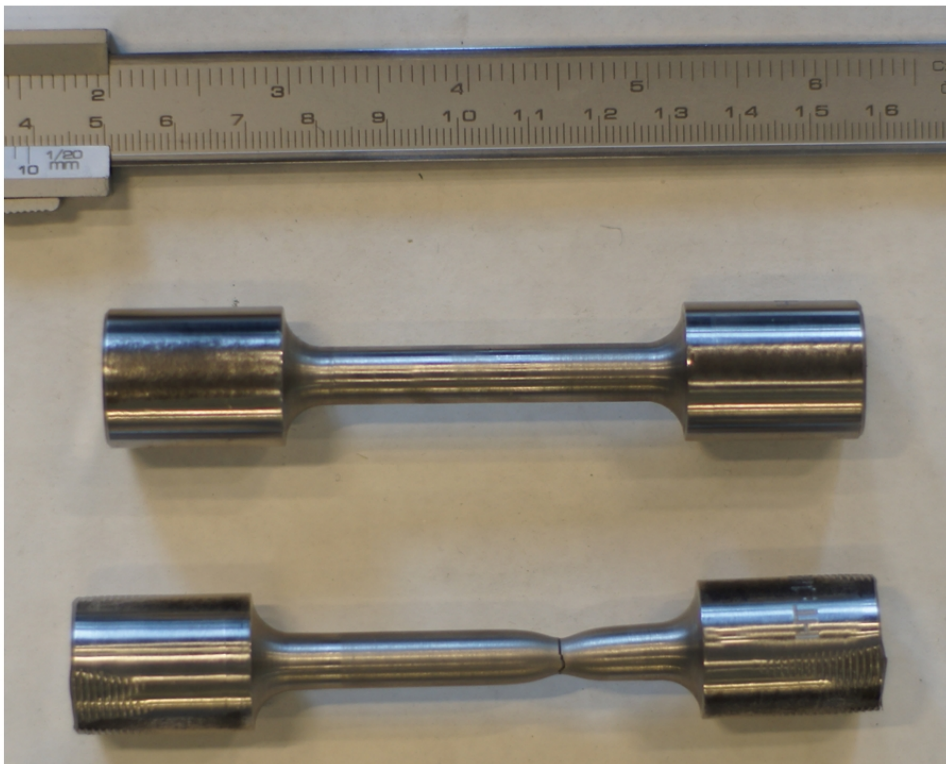
(c)



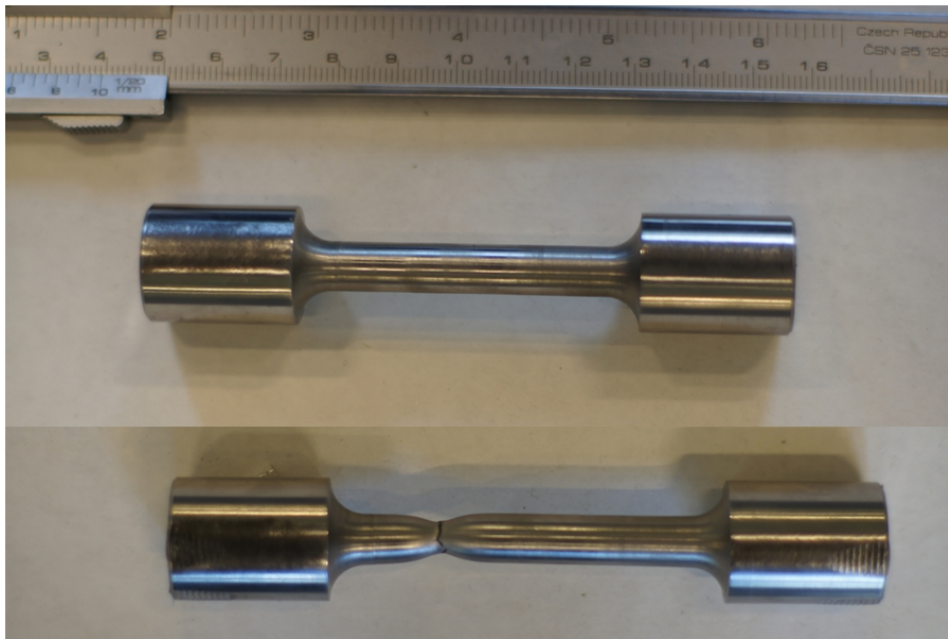
(d)



(e)



(f)



(g)

Figure H.0.1: Before and after uniaxial tensile test (a) TT1; (b) TT2; (c) TT3; (d) TT4; (e) TT5; (f) TT6; (g) TT7

Appendix I: Risk Assessment

NTNU	Risk assessment			Prepared by	Number	Date
				HSE section	HMSRV2603E	04.02.2011
HSE/KS				Approved by		Replaces
				The Rector		01.12.2006



Unit: IPM, Department of Engineering Design and Materials
Line manager: Torgeir Welo
Participants in the identification process (including their function): Julie Lund (student), Nils Petter Vedvik (supervisor)
Short description of the main activity/main process: Master project for student Julie Lund. Buckling of cylindrical members with respect to axial loads.
Signatures: Responsible supervisor: Nils Petter Vedvik *Nils Petter Vedvik*
 Student: Julie Lund *Julie Lund*

Date:

Activity from the identification process form	Potential undesirable incident/strain	Likelihood: Likelihood (1-5)	Consequence:			Risk Value (human)	Comments/status Suggested measures
			Human (A-E)	Environment (A-E)	Economy/material (A-E)		
Writing the Report	Lower-back pain, eyestrain, bacteria, stressful situations	1	A	A	A	1A	Good posture, regular exercise, breathing and relaxation techniques, hand sanitizer and antibacterial gloves
		2	A	A	A	2A	
Early Requirement Validation	Parts at high velocity Sudden acceleration at fracture/failure	1	B	A	A	1A	Glasses, helmet, screen, gloves
		2	B	A	A	2A	
Tensile Testing	Danger of pinching Sudden acceleration at fracture/failure	3	B	A	A	3A	Glasses, screen, safety shoes, gloves
		2	B	A	A	2A	
Testing of Setting Chamber Mandrel in Hydraulic Press	Parts at high velocity Hydraulic pressure Danger of pinching Big loads Sudden acceleration at fracture/failure	1	B	A	A	1A	Glasses, helmet, screen, lifting equipment, gloves
		2	A	A	A	2A	
		1	B	A	A	1A	
		2	A	A	A	2A	
Testing of Setting Chamber Mandrel in Hydrostatic Setting Unit	Sudden acceleration at fracture/failure	1	B	A	A	1A	Glasses, helmet, screen, lifting equipment.
		2	A	A	A	2A	